Single molecule studies of a voltage-gated potassium channel



Lauriane Angué

Department of Physics and Lincoln college, Oxford

University of Oxford

A thesis submitted for the degree of

Doctor of Philosophy

October 2013

Pour mes grand-parents, Yvette Steiner Cousin et Robert Steiner, avec amour

Acknowledgements

First, I would like to thank Dr Stephen Tucker and Dr Mark Wallace for having accepted me as a student. Their support, criticisims, patience have helped me all the way through this PhD. I am particulary grateful for the time they have spent reading this manuscript and tirelessly correcting it. Thank you!!!

I am indebted to the Berrow Foundation Scholarship for their financial support through these years. I feel particulary lucky to be part of such a diverse and friendly Scholars group and the Marquise de Amodio deserves all my gratitude for carrying this work through. Lincoln college has provided me during all of these years with an environment that many people would envy me, and does truly deserves a mention.

My collegues of Dr Stephen Tucker lab have been a big part of my life and I can only cherish all the fun moments we have spent together: Dr Vass Bavro, Dr Lejla Zubcevic, Dr Chetan Sharma, Matthias Schmidt, Dr Isabelle Andres-Enguix, Dr Lijun Shang, Dr Giovanna Bucci, Emma Sadler, Firdaus Abd Wahab, Conor McClenaghan, Alexandra Mackenzie. Thank you for having made me smile when the days were grim.

My collegues in Dr Mark Wallace laboratory have been part of this journey as well and I thank them for everything they have taught me: Dr

Olivier Castell, Dr Matthew Baker (thank you for your help on the photobleaching analysis!!!), Dr Charlotte Dodson, David Marshall, Jason Sengel, John Danila, Eve Wetherill, Mike Senior, Marc Szabo, Ed Down, Dr Brid Cronin, Dr Linda Gross, Chandini Mallick, Dr Lydia Hariss, Dr James Thompson, Dr Sebastian Leptihn.

I am deeply indebeted to Dr Constantina Fotinou, Dr Heidi de Wet, and Dr Holger Kramer for their support, and valuable scientific discussions. You have really made a difference for me and I thank you from the bottom of my heart.

A special thank you to Sylvia Elsner, for her help and wise advices.

My "Oxford family" deserves recognition as well. Firstly the rowdy boys: Dr David Yadin, Richard Passmore and Dr David Mulholland for all the fun we had under the same roof for a couple of years. Dr Richard Wheeler, Susanah Bell, Dr Penny Sarchet, Dr Thomas Skinner: thank you!! I have had the chance to make many friends in Oxford and they have helped me during this journey: Julie Miller, Marlena Whiting, Annika Bruger, Susana Hancock, Danielle Costa.

At last to the people who were there from the beginning: my family. My parents for their unconditional love and support, my sisters Amélie and Cécile,my grandparents, Yvette and Robert Steiner, my grandmother Huguette Angué Verchère. Merci pour tout!!!!

Abstract

This thesis aims to study the activation and deactivation mechanism of voltage-gated K^+ channels (K_v), through fluorescence and electrical measurements. Transmembrane voltage changes are detected by the voltage sensor (helices S3b-S4) among K_v, a phenomenon which triggers a conformational change to open or close the pore. By attaching a fluorescent tag on helices S3b-S4, voltage sensor movement can be followed by fluorescence and pore opening or closure by electrical recordings. K_vAP, a channel from an archaea organism was selected for this task. Channels were expressed, purified and fluorescently labelled before being reconsituted into droplet interface bilayers (DIB). The degree of labelling was determined by photobleaching measurements. Electrical activity and diffusion were recorded at the single molecule level. Further developments of the technique need to be achieved before successfully correlating fluorescence and electrical recordings at the single molecule level. However, both signals could be simultaneously recorded at bulk and single molecule levels, paving the way for future experiments.

Contents

Contents 1

List of Figures 2

List of Tables 3

1 Introduction 4

1.1 Bioelectricity 4

1.2 The action potential 6

1.3 Properties of ion channels 6

1.4 Potassium channels 8

1.5 KcsA 9

1.6 Voltage-gated channels 11

1.7 A simplified prokaryotic K_v channel (K_vAP) 13

1.8 The conventional model 15

1.9 The paddle model 16

1.10 Controversies 17

1.11 Modular voltage-sensor domain 19

1.12 Lipid regulation of K_vAP 21

1.13 Toxins . . . 22
1.14 Droplet interface bilayers (DIB) . . . 24
1.15 Ion channel single molecule fluorescence . . . 27
1.15.1 The importance of the signal to noise ratio . . . 28
1.15.2 Total internal reflection fluorescence (TIRF) . . . 29
1.16 Previous fluorescence studies on ion channels . . . 31
1.16.1 Fluorescence tracking experiments . . . 32
1.16.2 Subunit stoichiometry . . . 33
1.16.3 FRET . . . 34
1.17 Overall aim of this thesis . . . 35

2 Development of an Protein Production, Purification and Fluorescent Labelling Strategy for K_vAP-CL 37

2.1 Introduction . . . 37
2.1.1 Aim . . . 37
2.1.2 K_vAP-CL . . . 38
2.1.3 Choice of labelling site . . . 40
2.1.4 Methodology . . . 41
2.1.5 Affinity purification . . . 43
2.1.6 Thrombin protease reaction . . . 43
2.1.7 Gel electrophoresis . . . 43
2.1.8 Blue native PAGE electrophoresis . . . 44
2.1.9 Western blot . . . 45
2.1.10 Size-exclusion chromatography . . . 45
2.1.11 Labelling . . . 46

2.1.12 Dye/protein molar ratio 48
2.1.13 Ellman's reaction 49
2.2 Material 50
2.2.1 Gene 50
2.2.2 Vector 50
2.2.3 Strains 51
2.2.4 Purification 51
2.2.5 Western blot 51
2.2.6 Reconstitution 51
2.3 Methods 51
2.3.1 Site-directed mutagenesis 51
2.3.2 Production 52
2.3.3 Purification 52
2.3.4 SDS-PAGE 53
2.3.5 Blue native PAGE 53
2.3.6 Western blot analysis 54
2.3.7 Reconstitution 54
2.3.8 Planar lipid bilayer 55
2.3.9 Labelling 55
2.4 Results 56
2.4.1 Introduction of cysteines for labelling 56
2.4.2 Optimisation of Expression Protocol 58
2.4.2.1 Confirmation of K_vAP-CL expression 61
2.4.3 Optimisation of IMAC purification 62
2.4.4 FPLC 66

2.4.5 Functional analysis of purified protein 71
2.4.6 Development and optimisation of fluorescent labelling 73
2.4.7 Quantification of labelling efficiency 79
2.5 Discussion 80
2.5.1 Expression 80
2.5.2 Purification 81
2.5.3 Size-exclusion 81
2.5.4 Functional analysis of purified protein 82
2.5.5 Development and optimisation of fluorescent labelling 82
2.5.5.1 Reducing agents 82
2.5.5.2 Bufffer 83
2.5.5.3 Protective group and PEG-maleimide 84
2.5.5.4 Important considerations for labelling 85
2.5.6 Quantification of the fluorescence 86
2.6 Conclusion 87

3 Photobleaching Analysis of Labelled K_vAP-CL **88**
3.1 Introduction 88
3.1.1 First method: GMimPro 90
3.1.1.1 Single fluorophore detection algorithm (SFDA) . . . 90
3.1.2 Second method: Photobleaching analysis frequency code (PAFC) 92
3.1.2.1 Chung-Kennedy filter 92
3.1.2.2 The pairwise difference distribution function 92
3.1.2.3 Photobleaching analysis frequency code 93
3.2 Material and methods 94

3.2.1 Plasma cleaning . . . 94
3.2.2 Sample preparation and recordings . . . 95
3.2.3 Analysis . . . 96
3.2.4 TIRF microscopy setup . . . 96
3.3 Results . . . 97
3.3.1 GMimPro analysis . . . 97
3.3.1.1 Control: simulation with four photobleaching steps . 97
3.3.1.2 Control: simulation with one photobleaching step . . 99
3.3.1.3 Control: four Cy3 labelled DNA sample . . . 102
3.3.1.4 Labelled K_vAP-CL . . . 104
3.3.2 Photobleaching analysis frequency code . . . 108
3.3.2.1 Controls . . . 108
3.3.2.2 Labelled K_vAP-CL . . . 111
3.4 Discussion . . . 116
3.4.1 GMimPro analysis . . . 116
3.4.2 Photobleaching Analysis Frequency Code . . . 117
3.4.2.1 Controls . . . 117
3.4.2.2 Labelled K_vAP-CL . . . 118
3.5 Conclusion . . . 119

4 Combined Electrical and Fluorescent Measurements of K_vAP 121
4.1 Introduction . . . 121
4.1.1 Summary of the Chapter . . . 121
4.1.2 Droplet interface bilayer (DIB) . . . 122
4.1.2.1 System requirements . . . 124

4.1.2.2 Coupling with optical imaging 124
4.1.3 Membrane protein incorporation via vesicle fusion with a planar lipid bilayer 125
4.1.4 Lipids 126
4.1.4.1 POPE and POPG 126
4.1.4.2 DPhPC 128
4.1.4.3 TRITC-DHPE 128
4.1.5 Analysis of electrical and fluorescence traces 129
4.1.6 Particle tracking 129
4.1.7 Lateral diffusion coefficient 131
4.2 Material and Methods 132
4.2.1 Lipid preparation for electrical recordings 132
4.2.2 Lipid preparation for fluorescent lipids 133
4.2.3 DIB preparation for experiments with fluorescent lipids 134
4.2.4 Samples preparation 134
4.2.5 Plasma-cleaning of the coverslips 134
4.2.6 Cleaning of PMMA (polymethyl methacrylate) and equilibration device 134
4.2.7 DIB preparation for experiments with K_vAP 135
4.2.8 Droplet preparation 135
4.2.9 Electrical recordings 136
4.2.9.1 I/V curve 136
4.2.10 TIRF microscopy setup 136
4.2.11 Particle tracking and lateral coefficient diffusion calculation . . 137
4.2.12 Single particle trajectories and bulk fluorescent intensity analysis 138

4.3 Results . . . 138
4.3.1 DIB formation . . . 138
4.3.2 Electrical recordings . . . 141
4.3.3 I/V curve . . . 141
4.3.4 Lateral diffusion coefficient (D_{lat}) . . . 144
4.3.4.1 Fluorescent lipids . . . 144
4.3.4.2 K_vAP fluorescently tagged with TMR5M . . . 144
4.3.5 Correlation of fluorescent, voltage and electrical signals . . . 149
4.3.5.1 Single molecule measurements . . . 150
4.3.5.2 Ensemble-averaged measurements . . . 151
4.4 Discussion . . . 155
4.4.1 DIB formation . . . 155
4.4.2 Incorporation of vesicles . . . 155
4.4.3 Electrical traces and I/V curve . . . 156
4.4.4 Fluorescence experiments . . . 157
4.4.5 Diffusion coefficient . . . 158
4.4.6 Fluorescent, voltage and electrical correlation . . . 158
4.4.6.1 Technical difficulties . . . 158
4.4.6.2 Single molecule behaviour . . . 161
4.4.6.3 Ensemble level . . . 162
4.5 Conclusion . . . 163

5 Conclusions **165**

5.1 Summary . . . 165
5.2 Expression and purification of K_vAP . . . 166

5.3 Labelling of K_vAP 166
5.4 Incorporation of K_vAP into DIBs 168
5.5 Electrical measurements of K_vAP function 169
5.6 Measurement of fluorescent signals 170
5.7 Simultaneous electrical and fluorescent measurements 171
5.8 Future experiments 174
5.9 The mechanism of K_vAP voltage-gating and future directions 175

Appendix A **178**

A.1 K_vAP(ΔB13)-C247SC 178
A.2 pQE60-Lac vector 178
A.3 Four Cy3 labelled DNA sample 179
A.4 Microscope calibration 180

Bibliography **181**

List of Figures

1.1 Action potential. 7

1.2 Tetrameric cations channel superfamily. 9

1.3 KcsA structure. 10

1.4 Topology of voltage-gated potassium channels. 11

1.5 Tetrameric and monomeric structure of K−vAP. 14

1.6 Conventional model representation. 16

1.7 Paddle model representation. 17

1.8 Voltage sensing domain found in voltage-gated channels, in enzyme and as a whole unit. 20

1.9 Planar lipid bilayers. 25

1.10 Droplet interface bilayers. 26

1.11 Droplet hydrogel bilayer. 27

1.12 TIRF phenomenon between two media of different refractive indexes. 30

2.1 Cysteine mutated residues in (84). 39

2.2 Protein purification protocol for K_vAP-CL. 42

2.3 Principle of IMAC. 44

2.4 Principle of size exclusion chromatography. 46

2.5 TMR5M chemical structure and absorption and emission spectrum. . 48
2.6 Ellman reaction. 50
2.7 Site-directed mutagenesis on voltage-sensor of K_vAP-CL. 57
2.8 K_vAP-CL view as a dimer with the mutated residues highlighted. . . 58
2.9 Comparison of the K_vAP expression between cell lines at 37°C. . . . 60
2.10 Comparison of the K_vAP expression between cell lines at 28°C. . . . 61
2.11 Comparison of the K_vAP-CL expression with and without $BaCl_2$ . . . 62
2.12 Western blot of K_vAP-CL expression. 63
2.13 Different DM concentration tested during purification. 64
2.14 Different temperatures tested during purification. 64
2.15 Thrombin cleavage test. 65
2.16 SDS-PAGE gel of K_vAP-CL purification. 67
2.17 Elution profile of K_vAP-CL with changes of flowrate. 67
2.18 Elution profile of K_vAP-L121C-CL in octyl-β-glucoside detergent. . . 68
2.19 Elution profile of K_vAP-CL. 69
2.20 Elution profile of the FPLC analysed by Blue native-PAGE. 70
2.21 Aggregation of the 6xHis tagged protein, during FPLC. 70
2.22 Electrical trace recorded with the planar lipid bilayer showing opening and closing of one channel. 71
2.23 Electrical trace recorded with the planar lipid bilayer showing opening and cloing of two channels. 72
2.24 Electrical trace recorded with the planar lipid bilayer showing opening and closing of five channels. 72
2.25 Negative controls and unsucessfull labelling of K_vAP-CL in SDS-PAGE gel. 74

2.26 Control of site reactivity with PEG-maleimide. 76
2.27 Silver stained SDS-PAGE gel showing the fluorescently labelled K_vAP-CL mutant. 77
2.28 Coomassie stained SDS-PAGE gel showing the fluorescently labelled K_vAP-CL mutant and the purification through the desalting column. 78
2.29 Coomassie stained SDS-PAGE showing the absence of fluorescence of K_vAP-CL after labelling. 78
2.30 Reaction mechanism between DTT and a disulfide bond. 83
2.31 Reaction mechanism between MMTS and a disulfide bond. 85

3.1 Photobleaching traces of the four steps simulation with added noise analysed by GMimPro. 98
3.2 Photobleaching traces of the four steps simulation analysed by GMimPro. 99
3.3 Bargraph of the counted photobleaching steps by GMimPro for the two four steps simulations. 100
3.4 Photobleaching steps of the one step simulation analysed by the Ms-test (GMimPro). 101
3.5 Photobleaching steps of the one step simulation analysed by the drop test (GMimPro). 101
3.6 Bargraph of the counted photobleaching steps by GMimPro for the one step simulation. 102
3.7 Photobleaching steps of the four Cy3 labelled DNA analysed by the Ms-test (GMimPro). 103
3.8 Bar-graph of the four Cy3 labelled DNA analysed by the Ms-test (GMimPro). 104

3.9 Photobleaching steps of K_vAP-G101C-CL analysed by GMimPro. . . 105
3.10 Photobleaching steps of K_vAP-L121C-CL analysed by GMimPro. . . 106
3.11 Bar graph of labelled mutant of K_vAP analysed by GMimPro. 107
3.12 Photobleaching traces of the controls analysed by PAFC. 109
3.13 Histograms of the controls analysed by PAFC. 110
3.14 Example of photobleaching steps of K_vAP-G101C-CL/ L121C-CL label cycles 1-3 analysed by PAFC. 112
3.15 Example of photobleaching steps of K_vAP-A111C-CL/ G112C-CL/ L121C-CL purification 1 and 2 analysed by PAFC. 113
3.16 Histograms of labelled K_vAP-CL mutants analysed by PAFC. 114
3.17 Mutations done on the voltage sensor of K_vAP-CL. 115

4.1 PMMA devices. 122
4.2 DIB with TIRF beam. 123
4.3 Chemical structure of POPE and POPG lipids. 127
4.4 Chemical structure of DPhPC lipid. 128
4.5 Chemical structure of TRITC-DHPE lipid. 129
4.6 Example of electrical recording of K_vAP-CL. 142
4.7 Example of electrical recording of K_vAP-CL. 142
4.8 Example of electrical recording of K_vAP-CL. 143
4.9 I/V curve of K_vAP recorded in DIB. 143
4.10 Particle tracking of 0.00012 % of TRITC-DHPE in DPhPC bilayer. . 145
4.11 Calculation example of D_{lat}. 146
4.12 Particle tracking of fluorescently tagged K_vAP in DPhPC bilayer. . . 147

4.13 Standard deviation calculation of recordings of fluorescent lipids and fluorecently tagged K_vAP in DPhPC bilayer. 148
4.14 Individual fluorescent traces of K_vAP plotted along the applied voltage. 151
4.15 Macroscopic fluorescent traces of K_vAP plotted along the applied voltage and the current. 153
4.16 Bar-graph and normalised histograms of all fluorescent trajectories according to the voltage applied. 154

A.1 K_vAP(ΔB13)-C247S amino acids sequence. 178
A.2 Map of the pQE60-Lac vector. 179
A.3 Template gene sequence. 180
A.4 Strand with Cy3 fluorophore gene sequence. 180

List of Tables

2.1 Mutations list 56

2.2 Expression conditions for the production of K_vAP. + indicates expression. 59

2.3 Comparison of single channel currents between experimental values (single measurements) and the litterature 73

2.4 Labelling conditions tested with K_vAP(ΔB13)-Y59C-CL, and K_vAP(ΔB13)-A111C-CL after IMAC purification. 74

2.5 Labelling conditions tested with K_vAP(ΔB13)-Y59C-CL after IMAC purification with the use of a protective group. 75

2.6 Calculated protein/dye ratio for mutants of K_vAP-CL. Measures taken with the Nanodrop. 80

3.1 GMimPro conditions tested on the two simulations (20 fluorescent spots). The number of detected spots and the signal to noise ratio (SNR) calculated are shown. 100

3.2 Statistical values and standard error calculated by PAFC for the controls. 111

3.3 Statistical values calculated by PAFC for the samples tested 116

4.1 The droplets were incubated in the lipids/oil mixture for 20 min prior the experiment. 10 mM HEPES, pH 7.0 buffer was used in the rehydratation layer, in the droplet, and in the sample (K_vAP-G112C-CL) as well. 139

4.2 The droplets were incubated in the lipids/oil mixture for 20 min prior the experiment. 10 mM HEPES, pH 7.0 buffer was used in the rehydratation layer, in the droplet as well. 140

4.3 Coefficient diffusion and standard deviation of K_vAP-L121C-CL and K_vAP-G112C-CL analysed by the software Mosaic. 80, 53 and 79 trajectories were used in the calculation for TRITC-DHPE, K_vAP reduced mobility, and K_vAP freely diffusing. 148

A.1 Microscope calibration with a 60x optical magnification. 180

Chapter 1

Introduction

1.1 Bioelectricity

Cells constantly live and grow in contact with charged compounds. Solutes like amino acids, phosphate and inorganic ions necessary to every organism are present both in the intracellular and extracellular environment. Their transport across the lipid bilayer needs to be tightly controlled, to allow the organism to draw, retain essential compounds, and excrete unwanted molecules. However, the uneven distribution of solutes and in particular ions in the intracellular and extracellular environments creates an electric field, and the movement of charged ions across the lipid membrane can give rise to electrical currents.

Cells have evolved to deal with this voltage difference across the membrane and use it to their advantage for example in energy storage and synthesis of ATP. In addition in eukaryotic organisms, the movement of inorganic ions across the membrane has emerged as an efficient method for signaling. The lipid bilayer is essentially impermeable to charged ions, and the transport of species from one side of the membrane to

the other has to be carried out by specialized proteins within the membrane. Depending upon their use of energy, they can be classified into two distinct groups: active transport proteins, which use ATP as an energy source to move the species against their concentration gradient (pumps, transporters) and passive transport proteins, which facilitate the flow of the species down a concentration gradient. The second class does not require any use of energy, and ions flow through pores or "channels", inserted in the lipid membrane.

All electrical signaling in animal cells is the result of ion channels. Gradients of inorganic ions are maintained as a standard environmental condition through active transporters and pumps. The movement of ions through a channel is dictated by diffusion and electrical forces, and ion flow will stop when these two forces balance each other. This equilibrium state is described by the Nernst equation:

$$E_x = E^\theta - \frac{RT}{zF} \ln(c_{out}/c_{in}) \tag{1.1}$$

- E_x: Equilibrium potential for ion species x [V]
- E^θ: Standard equilibrium potential [V]
- R: Ideal gas constant [J $K^{-1}mol^{-1}$]
- T: Temperature [°K]
- z: Valence of the ion species [-]
- F: Faraday constant [C mol^{-1}]
- c_{out}: Concentration of the ion species in the external medium [M]
- c_{in}: Concentration of the ion species in the internal medium [M]

1.2 The action potential

Some animal cells, in particular neurons, have specialised in the generation, propagation and management of electrical signals in the most efficient and exquisite way. The information is carried from one point within a neuron down the nerves fibres, to a contact with either another neuron, or target such as a cell or a muscle. The electrical signal is propagated at a rate of several meters per second through the opening and closing of Na^+ and K^+ channels. At equilibrium in the nerves, Na^+ is present at a higher concentration in the external fluid (compared to a cell inside medium), whereas in the cytoplasm the K^+ concentration is higher (Figure 1.1). If Na^+ channels open, Na^+ ions will flow down its electrochemical gradient and enter the cell; the intracellular voltage will then change and become more positive. The signal will therefore propagate down the nerve fibres. Next, K^+ channel opening allows K^+ to leave the intracellular medium and restores the transmembrane voltage to its initial value.

1.3 Properties of ion channels

In order to fill their role, ion channels have to perform three basic but interconnected functions: selective ion permeation, gating (*i.e.* opening and closing) and sensing (regulation of gating in response to modulatory signal). Each channel must possess high ion throughput ($10^6 - 10^8$ ions per second) while maintaining high selectivity. The gating of the pore controls the flow of ions through the channel and this process is normally coupled to an environmental sensing mechanism of the channel.

Consequently, channels are classified according to the ions for which they are

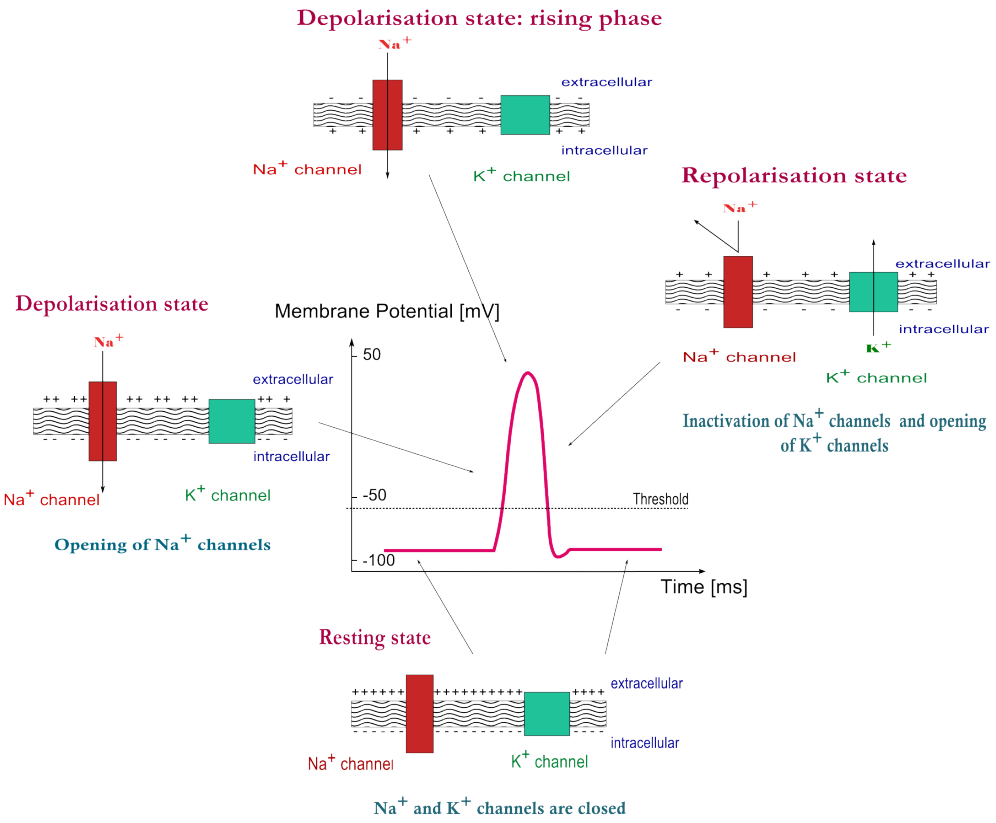


Figure 1.1: Movement of Na^+ and K^+ ions through the membrane via sodium and potassium channels, driven by the change in membrane potential. Different states are represented, the cell at rest (bottom), when the membrane is depolarized (middle left and top) and the repolarisation (right) to the resting state. Depolarisation needs to overcome a threshold value to generate an action potential.

selective, as well as their regulatory mechanisms. Typically, chloride, potassium, sodium, and calcium ions are the most common ionic species, whilst gating can be controlled by voltage, ligand binding (*e.g.* neurotransmitter, ATP, H^+, cyclic-nucleotide), light, pressure and covalent modification (*e.g.* phosphorylation).

1.4 Potassium channels

Potassium is one of the most abundant ions in the cytoplasm. Even in media deprived of K^+, unicellular organisms retain a high concentration (around 200 mM) of cytoplasmic potassium, and unlike other cations, a high internal K^+ concentration does not interfere with enzymatic and metabolic processes. It is thought that its presence inside the cell (along with other neutral molecules) provides the osmotic driving force required to sustain the turgor pressure necessary for cell growth (54).

Voltage-gated potassium channel genes are essential for any organism's survival; they are found in all kingdoms of life and were present even at life earliest forms. In the human genome, they form the third largest class of signaling molecules, with 78 members identified so far and can display a unitary conductance ranging from 1 to 1000 pS.

Their simple structure is highly conserved and the minimal unit to form a potassium ion channel seems to be two transmembrane α-helices separated by a pore forming loop (TM1-P1-TM2). This minimal channel is found in nature and the smallest identified so far (94 amino acids) has been found in a virus, PBCV-1 found in green alga (Chlorella).

Another very common structural motif, called the shaker motif, is formed by 6 α-helices, with the pore placed between TM-helices 5 and 6. This motif was first discovered in a voltage-gated potassium channel, the "shaker" K^+ channel which was the first to be cloned, from the fruit fly Drosophila. When mutated, the shaker gene causes the fly legs to shake under ether anesthesia and was cloned by positional genetics in the 1980's. Its topology represents the archetypal structure of a voltage-gated K^+ channel and its discovery has allowed the identification of many homologous

members of the K_v (voltage-gated channel) family in vertebrates.

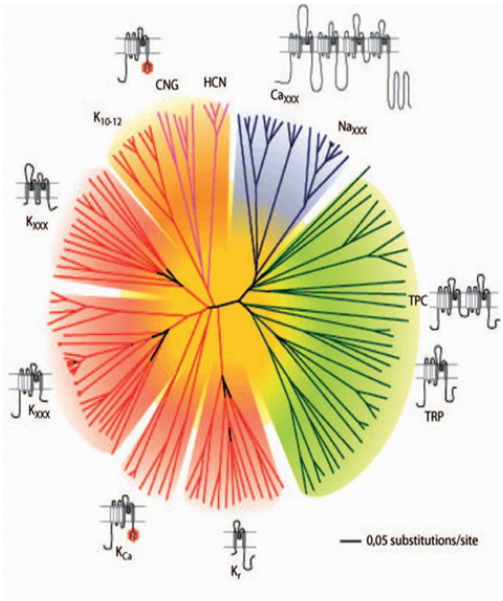


Figure 1.2: 143 members of the tetrameric cations channel superfamily classified into 7 groups with their membrane topology. Classification of the 143 members is done by the residue composition of the minimal pore region (106).

1.5 KcsA

Our first understanding of the 3D structure of the channel came from a K^+ channel (KcsA) from Steptomyces lividans, whose crystal structure was published in 1998 (31). They demonstrated that the size of the pore cavity determines the ion selectivity (Figure 1.3).

For K^+ channels, the mean diameter of the pore is 2.84 Å. Selectivity is achieved by the carbonyl oxygens of the canonical sequence of TXGYG residues from each of the four subunits that multimerises. The architecture of the pore is designed to

mimic the aqueous hydration shell carried by K^+ ions in solution. When the K^+ ions (diameter 1.33 Å) enter and pass through the filter, the energetic cost of removing their aqueous cargo is minimal (31). On the other hand, if a Na^+ ion comes close enough to the mouth of the filter, the free energy cost of dehydration is unfavourable, and the smaller (diameter 0.95 Å) Na^+ ions do not not bind as well to the filter. The fine design of the filter allows a factor of discrimination between K^+ and Na^+ of 10^5.

The activation gate of the channel is located on the intracellular side and is formed by the intersection of four pore-lining transmembrane segments at the bottom of the filter to seal the pore. A small vestibule exists between the gate and the filter in the form of a filled cavity with water.

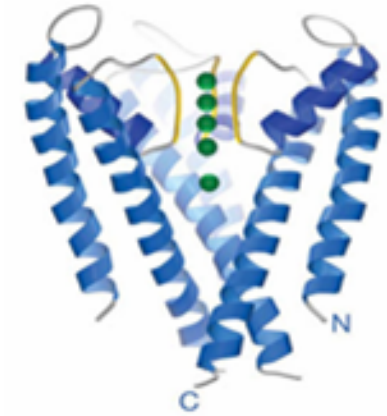


Figure 1.3: KcsA structure with potassium ions (green) are sitting in the pore filter sites (yellow) highlighted (70).

1.6 Voltage-gated channels

This class of potassium channels is mainly expressed in excitable tissues where they are primarly responsible for repolarisation of the membrane during an action potential. Like KcsA, they are functional as tetramers.

Each subunit is composed of 6 transmembrane α-helices, 5 linker regions and the N and C termini both being intracellular (Figure 1.4). Two domains exist within each subunit: the pore-forming domain composed of helices 5 and 6 (S5 and S6, which is similar to KcsA) and the voltage-sensor domain composed of helices 1 to 4 (S1 to S4). Each subunit assembles with its voltage-sensor domain at the periphery and its pore-domain facing each other in the middle, forming a four-fold symetrical unit.

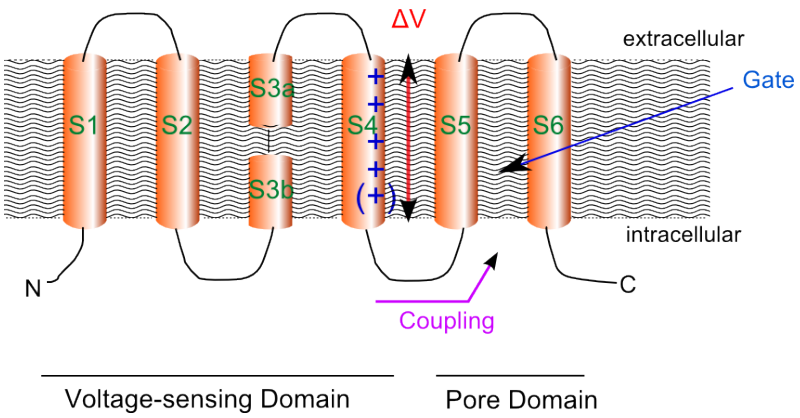


Figure 1.4: Topology of K_v channels. Six α-helices are inserted into the bilayer with the N and C termini being intracellular. α-helix S3 is composed of two parts, a and b. α-helix S4 carries four or five positively charged residues.

Each member of the family possesses 4 to 5 positively charged amino acids on the S4 α-helix. These positively charged amino acids are thought to "sense" the voltage change across the membrane and use this to drive conformational motion in the channel. A plethora of studies have shown that this charged S4 helix is essential

for voltage activation and its movement is coupled to the opening or closing of the channel gate (3, 4, 8, 11, 56, 61, 75, 78, 90, 92).

Upon changes in transmembrane potential, the S4 helix moves in the membrane, giving rise to a small "gating current" of approximatively 12-14 electronic charges (3.0-3.5 charges per subunit). These positively charged residues are crucial for the detection and the response to changes in the transmembrane potential and are highly conserved among voltage-gated channels (12).

The Na_v channel family is structurally similar to voltage-gated potassium channels. Its central subunit, the α-subunit is composed of four repeated motifs linked together: the 6 α-helices forming the pore and the voltage-sensing domain. Similar to K_v channels, the S5-S6 helices are packed at the centre of the channel to form the conduction pore, whereas the S4 helices mediate the channel activation through positive residues with two hydrophobic resides intercalated in between. This highly glycosylated 260 kDa subunit is surrounded by four β-domains subunits (in mammals), each one composed of an intracellular C-terminus, a transmembrane domain and two extracellular β-sheets. Only two of the β-domains are covalently linked to the central α-subunit via disulfide bonds ($\beta 2$, $\beta 4$). These domains are thought to regulate the biophysical properties of the channels and to control their surface density on the membrane. In the nervous system, both Na^+ and K^+ channels families act in concert to produce the action potential.

In prokaryotic cells, K_v channels function as homotetramers; in humans they are present as heterotetramers. 40 genes code for K_v channels in humans forming 12 subfamilies, but their diversity is even greater due to alternative splicing and heteromultimerisation (104).

The channels are composed of three domains. 4 monomers assemble together

relatively freely and form the membrane domain. The heteromultimerisation results in a large variety of biophysical and pharmacological properties for each channel combination. In contact with the cytosolic part of the channel sits the tetramerisation domain, which controls the ability of different K_v channels to heteromultimerise. In eukaryotes, the properties of the channel can also be modified by glycosylation, phosphorylation, ubiquitylation, palmitoylation and even sumoylation. Consequently, the molecular diversity which arises from such complexity makes it challenging to identify which channels are produced in a native tissue. Our ability to define their biophysical and pharmacological properties compared to cloned channels produced in isolated systems is thus restricted.

1.7 A simplified prokaryotic K_v channel (K_vAP)

In 2003, the Mackinnon group presented the first x-ray structure of a voltage-gated potassium channel, K_vAP, at a resolution of 3.2 $\mathring{A}$ (Figure 1.5) (49). This channel comes from a hyperthermophilic archaebacterium, *Aeropyrum pernix*, from a coastal thermal vent of 95°C. Like other voltage-gated channels, it is functional as a homotetramer, with each subunit composed of one pore domain and one voltage-sensing domain. Five arginines within S4 are responsible for sensing the transmembrane voltage. The reported conductance of the channel is 170 pS, in 150 mM KCl, 10 mM HEPES, pH 7.0 (on both sides) (83). K_vAP was the first voltage-gated potassium channel structure to be resolved near atomic resolution. Along with the full channel structure, the voltage sensor was crystallised separately and its x-ray structure presented at a resolution of 1.9 Å. Due to the high mobility of the voltage sensor domain, monoclonal antibodies, Fab fragments, were used during the crystallisation

process to hold the channel in a defined position. A library of Fab fragments was generated and the ones which could bind to the voltage sensor were selected. The crystal structure revealed a tetrameric channel with a Fab fragment bound to each voltage sensor.

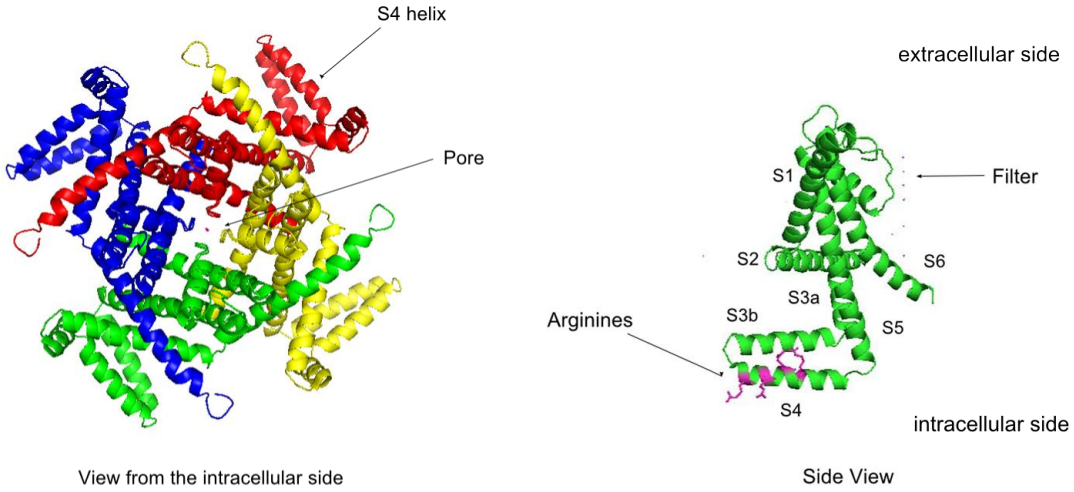


Figure 1.5: Crystal structure of K_vAP as published in 2003, without the Fab fragments. The protein was purified with decylmaltoside and *n*-octyl-β-glucoside detergents. The left image represents a view from the intracellular side. Each monomer has a different colour. The right image shows a monomer with the annotated transmembrane α-helices. The four arginine residues are represented in magenta colour. PDB: 1ORQ.

In another article from the same group, the authors convincingly proved that the gating properties of K_vAP are similar to the eukaryotic K_v (83). These studies compared sequence alignements, toxin studies targeting both the filter and the voltage domain, and showed that the channel is structurally similar to eukaryotic voltage-gated channels. Studies of the voltage-dependence of gating and determination of K^+ selectivity versus Na^+ both in (3/1) POPE/POPG (1-plamitoyl-2oleoyl-*sn*-glycero-3-phosphoethanolamine/1-plamitoyl-2 oleoyl-*sn*-glycero-3-phospho-(1'-*rac*-glycerol)) at room temperature also demonstrated that K_vAP is functionally similar to eukary-

otic K_v channels. However, this x-ray structure came as a shock to the field, because it contradicted most existing models of how voltage-gated potassium channels actually work.

1.8 The conventional model

Over 20 years of previous studies on K_v channels had concluded that the voltage sensor domain is tightly packed, with the S4 helix sitting in the middle, isolated from the hydrophobic core and perpendicular to the plane of the membrane. Aqueous vestibules located along S4 were thought to insulate the positively charged amino acids from the rest of its surrounding (46). Upon depolarisation, the S4 helix is thought to move outwards (towards the extracellular region of the bilayer) by less than 15 Å, while the rest of the voltage-sensing domain sits in the membrane (Figure 1.6). The S4 helix was thought to move by tilting, rotation or axial translation according to the different variations of the conventional model. The presence and the movement of charges in a low dielectric medium is energetically costly. Therefore solvation of the majority of S4 charges and stabilising interactions with negative charges in the pore domain have the effect of decreasing this energetic cost and allow a minimal contact between the gating charges and their hydrophobic surroundings (4).

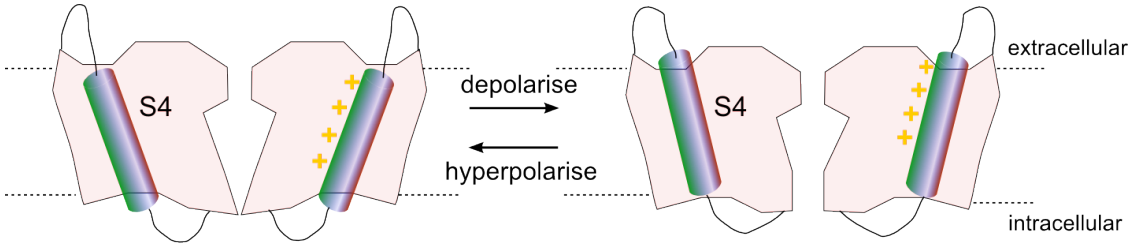


Figure 1.6: Conventional model of voltage-sensing. The S4 helix is surrounded by the rest of the channel and is perpendicular to the membrane plane. This α-helix moves outwards upon depolarisation.

1.9 The paddle model

The paddle model was proposed by the MacKinnon group after the K_vAP x-ray structure was published. In this structure, none of the α-helices are normal to the membrane plane and the S3 helix is divided into two segments, a and b, separated by a loop. The S3b and S4 α-helices form a rigid structure, helix-turn-helix, central to the voltage detection, and placed almost isolated to the voltage-sensor domain. Most significantly however, the first four arginines are exposed to the lipid bilayer (117, 120, 123, 126) and the fifth one is thought to make a salt bridge with an aspartate on S2. This "paddle" was proposed to undergo a large movement in the membrane upon depolarisation, more than 20 Å, spanning the lipid bilayer (Figure 1.7). But the model also requires these gating charges to be in direct contact with the hydrophobic core of the membrane, which is energetically unfavourable.

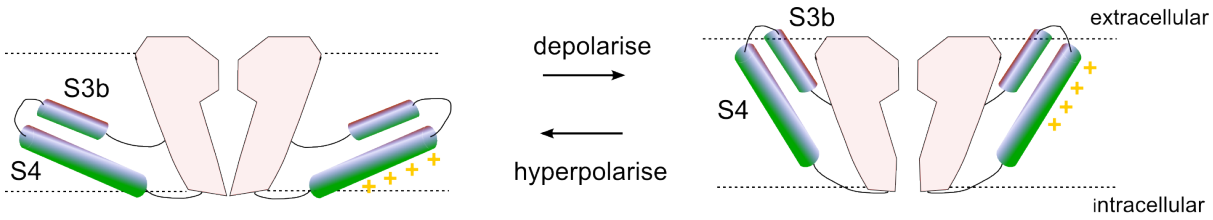


Figure 1.7: Paddle model of voltage-sensing. The S3b and S4 helices are located outward of the channel, quite in contact with the hydrophobic surrounding. Upon depolarisation, the "paddle" travels outwards in the membrane by a large extent.

1.10 Controversies

Many experiments carried out on voltage-gated potassium channels contradicted this paddle model. Hydrophilic probes such as antibodies (49), hydrophilic cysteine reagents (35) and toxins targeting extracellular loops (57) all favoured the conventional model, in which all α-helices are normal to the membrane.

The accessibility of the S4 segment was probed by examining the reactivity of mutated cysteines with methanethiosulfonate (MTS) reagents (35). Because of the charged nature of the MTS compound, it cannot enter the lipid core of the membrane. Moreover, the thiol functional group should be protonated in a hydrophobic medium. Therefore the reaction should only occur in a hydrophilic environment which has been interpreted as aqueous vestibules surronding the S4 helix. These data contradict the paddle model where S4 is embedded in lipids and where it would be inaccessible to MTS reagents.

The major difference between these models lies in the location and the movement of the paddle sensor (the helix-turn-helix S3b-S4). The paddle model places this unit on the intracellular side which undergoes a large outward movement at depolarized

voltage. On the other hand, the paddle motif permanently lies close to the extracellular surface. Data from both eukaryotic channels and K_vAP appear to contradict each other. For example, toxin studies on K_v2.1 (an eukaryotic channel) binds on the S3b-S4 loop both at depolarised and hyperpolarised voltage (57). Two studies performed on a voltage-gated Na^+ channel and the Shaker K^+ channel, where cysteines were mutated on the S3b helix show very little change of reactivity with voltage change (37, 73).

By contrast, the VSTx toxin (tarantula venom toxin) and an antibody only bind to the extracellular side of the voltage sensor domain at depolarised voltages.

In other studies (50, 84), the accessibility of K_vAP segments to a tethered biotin was tested. Avidin is a bulky hydrophilic protein (diameter >100 Å), which cannot penetrate the inside of the membrane. Attached to it, a tethered biotin which can enter the bilayer and react with a cysteine carried by the channel to lock it in a definitive position. However, the reaction depends on the accessibility of the tethered biotin to the cysteine, and can be probed from both sides of the membrane. The voltage and the length of the tether were varied between experiments to assess the translational movement of the helices inside the membrane. The results showed that the S4 helix underwent a large (15-20 Å) movement in the membrane, which was interpreted as supporting the paddle model.

But despite this evidence, the modified paddle model still did not explain the energetic cost of moving 5 positive charges within the hydrophobic core of the membrane.

In 2005, a second voltage-gated K^+ channel (K_v 1.2) was crystallized at 2.9 $\mathring{A}$ resolution, (62). This channel comes from the same family as the Shaker channel, and was coproduced and cocrystallised with an accessory β2 subunit. However, in

this structure the S3b-S4 helices are located closer to the voltage-sensing domain than in the K_vAP structure and perpendicular to the plane of the membrane. Despite being nearly two helical turns longer, and therefore more flexible, the voltage paddle's position in the membrane is more consistent with the experimental data and is considered the one that the protein adopts in the membrane (62).

Interestingly, a recent paper has presented a radically new conformation of K_vAP, that is different to all previous structures presented to date (91). The structure analysed by 2D electron crystallography (resolution up to 6.5-7 $\mathring{A}$) shows the voltage-sensor domains forming a concentrating ring around the central pore of the channel. The authors concluded that the conformation adopted by the channel is the physiological inactivated state. However, less than two months after its publication, the structure was retracted due to mistakes in the analysis of the protein density and incorrect indexing of cell parameters.

1.11 Modular voltage-sensor domain

The voltage sensor domain is composed of four α-helices and can form a domain by itself in the membrane. Interestingly, this voltage sensitive domain has been identified in two non-classical membrane proteins in eukaryotes (Figure 1.8). A voltage-sensitve phosphatase (Ci-VSP), from *Ciona intestinalis* has been discovered in transparent sea squirt. This enzyme is formed of two parts, a catalytic cytosolic domain and the S1-S4 embedded in the membrane which controls the hydrolysis of phosphoinositides (71), (53). It is the first enzyme identified which is controlled by membrane voltage. It is thought to function as a monomer and the catalytic activity of the protein is determined by the voltage-sensitive part (Figure 1.8 right).

The voltage activated proton channel H_v1 is also composed of two voltage-sensor domain-like proteins. This channel was first identified in snail neurons and the proton pathway appears to be internal to the voltage-sensing domain itself (Figure 1.8 in the middle). The general hypothesis is that protons move through the pore in the channel-depolarised state. In other voltage-gated cation channels, this voltage-sensor domain pathway does not exist and appears to be blocked. However, when internal residues are mutated within the voltage-sensor domain, the pathway can open up again to form the so-called gating pore pathway or Omega (Ω) current.

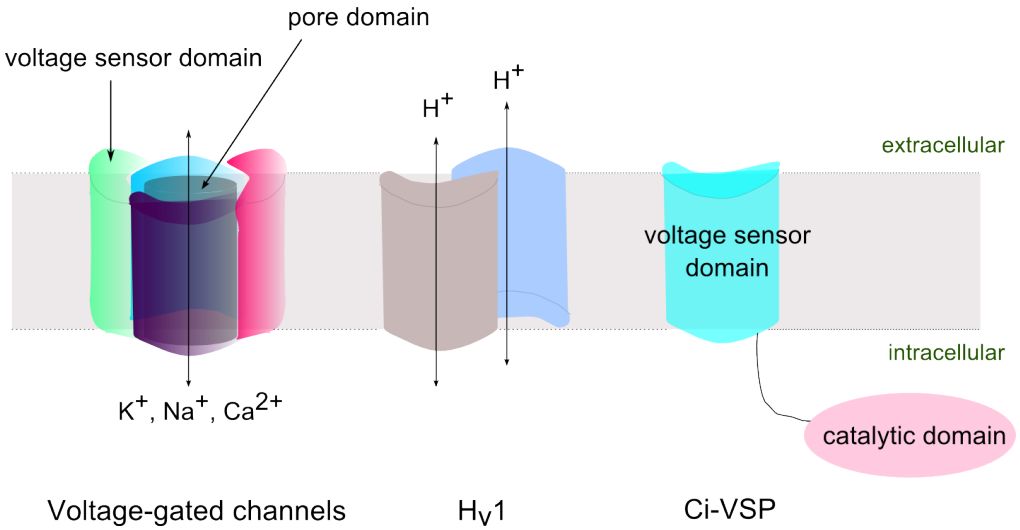


Figure 1.8: Modular nature of the voltage sensing domain. The voltage-gated channel is shown on the left as a tetramer with the conduction pore situated in the middle of the protein. In the middle, H_v1 is represented, functional as a dimer, with two conduction pathways. On the right, the Ci-VSP phosphatase is shown as a cartoon, with its separated membrane one and the cytoplasmic catalytic domains.

1.12 Lipid regulation of K_vAP

Lipids interact closely with membrane proteins, and ion channels are no exception. They are often present until the final stage of the purification process or are added during biochemical process for stability reasons, as can be seen in membrane proteins structure resolved by x-ray. For example, in the K_v2.1 crystallographic structure, lipids were found intercalated between helices, the pore domain and the voltage sensing domains, and even between adjacent subunits(63).

K_vAP is found in an archaebacterium that lives at high temperatures (95°C). It is thought that the typical membrane lipid composition of *E. coli* is best mimicked by a mixture 3 to 1 of POPE (1-plamitoyl-2oleoyl-*sn*-glycero-3-phosphoethanolamine) and POPG (1-plamitoyl-2 oleoyl-*sn*-glycero-3-phospho-(1'-*rac*-glycerol)). However, the lipid composition of extremophile archaea, due to its high diversity and complexity, is still under debate (1). For example, unusual lipids, such as glycerol-ether lipids (instead of glycerol-esther lipids among eukaryotes and bacteria organisms), side-branches hydrocarbonchain, or bolaamphiphiles (an hydrophobic chain endowed with two hydrophilic heads) are found in these extremophiles organisms.

K_vAP was first characterized in (3:1) POPE:POPG; and all the subsequent studies have used this lipid composition as a standard reference for macroscopic and single channel electrical traces, (83). These two phospholipids are quite similar: they both have the same length of fatty acid with a single double bond but carry a different functional group: POPE carries a positively charged primary amine and POPG carries two alcohol groups.

One of the first articles to thoroughly study the effect of lipids on K_vAP was published in 2006. This article focused on the interaction of K_vAP with differ-

ent types of lipids and their impact on macroscopic channel gating properties (88). This study identified a crucial role for phospholipids in K_vAP function. When the channel was surrounded by DOTAP (1,2-dioleoyl-3-trimethylammoniumpropane), a non-phospholipid, K_vAP lost all functionality, but when the types of phospholipids were varied, its gating properties could be modulated. The presence of the negatively charged phosphate group seemed to be a key factor in the channel's ability to respond to a change in transmembrane voltage. It was thought that the negative charge of the lipids directly interacts with the arginine residues, helping to stabilize the "open state" under depolarisation.

Furthermore this study presented some interesting results with cholesterol. K_vAP appeared to lose function when cholesterol was present. Even at low concentration (10%), this molecule appears to disturb the packing of both headgroups and acyl chains preventing K_vAP to respond to changes in transmembrane voltage. This finding was quite surprising since the prokaryotic channel is a good homologue of eukaryotic ones and cholesterol is found in the native membrane environment of eukaryotic cells. However, eukaryotic channels might have evolved to cope better with the presence of cholesterol in their surroundings and therefore its effect on prokaryotic channels may be much stronger than on eukaryotic ones.

1.13 Toxins

Toxins are small compact peptides (8 to 70 amino acids) present in the venomous ducts of snakes, spiders, sea anemone and marine snails. These poisonous creatures inject a cocktail of toxin peptides in their prey's blood to immobilise them and devour them at leisure. Among the injected components, many toxins target voltage-gated

potassium channels. By inactivating K_v channels, electrical signaling becomes disrupted, thereby paralysing, or even killing the victim.

Toxins targeting voltage-gated potassium channels are divided into two classes according to their modes of action: pore-blocker toxins and voltage-sensor toxins. Pore-blocker toxins act by association with the pore's entry on the extracellular site, permanently blocking the potassium ions' flow. Voltage-sensor toxins target the voltage-sensors domains of potassium channels, by binding to them. It is thought that the binding of toxin to a single voltage-gated domain is enough to prevent the channel from opening (stoichiometry of 1 to 4) (94). Hanatoxin and VSTX1 from tarantula spider venom are two toxins that target the voltage-sensor part of potassium channels and trap the voltage-sensor domain in the resting state (K_d in the range of 10-100 nM range) (58, 67).

The toxin studies complement the work on ion channels. Along with ligands, antidepressants, anesthesics, toxins exert a direct effect on the function of the channel through binding. Toxins help to identify structural motifs and key residues important for voltage-gated potassium channels. Likewise, channels have also been used to screen for pharmaceutical compounds in venoms. Once purified, these newly discovered substances can be studied and used as therapeutic agents. For example, procoagulants and anticoagulants found in venoms can be used to correct clotting problems. Hannalgesin, a toxin present in king cobra venom, can be used as an analgesic in small quantities (52).

1.14 Droplet interface bilayers (DIB)

Our current understanding and knowledge about ion channels has only become possible thanks to the advanced biological and electrophysiological methods available to study this functional properties. Hodgkin and Huxley first recorded ionic current from the giant axon of the squid. Since then our comprehension and grasp of this class of membrane proteins has grown remarkably due to development of experimental methods, such as the patch-clamping technique, the planar lipid bilayer and more recently in the Wallace laboratory, the droplet interface bilayers.

In 1972, Montal and Mueller published an article where they presented a new experimental procedure to study ion channels in a reconstituted environment (Figure 1.9) (69). A Teflon film separating two aqueous chambers is pierced in the middle (average hole diameter: 50-250 μm). The two chambers are filled with buffer carpeted by a lipid monolayer dissolved in an apolar solvent. The level of the two chambers is raised to create a bilayer (from the two monlayers) on the Teflon film. In order to diminish the tension of the newly formed bilayer at the edge of the hole, the Teflon film is pre-painted with hexadecane. A solution of ion channels reconstituted into vesicles is added to one chamber. If an osmotic gradient exists between both chambers, vesicles can then fuse with the bilayer, therefore incorporating channels to the bilayer. The current passing through the channel can then be controlled and measured by two electrodes present in both chambers.

This methodology was the first *in vitro* technique developed for the electrophysiological study of ion channels. One of the greatest advantages of this type of experimental procedure over *in vivo* methods is the control of the environmental components, such as the lipids, the salt concentration, but also the number of channels in the

bilayer, which allows the experimenter to perform single channel recordings (difficult to achieve by the patch-clamp technique). Unfortunately, the bilayer is quite fragile due to the annulus instability which makes the experiment more difficult and short lived.

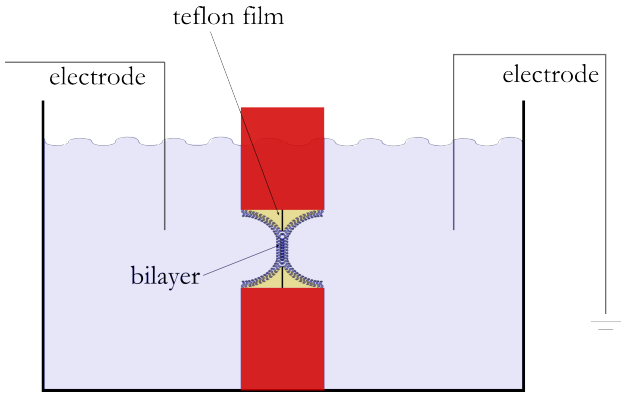


Figure 1.9: Planar Lipid Blayer. Both chambers (cis and trans) are separated by a Teflon film pierced in the middle. A lipid bilayer is formed on the hole allowing the transport of ions from one chamber to the other one, if at least one ion channel is inserted in it. Two electrodes record the current passing through the bilayer. By convention, the channels are inserted on the side of the recording electrode called the "cis" side while the ground electrode side is called the "trans" side.

In 2005, a new method was developed to form bilayers between two aqueous droplets in a lipid in an oil mixture, the droplet interface bilayer (DIB) (Figure 1.10). This experimental procedure rapidly developed into a new way to study or screen membrane proteins including ion channels. Two aqueous droplets (with a volume being as low as 100 nl) are sunk in mixture of lipids in oil (squalene or hexadecane) which drives the formation of a monolayer around the droplet. If the two are brought in contact, a bilayer should form between them.

Similar to the Montal-Mueller approach, two electrodes inserted in the water phase can monitor and record the current passing between each droplet, if an ion channel is

inserted in the bilayer. Since the droplets are immersed in an incompressible liquid, hydrostatic shocks are minimised which also makes the system significantly more robust. Furthermore, a lipid reservoir can constantly supply the bilayer, avoiding lipid loss in the aqueous phase and reduction of the bilayer, like in the planar lipid bilayer method. The lifetime of the DIB is thus greatly extended compared to the Montal-Mueller approach, and bilayers can last for days or weeks compared to hours/minutes for the more traditional approaches to bilayer formation.

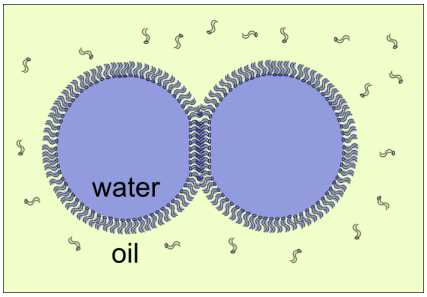


Figure 1.10: Droplet Interface Bilayer. Two aqueous droplets immersed in a lipid oil mixture are brought into contact to form a bilayer.

This procedure has given birth to a modified version of the DIB, by replacing one of the droplets with a hydrogel surface. The principle of bilayer formation is exactly the same, only the hydrogel surface has to be hydrophilic and offers a support for lipid monolayer self formation. The droplet is immersed in a lipid/oil solution and brought into contact with an agarose surface by gravity (Figure 1.11). This experimental setup has a high resistance (to 100 GΩ), can sustain a relatively large potential difference across the bilayer (around 150 mV). In addition, the bilayer capacitance can be measured and changed by manipulating the bilayer's area through upward or downward movements of the Ag/AgCl electrode which is inserted in the droplet (42).

Many different approaches have been used to study ion channel conformational

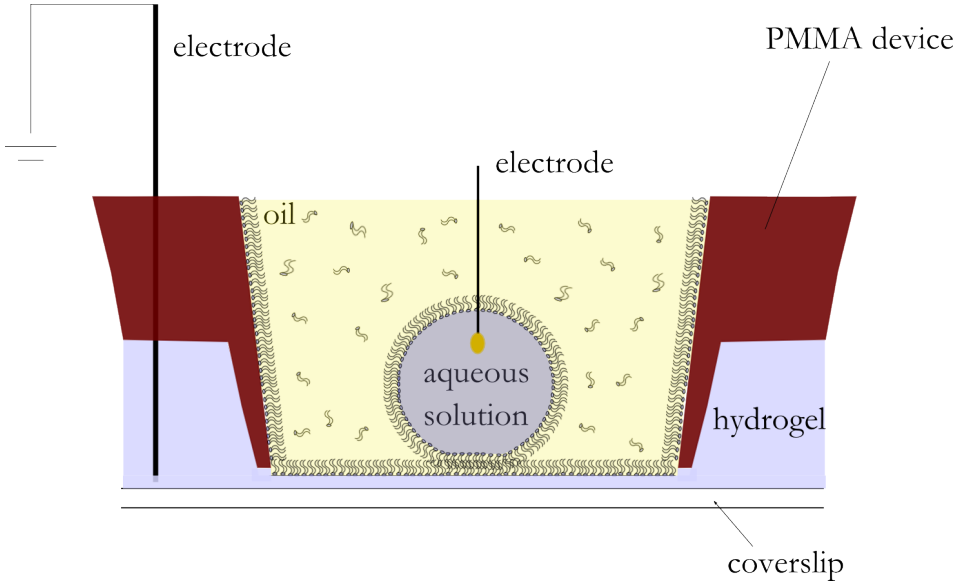


Figure 1.11: The Droplet Hydrogel Bilayer. An aqueous droplet immersed in a lipid/oil mixture in a PMMA device (polymethyl methacrylate) makes contact with a planar lipidic monolayer on top of an hydrogel. A bilayer is created between both media; and electrodes inserted on both sides can record the ions flowing from one side to the next one.

changes but fluorescence-based methods have often proven the most successful for the detection of dynamic changes (108), (14). One of the other major developments has been the ability to combine these measurements with simultaneous recording of channel electrical activity (64).

1.15 Ion channel single molecule fluorescence

Single molecule techniques use a different approach from ensemble measurements. Instead of measuring bulk properties of a large group of molecules, individual molecules are observed over a certain period of time. Thereby the distribution of a variant property rather than measuring an average is determined. This gives us more information on the system under study. For example, the observation of different intermediates

during an enzymatic cycles (107). Using this approach, we therefore gain access to information inaccessible by classical measurements, such as the characterisation of static and dynamic inhomogeneities, or the existence of heterogeneity in complex systems (51). Using single molecule methods, subpopulations can be assessed and kinetic pathways determined under the equilibrium condition. Moreover, comparison of single molecule results with computer simulation and theory is straightforward, as both are inherently molecular measurements (39).

1.15.1 The importance of the signal to noise ratio

A major obstacle to single molecule experiments is the detection of small signals from individual molecules over the background noise. Instruments and techniques with high precision and sensitivity are required.

Over the last few decades, fluorescence has become a popular choice for single molecule measurements. When a molecule absorbs a photon, it enters an electronically excited state. One way to release its energy is to emit a photon (fluorescence), after having lost a small amount of the excitation energy, due to relaxation. The excitation and emission spectra are characteristic of each molecule and their maxima are separated by the Stokes shift. In order to detect fluorescence, the emission light needs to be separated from the excitation one; the larger the Stokes shift, the easier this task. This configuration makes fluorescence spectroscopy highly sensitive (around 1000 times greater than absorption). Nevertheless, the amplification provided by fluorescence alone is not enough to exceed the crucial signal to noise ratio for single molecule experiments.

All the single-molecule fluorescence techniques which have emerged over the last decades focus on the reduction of the fluorescence background. One of the most

obvious way of doing this is to simply minimise the background signal by reducing the excitation volume.

1.15.2 Total internal reflection fluorescence (TIRF)

TIRF principle is based on Snell's law which describes the light path between two media, of different index of refration. The incoming light gets split into two light beams, the transmitted light and the reflected light. The angle of the incident light and the indices of refraction determine the angle of the transmitted light.

$$n_1 \sin(\theta_1) = n_2 \sin(\theta_2) \tag{1.2}$$

- n_1: Refractive index of medium 1 [-]
- n_1: Refractive index of medium 2 [-]
- θ: Angle from the normal to the interface to the boundary [°]

If the angle of the incoming light is greater than a critical angle, typically 90° (depending on two refractive indices), the light is reflected and total internal reflection is achieved (Figure 1.12). A small component of the reflected light is present within the lower refractive index medium and produces an evanescent wave of the same frequency as the incoming light. This evanescent wave creates an electromagnetic field, whose intensity decays exponentially with increasing distance from the interface. For a glass/air interface, this electromagnetic field decay is approximately 150 nm. This exponential decay results in excitation volume reduction.

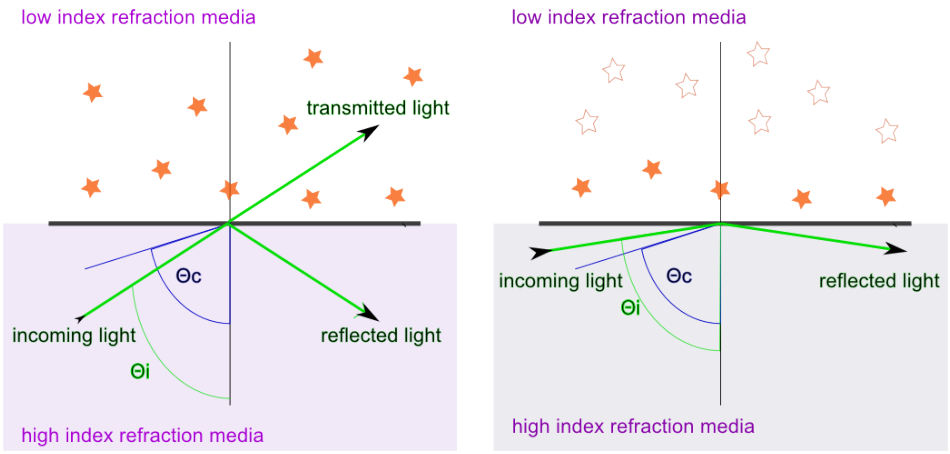


Figure 1.12: TIRF phenomenon. If the angle of the incoming light is under the critical angle value, the light is reflected and transmitted at the interface. If the incoming light exceeds this value, an electromagnetic field is created in the low index refraction media, typically 1-150 nm.

Two microscope configurations exist: prism-based TIRF, and objective based TIRF. In the first setup, a prism is used to direct the incoming light to the sample. Fluorescence is collected by an objective placed under the sample, while the reflected light passes through the prism.

The second configuration requires an objective with a high numerical aperture. The laser beam is focused on the back focal plane of the objective at a position which allows the light to reach the surface above the critical angle. Both the fluorescence of the sample and the reflected beam are collected through the same objective. The separation of the emission and excitation light is more difficult than with the prism-based TIRF. However, the second technique is better when one wants to look at thicker samples than the prism based technique, since the evanescent wave is generated on the same side than the objective (where the fluorescence light is collected). Additionally, collecting photons is more efficient within the high index material than through the low index one (6). Finally, it is easier to couple this configuration with

another technique because of free access of the sample on the opposite side of the objective.

1.16 Previous fluorescence studies on ion channels

The simultaneous measurement of ion channel electrical current and conformational movement of the voltage sensing domain has been performed at the macroscopic level using voltage-clamp fluorometry (18, 19, 20, 36, 41, 64). Fluorophores used as molecular sensors are attached to the moving part of ion channels reporting real-time structural changes, which are correlated with changes in channels function via simultaneous electrical recording. However, it remains challenging to do this at the single molecule level.

Only recently fluorescence techniques have been applied to the study of ion channels. In 1996, the first article was published investigating the conformation change of the helix S4 labelled with tetramethylrhodamine maleimide (TMRM) of the Shaker channel produced in oocytes (64). Since then, the techniques and the fields of investigations have expanded. Work is now done using confocal microscopy (66), voltage-clamp fluorimetry (36), TIRF (14), various fluorescent reporters are used such as dyes of fluorescent proteins like EGFP, in different systems including oocytes, cells or reconstituted systems.

In 2002, the Romano-Silva group reported the visualization and tracking of sodium channels in live cells using confocal microscopy and fluorescently labelled toxins (66). Groups have studed the voltage gating mechanism in K^+ channels by combining oocyte recording with fluorescence measurements. The studies have always been carried at the ensemble level, using TMRM as a fluorescent reporter, while the cur-

rent was recorded in response to voltage changes (18, 36). Unfortunately, ensemble-averaged measurements only report a raw change of fluorescence without any detailed information, such as the stoichiometry of the channel or which part of the S4 helix undergoes the largest movement inside the membrane.

Many other channels and transporters have been studied using combined fluorescence-electrophysiological methods, including TREK channel, and the eag K^+ channel (10, 85).

Most of the fluorescence-electrophysiological studies used oocytes and the voltage-clamp technique. Very few have used reconstituted bilayers systems; although one of them has examined the cooperativity of KcsA (14) which use labelled KcsA with TMRM and Atto 565 maleimide in supported bilayers.

1.16.1 Fluorescence tracking experiments

Most of the single molecule tracking experiments on voltage-gated potassium channels have been done in living cells, neurons, or synapses. The preferred labelling methodology for tracking uses quantum dots. BKCa and K_v10.1 channels are two of the few which have been studied *in vivo* (102, 103). In both cases, the ion channel of interest was produced in established cell lines and a fluorescent tag was attached to the protein. The channels demonstrated different classess of 2D motions dependent on the environmental conditions, the expression system and their subcellular location. For example, when BKCa channel is produced in COS-7 cells, it exhibits a confined diffusion. When the same channel is produced in neurons, its diffusion behaviour changes depending on its location: in somata, its coefficient diffusion is 36-fold lower than in axodendrites and 11 times lower than in COS-7 cells.

In a similar way, K_vAP has been used as a model of membrane protein mobility in

planar and tubular bilayers (30). Fluorescent quantum dots were attached through a PEG linker to the channel and its 2D diffusion behavior was compared with the ones experienced by lipids in GUVs (giant unilamellar vesicles). The radius of the vesicles was varied with a micropipette. For both the lipid and K_vAP, the diffusion was found to decrease with the radius of the tubular bilayer by a factor of 5 for the ion channel. The protein seems to reach a diffusion coefficient maximum on flat surface. The reported diffusion coefficient in planar lipid is 3.3 $\mu m^2/s$ in (9/1) EPC (egg phosphatidylcholine)/EPA (egg phosphatidic acid), a value much higher than ion channels reported mobility in cells (D_{lat} =0.033 $\mu m^2/s$ for BK channel in COS-7, D_{lat} of K_v10.1 channels in neurons and synapses varies between 0.008 and 2 $\mu m^2/s$). Obviously, the environmental conditions and the membrane composition are quite different between *in vivo* and*in vitro* systems and the presence of the cytoskeleton is likely to affect the motion behavior of membrane proteins and lipids within the membrane.

1.16.2 Subunit stoichiometry

The counting of photobleaching steps has been used recently to quantify a channel stoichiometry: the first paper which described the methodology was published in 2007 (100). The ion channel under interest was genetically fused with GFP (green fluorescent protein) and produced in *Xenopus laevis* oocytes. The membranes are then ruptured and imaged on coverslips by TIRF. Through careful control of the ion channel expression, individual fluorescent spots can be resolved. Constant illumination of the coverslip surface causes photobleaching of the GFP. Therefore by counting the number of photobleaching steps coming from an individual fluorescent spot, the number of subunits carrying a fluorescent reporter can be revealed. One of

the main advantages of the methodology is that the analysis of the ion channels can be performed directly at the membrane, after expression. This approach is therefore particularly useful for heterogenous ion channels which have ambiguous stoichiometry. Different populations of ion channels can be uncovered, dimerization/recruitement of auxiliary units in signaling processes can be studied. Many different multisubunit channel types have been studied using this approach: Mpiezo, HCN, NMDA receptors and even H_v1 channels have been investigated with this method subsequently (9, 26, 28, 99, 100).

However, this method is more reliable to the study of channels with a maximum of 5 subunits, since the distribution of bleaching steps start to become indistinguishable and the assessment of the number of subunits more difficult (100).

1.16.3 FRET

Fluorescence resonance energy transfer (FRET) is a phenomenon using two distinct dyes as distance reporter. If the two dyes are spatially close enough and the donor is in its excited state, a radiationless transfer of energy can occur between the donor and the acceptor and the acceptor fluorescenses. The energy transfer depends on the spectral overlap between the donor emission and the acceptor absorption spectra, the dipole moment orientation between the two fluorophores and their separation distance, following the relation $1/R^6$. If the donor and the acceptor come close together [1-10 nm] the fluorescence emission of the acceptor will increase due to the FRET, through excitation of the donor. However, the dipole orientation dependence means that each fluorescent tag must move relatively freely in their environments as well. The FRET technique is extremely useful for detecting protein interactions or probe intermolecular movements.

Gramicidin ion channels have been successfully investigated using FRET, and in addition the fluorescence readout has been coupled with electrical recordings. Single ion channel currents were recorded along with the FRET signal arising from Cy3 and Cy5 dyes (15). The diffusion coefficient of the channel was measured with detection of homodimers and heterodimers via FRET. The conformations of labelled gramicidin were also measured in a patch-clamp micropipette through FRET and fluorescence self-quenching with single channel currents recordings, demonstrating a correlation between the closed/open states of the channels and its conformation changes (44).

1.17 Overall aim of this thesis

Given the apparent controversy over the proposed movements of the voltage sensor domain and the mechanism by which these movements couple to opening of the channel, the overall aim of this thesis was to perform simultaneous electrical and fluorescent measurements of the K_vAP potassium channel at the single molecule level.

Such measurements might enable us to dissect the electromechanical coupling of the voltage sensing domain to the pore domain in this tetrameric channel with a level of precision not possible using more conventional macroscopic approaches. Correlating simultaneous electrical and fluorescence signals at this low scale represents a technical challenge in itself. But moreover, this level of analysis can let us unravel the link between activation/deactivation through voltage and the K^+ flux in this important class of ion channels. This process, central to life, remains unclear and new investigations would allow us to shed a new light on those questions.

In this regard, the aim was to exploit the single molecule fluorescence detection

methods developed in the Wallace lab which combine single channel recording in droplets with TIRF.

Chapter 2

Development of an Protein Production, Purification and Fluorescent Labelling Strategy for K_vAP-CL

2.1 Introduction

2.1.1 Aim

This chapter describes the expression, purification, labelling and reconstitution of different mutants of K_vAP-CL. Following purification, ion channel function was tested at the single molecule level, using planar lipid bilayers. Cysteine mutants of the protein were generated and labelled with the fluorescent dye tetramethylrhodamine-5-maleimide (TMR5M).

2.1.2 K_vAP-CL

K_vAP-CL (K_vAP-C247S) was chosen as our model system to study the voltage-gated potassium channels. Despite having been isolated from a prokaryotic organism, it possesses similar gating properties to eukaryotic channels, and thereby repesents an archetypal voltage-gated potassium channel (83). It is also one of the few voltage-gated potassium channels whose three dimensional structure has been resolved at the atomic scale, thus allowing an accurate interpretation of its structural mechanisms and enabling a more rational choice of labelling site to be informed by this structure (49).

Furthermore, although it would be possible to do these experiments with produced/purified eukaryotic K_v1.2 channels, prokaryotic channels are more robust than eukaryotic channels, therefore making development of this method easier than using eukaryotic channels (2).

In order to achieve this aim, we can exploit a recent study investigating the position of S3b-S4 helices, both in the closed and open states of the pore (84). These experiments were based on the reaction between a biotinylated cysteine residue and a tethered avidin. Mutations on S3b-S4 (residues 101 to 127) to cysteine residues were generated and channels produced, purified and reconstituted into lipid vesicles. In a planar lipid bilayer experiment, following fusion of proteoliposomes with the bilayer, their function was tested after having been in contact with biotin, by exposing them to diverse length tethered avidin reagents, capable of penetrating into the lipid bilayer core. If the cysteine could move in the bilayer during the activation/deactivation in proximity to the biotin, a covalent bond might form and the S3b-S4 voltage paddle would be permanently locked in this position. The range at which the biotin can

penetrate into the bilayer is controlled both by the tether length (varied from 1 $\mathring{A}$ to 17 $\mathring{A}$) and the avidin, which is too large and hydrophilic to enter the lipid bilayer. The investigation could assess the range of motions of the voltage sensor inside the bilayer, 15-20 $\mathring{A}$, and identify residues that are particulary mobile.

However, this study does not take into account clefts, thinnings, surface irregularities of the lipid bilayer in proximity of the channel, which will affect the membrane diameter. Furthermore, the tether length is unlikely to penetrate the lipid core fully straight, but may bend or wring while it moves around secondary structures, especially due to thermal motions. Finally, it also may unspecifically interact with other parts of the ion channel (particulary at high concentrations), hindering the α-helices range of motion during activation/deactivation. In conclusion, the study offers valuable guidelines to identify residues with a large range of motion, but its motion accuracy in the lipid core (especially at the $\mathring{A}$ level) may be compromised by the above effects.

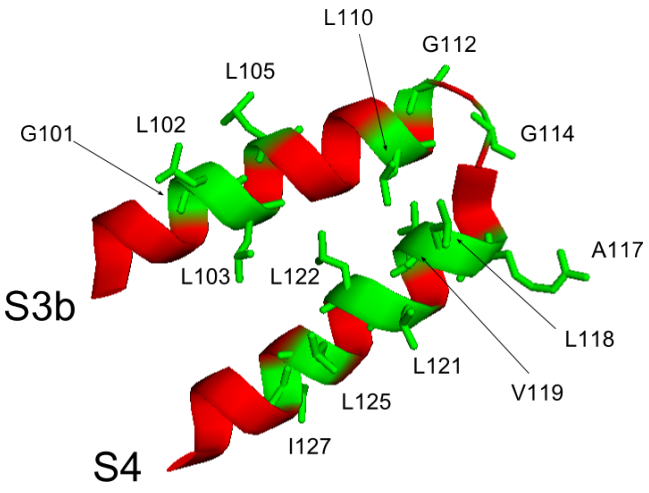


Figure 2.1: Voltage-paddle sensor of K_vAP-CL (S3b-S4 helices) with the residues in green which were mutated to cysteines in (84). All the mutants were functional proteins.

2.1.3 Choice of labelling site

The optimization of the production and expression of K_vAP, was carried out on K_vAP-CL, (K_vAP-C247S) from which the endogenous cysteine has been removed. This serves as the background channel on which all the cysteine mutants will be constructed. Furthermore, it constitutes a negative control for the fluorescence detection. A previous study was used as a guideline for the choice of the mutations site (84). The experiments were done on K_vAP(B13)-CL and mutations were introduced all along the voltage-sensor to study its movement upon depolarisation/hyperpolarisation (Figure 2.1). The functionality of the protein was established through macroscopic electrical measurements in oocytes. According to the article (84), the L121C and L122C residues are the most mobile (both accessible to avidin on both sides at 10 Å), followed by L125C, I127C, L118C and V119C (all on the S4 helix). Despite the high mobility of the loop, its residues as well as the ones located on the S3b helix are only accessible from the extracellular side. One curious fact is that at every length of the biotin, the accessibility results for each residue are the same on both spatial conformations. This suggests that the voltage sensor paddle travels in the lipidic bilayer as a fixed unit, without any changes of secondary conformation.

Another article published 5 years later, which deconstructs the voltage sensor of the Shaker channel, brings a new light on the structure of the unit, especially on the necessary components for the detection of the transmembrane voltage (105). The paddle comprises a large modulatory part and a smaller core structure. The intercalation of two hydrophobic amino acids between the charged arginines is an essential feature for voltage detection. This new result questions the ion channel functionality of mutating some of the intercalated hydrophobic residues on K_vAP-CL

(L118C, V119C, L121C, L122C, L125C) into cysteines. Nonetheless, the publication demonstrates that changing all hydrophobic amino acids alters the voltage detection. Moreover, this study shows that the ion channel conserves its functionality for every mutated cysteine. Because we did not want to alter the ability of the ion channel to detect the transmembrane voltage, none of the voltage-sensor arginine residues (117, 120, 123, 126) were mutated.

A control was also chosen at position 59 on the S2 helix, close to the extracellular side. This region is not predicted to undergo a large movement during the gating process. It is further away to be kept out of the coupling mechanism and should remain in the lipid core, experiencing a minimal environmental change upon voltage change.

2.1.4 Methodology

The protein was produced and purified according to standard protocols and methods from the MacKinnon group with some modifications (83). The channel was first produced in *E. coli* cells, before undergoing a multi-steps purification process (Figure 2.2). Labelling with a fluorescent dye was performed at the last stage before the reconstitution of the ion channel in POPE/POPG (1-plamitoyl-2oleoyl-*sn*-glycero-3-phosphoethanolamine)/ 1-palmitoyl-2 oleoyl-*sn*-glycero-3-phospho-(1'-*rac*-glycerol)) (3:1) lipid vesicles.

Reconstituting ion channels in lipid vesicles keeps them functional for long-term storage. They tend to precipitate while kept in detergent for a long time. Moreover, the presence of detergents affects bilayer stability. Thus, working in a detergent-free environment for electrical recordings experiments enhances the lipid bilayer lifetime and avoids mistaking electrical openings caused by detergent for single channel states.

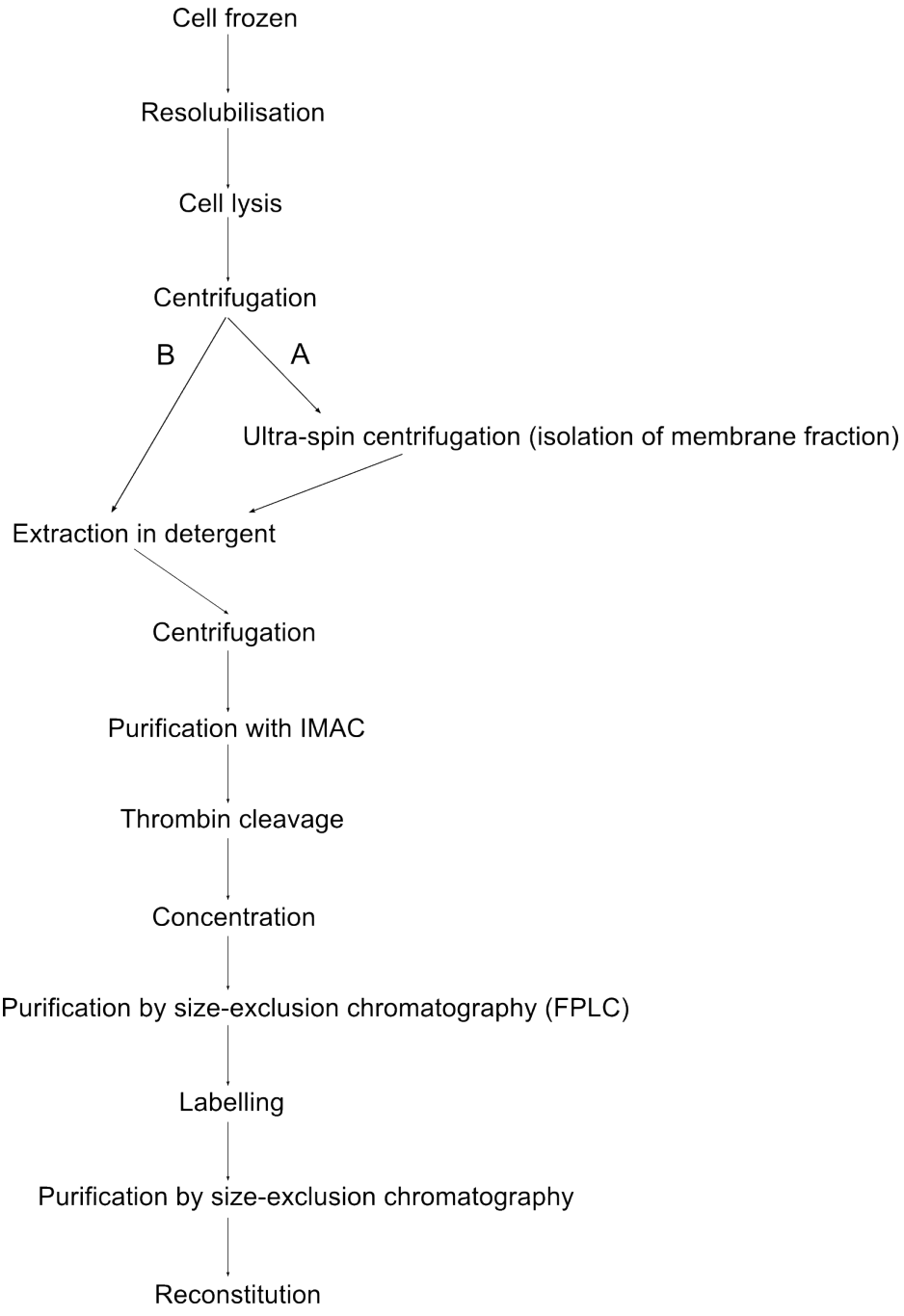


Figure 2.2: Brief outline of the K_vAP-CL purification protocol used in this study. The protein could be either directly extracted from the cell lysis (B path) or from the membrane fraction after an additional centrifugation (A path).

2.1.5 Affinity purification

A histidine tag, attached either on the N or the C-terminal of a protein of interest has high affinity for metal divalent cations (nickel, cobalt, copper) immobilized on a resin and allows for purification of the protein of interest quickly and efficiently. The protein is recovered by elution by a high concentration of imidazole (200-400 mM) or chelator (such as EDTA), or at low pH. Immobilized Metal Affinity Chromatography (IMAC) has now become a standardized purification procedure. Furthermore, anti-His tag antibodies have been developed and are used in different assays to detect the recombinant protein.

The TALON Metal Affinity Resin (Clontech) has been designed for the purification of proteins tagged with 6 histidines (Figure 2.3). The resin is stable under a large range of pH (2-14 for 2 hours) and can be used in batch or gravity flow mode. Its binding capacity is 5-15 mg protein/ml adsorbent.

2.1.6 Thrombin protease reaction

Thrombin is an endoprotease which recognises the amino acids sequence Leu-Val-Pro-Arg-Gly-Ser and cleaves between the Arginine and the Glycine residues with high affinity. This 6 amino acid sequence was inserted between the recombinant protein and the 6xHis tag.

2.1.7 Gel electrophoresis

SDS-PAGE (sodium dodecyl sulfate polyacrylamide gel electrophoresis) is one of the most common and significantly used analysis and separation methods of proteins in molecular biology. A mixture of proteins solubilised in the charged detergent SDS is

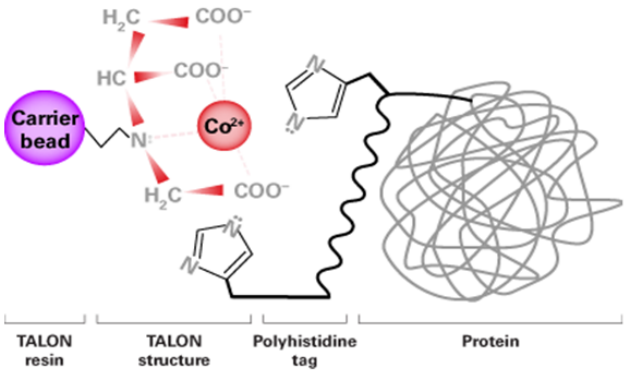


Figure 2.3: Schematic representation of IMAC. A protein with a 6xHistidine tag attached to it, retained by the TALON resin (image courtesy from Clontech).

run in a discontinuous electrophoretic gel/buffer system. Proteins migrate towards a positive electrode into the stacking gel first (4 % (w/v) of acrylamide/bisacrylamide) where they all enter the separating gel (4-12 % (w/v) of acrylamide/bisacrylamide) at the same time. The separation occurs according to the electrophoretic mobility of the proteins. The percentage of acrylamide used controls the pore size of the matrix, and hence the speed of progression through the gel. The SDS detergent (negatively charged) denatures proteins, by linearising them through binding. In consequence, the charge each protein carryies depends on the number of bound SDS molecules determined by the proteins length (and therefore its mass).

2.1.8 Blue native PAGE electrophoresis

Blue native-PAGE shares the same separation principle as SDS-PAGE. The main difference lies in the fact that proteins in SDS-PAGE gels have lost their native state,

due to the presence of denaturing conditions (SDS detergent, 2β-ME). Blue native-PAGE tries to retain the original secondary structure of the sample under analysis by using a charge-shift molecule, for example G-250. This technique allows us to preserve the oligomeric forms present in solution.

2.1.9 Western blot

Western Blotting is an analytical method used for the detection of specific proteins. It makes use of the protein separation in SDS-PAGE gels (1st step). The proteins are then transferred from the gel to a membrane (nitrocellulose or PVDF). The membrane is first incubated in a solution of BSA protein (bovine serum albumin) or milk powder, in order to block any unspecific sites on the membrane and reduce the background. A dilute solution of a primary antibody designed to recognise the protein under interest when exposed to it is incubated with the membrane. In this case, an antibody directed towards the 6xHis tag was used. A second solution of a secondary antibody is incubated with the membrane. The secondary antibody recognises the primary antibody and binds to it. Its purpose is to reveal itself, to allow the detection of the"secondary antibody-primary antibody-protein" complex. Different methods such as chemiluminescence, fluorescence, colorimetry, or radioactivity are then used to reveal binding of the antibody.

2.1.10 Size-exclusion chromatography

The separation principle is the same as other forms of chromatography: compounds are separated on their own affinities for two media. A mobile phase, the buffer media is passed through a stationary phase, a porous resin. Depending on the sample properties (polarity, size), some components will take a longer time to pass through

the porous resin. Components larger than the pores will be excluded and will pass through the matrix without entering it. Molecules of intermediate size will be able to partially penetrate the beads, while the smallest molecules will take the longest path inside the column and exit last (Figure 2.4). Thus, this technique can be used to separate the different oligomeric forms of a protein, by size-exclusion.

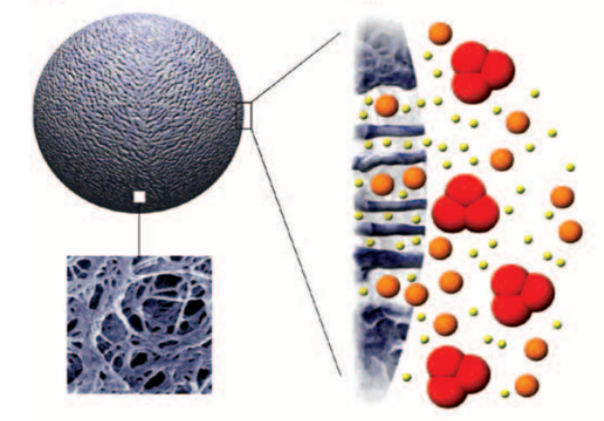


Figure 2.4: Size-exclusion principle. Schematic view of a bead with an electron microscopy enlargement picture. (image courtesy of GE Healthcare, Gel filtration principles and methods).

The size-exclusion column used in this work is the Superdex 200 10/300 (GE Healthcare). Its matrix is composed of spherical composite of cross-linked of agarose and dextran with an average particle size of 13 μm. The column material is stable at a large working range pH, (3 to 12) and possesses a good resistance towards most common buffers used in molecular biology liquid chromatography.

2.1.11 Labelling

A protein offers a large number of possible sites for chemical modification through labelling. Not all the side chains of the 20 standard amino acids will have the same reactivity under moderate aqueous conditions: the hydrophobic side-chains of Ala-

nine, Valine, Leucine, Isoleucine, Proline and Phenylalanine, the amides functions of Asparagine and Glutamine, the hydroxyls groups of Threonine and Serine show little reactivity. Tryptophan, Methionine, Tyrosine, Histidine, Arginine are either not useful, or have not been used for conjugation purposes. The functional groups carried by Lysine (amino group), Cysteine (thiol), and Aspartic acid, and Glutamic acid (carboxyl) are the most reactive under moderate aqueous conditions and therefore the majority of labelling reactions are directed towards them. Many factors need to be taken into account, when trying to tackle protein labelling: the buffer, the pH, the temperature, the reaction time, the label/protein ratio as well as the molar ratio of the species in solution. If a certain modification is expected at a certain label to protein ratio, diluting the protein species by a factor of 5 for example, and keeping the same ratio, will affect the reaction time. The modification will take place 25 times slower, but also other reactions, such as hydrolysis by example will dominate at this lower protein concentration (38).

Thiol chemistry allows high specificity of reactant and high reactivity of the functional group. Furthermore, cysteines are not so common as amino acids found in peptides, they are in most cases present at disulfides. For these reasons, cysteine modification is by far the most widespread method to carry selective labelling of proteins.

The labelling reaction presented in this work is a thiol (pKa= 8.2) alkylation with a maleimide reagent (Figure 2.5).

TMR5M (tetramethylrhodamine-5-maleimide) is a red-orange fluorescent conjugate which reacts with thiol functions with a high specificity under physiological conditions. It is photostable, pH-sensitive and soluble in DMF or DMSO (Figure 2.5).

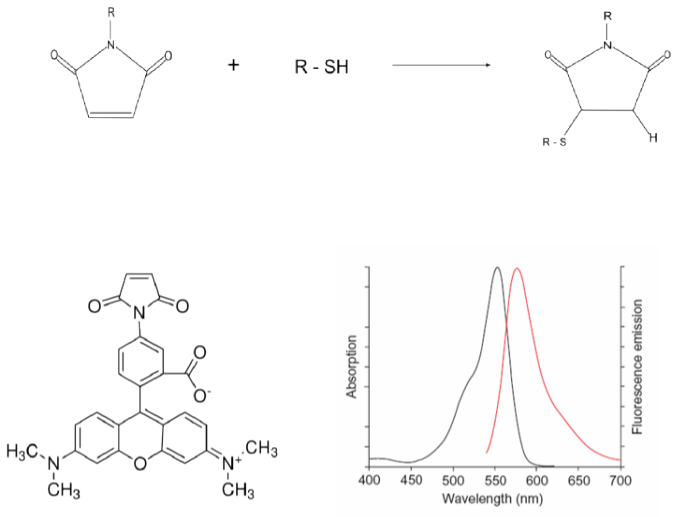


Figure 2.5: Thiol maleimide alkylation, chemical structure and spectrum of TMR5M (tetramethylrhodamine-5-maleimide). Absorption and emission spectra of TMR (tetramethylrhodamine) in 0.1 M phosphate buffer pH=7.0. The maximum λ_{ex} and λ_{em} are 543 nm and 575 nm respectively.

2.1.12 Dye/protein molar ratio

Due to the fluorescent dye absorption at λ_{280}, the protein concentration cannot be calculated by simply taking its absorbance measure at this wavelength. Instead, the formula below is used.

$$c_{prot} = \frac{A_{prot/dye}^{\lambda_{280}} - (A_{dye}^{\lambda_{max}} CF)}{\varepsilon_{prot} b} \tag{2.1}$$

- c_{prot}: Protein concentration [M]
- $A_{prot/dye}^{\lambda_{280}}$: Absorbance of the dye labeled protein at λ_{280} [-]

- $A_{dye}^{\lambda_{max}}$: Absorbance of the dye taken at its maximum emission λ [-]
- CF: Correction factor of the dye contribution to the $A_{prot/dye}^{\lambda_{280}}$
- ε_{prot}: Protein molar extinction coefficient [$M^{-1}cm^{-1}$]
- b: Path length [cm]

The degree of labelling is calculated by:

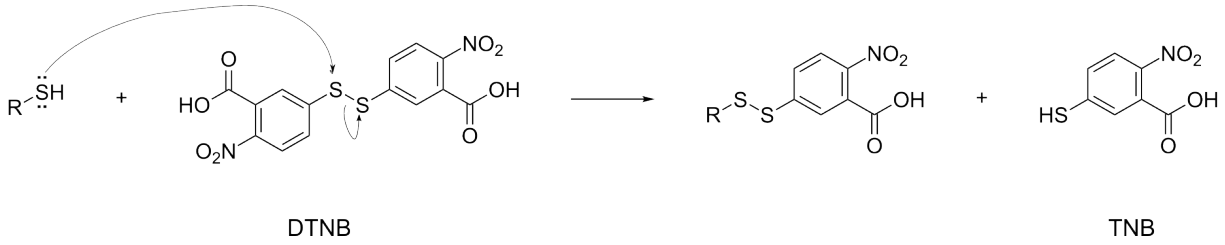
$$mol_{dye}/mol_{prot} = \frac{A_{prot/dye}^{\lambda_{max}}}{\varepsilon_{dye} c_{prot}} \tag{2.2}$$

- $A_{prot/dye}^{\lambda_{max}}$: Absorbance of the dye labeled protein at λ_{dye}^{max} [-]
- ε_{dye}: Dye molar extinction coefficient [$M^{-1}cm^{-1}$]
- c_{prot}: Protein concentration [M]

2.1.13 Ellman's reaction

The Ellman reaction is used to quantify free sulfhydryl groups in solution (32). A dye, DTNB, (5,5'-dithio-bis-(2-nitrobenzoic acid)) reacts with a free thiol group and produces a yellow-coloured dye, TNB (2-nitro-5-thiobenzoic acid), whose concentration is proportional to the amount of reacted sulfhydryls (Figure 2.6). The high molar extinction coefficient (14,150 M^{-1} cm^{-1}) and its stability at pH 7.6 to 8.6 makes it a good tool to work with biological samples.

The objective of this chapter is to express, purify K_vAP-CL mutants and to develop a labelling protocol. Different conditions at each stage of the procedure were



DTNB TNB

Figure 2.6: Reduction of Ellman's reagent (DTNB).

tested in order to optimise each step. The channel functionality was tested through recordings with PLB.

2.2 Material

2.2.1 Gene

The K_vAP gene is 890 bp long and carries a 6x Histidine tag (6xHis-tag) on the C-terminus. Two silent mutations were introduced on the wildtype gene of K_vAP in order to delete two endogenous *BamHI* restriction sites (K_vAP(ΔB13)) (see Appendix A.1, 178).

2.2.2 Vector

The K_vAP gene has been introduced in a modified version of the pQE-60 vector (Qiagen). The pQE-60 vector is a low-copy bacterial vector carrying ampicillin resistance. The pQE-60lac plasmid is an in-house derived vector with an additional lac repressor gene inserted in the backbone so as to control the expression of the target gene tightly (see Appendix A.2, 178). Previous work has suggested that the expression and the production of potassium channels in *E. coli* is toxic to the cell and requires tight

repressive control.

2.2.3 Strains

The porin-deficient expression strain *E. coli* PC2889E [BL21(DE3)ΔlamB ompR] was selected for the production of K_vAP-CL (K_vAP-C247S). This strain has been developed for the expression of porins, able to rescue the growth of porin-deficient bacteria.

2.2.4 Purification

- Resuspension Buffer: 20 mM Tris, 100 mM KCl pH 8.0.
- Column buffer : 5 mM DM (n-decyl-β-D-maltoside), 20 mM Tris, 100 mM KCl pH 8.0.

2.2.5 Western blot

- Incubation Buffer: 0.05% (m/v) TBST (Tris-buffered Saline Tween-20).

2.2.6 Reconstitution

- Buffer A: 10 mM HEPES, 150 mM KCl pH=7.0.

2.3 Methods

2.3.1 Site-directed mutagenesis

The mutations were made by Site-Directed Mutagenesis, using the Stratagene Quick-change kit according to the manufacturer's protocol. The PCR cycle used for the

reaction was: 95°C for 1 min, 95°C for 50 sec, 60°C for 50 sec, 68°C for 12 min, 68°C for 7 min, (for 25 cycles). Successful incorporation of each mutation was confirmed by sequence analysis.

2.3.2 Production

One single colony of *E. coli* PC2889E containing plasmid pQE60lac-K_vAP-CL was selected and used to inoculate a 1 L-flask containing 200 ml of LB media supplemented with carbenicillin (0.1 mg/ml). The preculture was incubated overnight at 37°C under 210 rpm agitation and used the next morning to inoculate a 2l-flask containing 500 ml of LB media supplemented with carbenicillin (0.1 mg/ml) to yield an OD_{600} of 0.1. When the culture reached an OD_{600} of 1.0, IPTG (isopropyl-β-D-thiogalactopyranoside) was added to an ending concentration of 0.4 mM to induce protein expression. The culture was harvested 4 hours after the induction by centrifugation (Beckman rotor JLA 8.1000). The cell pellet was stored frozen at -80°C.

2.3.3 Purification

Protein was purified following a previous method with minor modifications as described below (83). Briefly, the cell pellet was thoroughly resuspended in Resuspension buffer prior to lysis through a cell disrupter (Stansted Fluid Power, Model TC5W-0612-332) adjusted to 6.9 10^4 kPa. Immediately after resuspension, the cell slurry was centrifuged by low spin at 4000 rpm for 10 min at 4°C. The cell slurry was either directly used for resolubilisation or centrifuged again at 50 000 rpm, for 45 min at 4°C to isolate the membrane fraction. The cell slurry/ the membrane fraction was extracted in the above buffer supplemented with 40 mM DM (n-decyl-β-D-maltoside) and rotated at 20°C for three hours. The protein was extracted by IMAC using the

Talon Co^{2+} affinity resin (Clontech) and eluted with 400 mM imidazole following affinity purification. The hexahistidine sequence was cleaved overnight at 20°C by adding 1.0 units of thrombin per 3.0 mg of channel. The mixture was successively passed through a benzamidine-agarose (GE Healthcare) and Talon Co^{2+} (Clontech) affinity resins to remove both the enzyme and the uncleaved channel. The protein was then concentrated to 3.5 mg/ml and run on a Superdex 200 10/300 GL column at a flowrate of 0.3 ml/min in Column buffer. The fractions were collected and kept at 4°C for subsequent analysis or reconstitution.

2.3.4 SDS-PAGE

Samples taken during the purification were mixed with NuPAGE LDS Sample buffer (Invitrogen) supplemented with 4 mM DTT (dithiothreitol) in a 3 to 1 ratio. The mixture was incubated at 90°C for 2 min prior to loading to a NuPAGE 4-12% Bis-Tris Gel 1.0 mm x 15 well precast gel (Invitrogen). Electrophoresis was run at constant 180 V for 40 min in a MES running buffer. 5 μl of Novex Sharp Pre-Stained Protein Standards was used as molecular weight standard. To allow the visualisation of proteins, the gel was stained with Coomassie blue and destained according to the manufacturer's recommendations.

2.3.5 Blue native PAGE

Samples taken during the purification were mixed with the Native Page Sample buffer (Invitrogen) supplemented with 0.5 μl of Native Page 5% G250 in a 3 to 1 ratio. The mixture was loaded to a Native PAGE Novex 4-12% Bis-Tris Gel 1.0 mm x 10 well precast gel (Invitrogen). The electrophoresis was run at constant 150 V for 115 min in 1% Native PAGE Running Buffer. 3 μl of Native Mark Unstained Protein Standards

was used as molecular weight standard. To allow the visualisation of proteins, the gel was stained with Coomassie blue and destained according to the manufacturer's recommendations.

2.3.6 Western blot analysis

Proteins from a SDS-PAGE gel were electrotransferred to a PVDF membrane using an iBlot Gel Transfer Device (Invitrogen) for 9 min at 20 V. The PVDF membrane was soaked at °C in incubation buffer supplemented with 16.7% (w/v) dried milk powder and subsequently, in 10 ml of incubation buffer containing 5 μl of Anti-His (C-terminal)/AB AP (Sigma-Aldrich) for 2 hours. Excess antibody was removed by washing the membrane. The gel was then soaked in 10 ml of Novex AP Chromogenic Substrate (BCIP/NBT) (Invitrogen) in the dark at 20°C to visualise the bound antibody.

2.3.7 Reconstitution

The lipids, (3:1) POPE (1-plamitoyl-2oleoyl-*sn*-glycero-3-phosphoethanolamine) and POPG (1-plamitoyl-2 oleoyl-*sn*-glycero-3-phospho-(1'-*rac*-glycerol) (sodium salt)), were dissolved in 4 ml of *n*-pentane and then dried under a N_2 flux. They were then hydrated in 4 ml of Buffer A (end conc: 1.5 mg/ml) and sonicated for 2 min to create a vesicle suspension of (3:1) POPE:POPG. CHAPS (3-[(3-Cholamidopropyl)dimethylammonio]-1-propanesulfonate) was added to the solution to achieve an ending concentration of 34 mM, which was sonicated until clarity to form a mixed lipid-detergent micelles. The lipid detergent mixture was kept at 20°C for 30 min and protein was added to 200 μg/mg (protein/lipid). The mixture was dialyzed with a membrane of 5000 MWCO cut-off in 5 L of Buffer A at 20°C. The buffer was changed 3 times:

after 2 hours, overnight and after 3 hours. The vesicles were then collected, flash frozen with liquid N_2 and stored at -80°C.

2.3.8 Planar lipid bilayer

A 10 % (v/v) hexadecane in *n*-pentane solution was spread on a 100 μm hole in a Teflon film separating two aqueous chambers. The chambers were then filled with 150 mM KCl, 10 mM HEPES pH 7.0 (cis) and 15 mM KCl, 10 mM HEPES pH=7.0 (trans). A (3:1) mixture of 14.2 mg/ml POPE and POPG dissolved in *n*-pentane was painted over the hole. Membrane formation and thinning was recorded through electrical capacitance. Vesicles were thawed on ice, sonicated for 10 sec prior to loading to the cis side. After vesicle insertion, the KCl concentration on the trans side was raised at 150 mM. An Axopatch 200B amplifier connected to a PC via a MiniDigi 1A converter (Axon Instruments) was used to record the voltage-clamp measurements in whole-cell mode. Axoscope software was used to control the hardware. Signals were sampled at 1000 Hz. The trans side was taken as ground.

2.3.9 Labelling

Tetramethylrhodamine-5-maleimide and PEG-maleimide were both kept in DMF at -20°C, under a N_2 atmosphere. Upon cell lysis, MMTS (methyl methanethiosulfonate) was added at a 4000x expected protein concentration to the cell slurry. The channel was purified as described above. Prior to size-exclusion separation, the samples were incubated with 10 mM DTT (dithiothreitol) (end concentration), for 30 min at 0°C. After the size-exclusion, fractions were collected and immediately reacted with 10x dye for 30 min-1 hour at 20°C, in the dark. The sample was then passed through a PD-10 Desalting column (GE Healthcare) in 20 mM Tris, 100 mM KCl, 5 mM

DM pH 8.0 and concentrated to separate the dye-labelled protein from the free dye. Samples were directly used for reconstitution.

2.4 Results

2.4.1 Introduction of cysteines for labelling

All mutagenesis were carried onto the K_vAP(ΔB13) gene. ΔB13 stands for two silent mutations which were introduced into the nucleotide sequence to remove two endogenous *BamHI* sites. The single endogenous cysteine (C247) of the K_vAP(ΔB13) gene was mutated into a serine by site-directed mutagenesis to produce a cysteine free version of the protein (see Appendix A.1). Single cysteines were then introduced on the paddle voltage sensor (S3b-S4 helices) using the same methodology. The mutation sites were chosen according to the results of (84) to successfully produce the following constructs. (Table 2.1).

K_vAP(ΔB13)-G101C-CL	K_vAP(ΔB13)-L102C-CL
K_vAP(ΔB13)-L103C-CL	K_vAP(ΔB13)-L105C-CL
K_vAP(ΔB13)-L110C-CL	K_vAP(ΔB13)-A111C-CL
K_vAP(ΔB13)-L112C-CL	K_vAP(ΔB13)-L113C-CL
K_vAP(ΔB13)-G114C-CL	K_vAP(ΔB13)-L115C-CL
K_vAP(ΔB13)-F116C-CL	K_vAP(ΔB13)-L118C-CL
K_vAP(ΔB13)-V119C-CL	K_vAP(ΔB13)-L121C-CL
K_vAP(ΔB13)-G122C-CL	K_vAP(ΔB13)-L125C-CL
K_vAP(ΔB13)-I127C-CL	K_vAP(ΔB13)-Y59C-CL

Table 2.1: Mutations list

Figure 2.7 and Figure 2.8 respectively show the location of the mutations on the

voltage-sensor and the protein dimeric form. A mutant for the negative control was chosen on the S2 helix, at the entrance of the pore, K_vAP(B13)-Y59C-CL (Figure 2.8). A mutant for the negative control was chosen on the S2 helix, at the entrance of the pore. K_vAP(B13)-Y59C-CL (Figure 2.8).

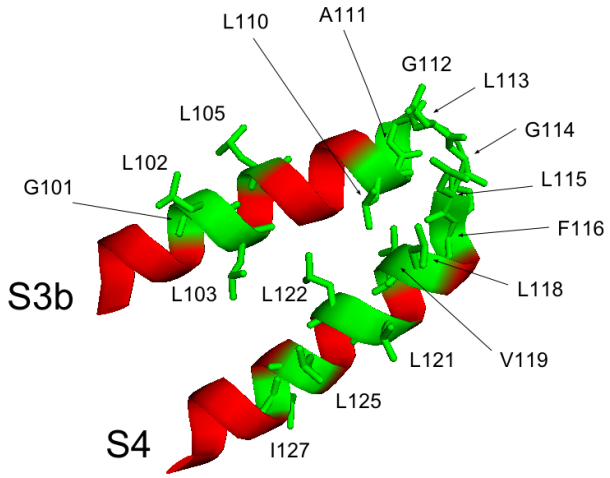


Figure 2.7: Voltage-paddle sensor of K_vAP-CL (S3b-S4 helices) showing residues in green which were mutated to cysteines in this study.

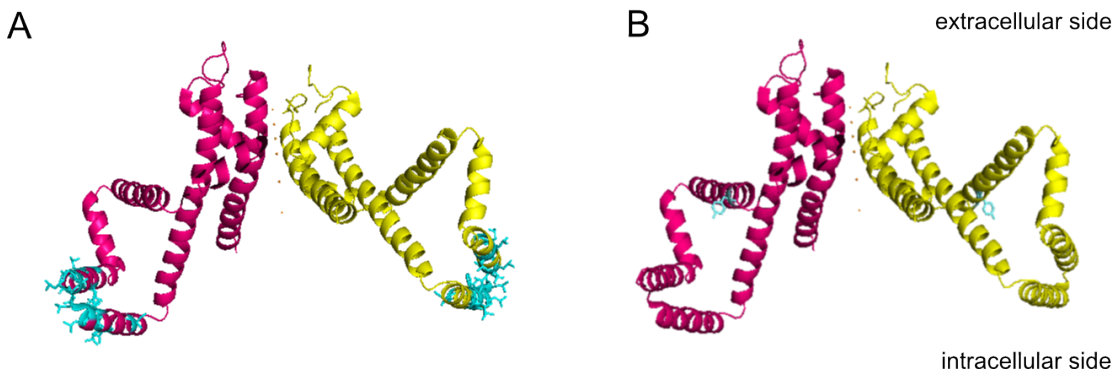


Figure 2.8: K_vAP-CL dimer viewed from the planar bilayer with the pore in the middle. On panel A, the voltage sensor mutated residues are represented in cyan ribbon while the Y59C control residue is represented on panel B.

2.4.2 Optimisation of Expression Protocol

Different tests were made regarding the vector and the cell line to find a proper expression system to allow a good expression of the gene. Membrane proteins are notoriously hard to express in *E. coli* cells, so the expression system and the growth conditions need to be optimised.

Three *E. coli* strain lines were tested, two developed by companies: BL21-Codon + competent cells (Stratagene) and XL1-Blue competent cells (Agilent). Both of them are commonly used for the production of membrane proteins; the first one is designed to have a larger supply of *E. coli* tRNAs, the second one is endonuclease deficient. The third strain came from the Netherlands Culture Collection and is a porin deficient *E coli* cells [BL21(DE3)ΔlamB ompR], PC 2889E. One of the common problems with ion channel reconstitution is the contamination by endogenous porins (2, 76) and this strain has the advantage to be porin-free. The modified K_vAP-CL genes were cloned into two vectors, pQE60 (Qiagen) and pQE60lac (see

	Without $BaCl_2$				With $BaCl_2$
	28°C		37°C		37°C
	pQE60lac-K_vAP(ΔB13)-CL	pQE60-K_vAP(ΔB13)	pQE60lac-K_vAP(ΔB13)-CL	pQE60-K_vAP(ΔB13)	pQE60lac-K_vAP(ΔB13)-CL
BL21+	+	+	+	+	+
XL1 blue	+	+	+	+	+
PC 2889E	+	+	+	+	+

Table 2.2: Expression conditions for the production of K_vAP. + indicates expression.

Appendix A.2). The second vector is a modified version of the previous one, where a supplementary *lacI* gene has been inserted to have a tighter expression of the protein of interest (Table 2.2).

The Table 2.2 summarises the tested conditions and Figures 2.9 and 2.10 show the purified protein by IMAC on SDS-PAGE gels.

PC 2889E and pQE60lac were chosen for the expression of the protein K_vAP-CL. The cells were grown for 4 hours before being harvested and the temperature was set to at 37°C, since it gave rise to a better production of the ion channel. Expression of some potassium channels is toxic to the cell due to leak current through the membrane, and so $BaCl_2$ can be used to block the channels and allow the cells to fully grow and enhance the expression. However in our case, the presence of the additional *lacI* gene provides a tight expression regulation and the presence of 10 mM $BaCl_2$ gives rise to a lower expression of the ion channel, probably due to the toxicity of Ba^{2+} itself (Figure 2.11). Different concentrations of isopropyl-β-D-1-thiogalactopyranoside (IPTG) were used to optimise the protocol and 0.4 mM was

chosen to be the best working one. The growth speed was also tested after IPTG induction, at 200, 210 and 220 rpm and the 210 rpm was found to be optimal for the ion channel expression.

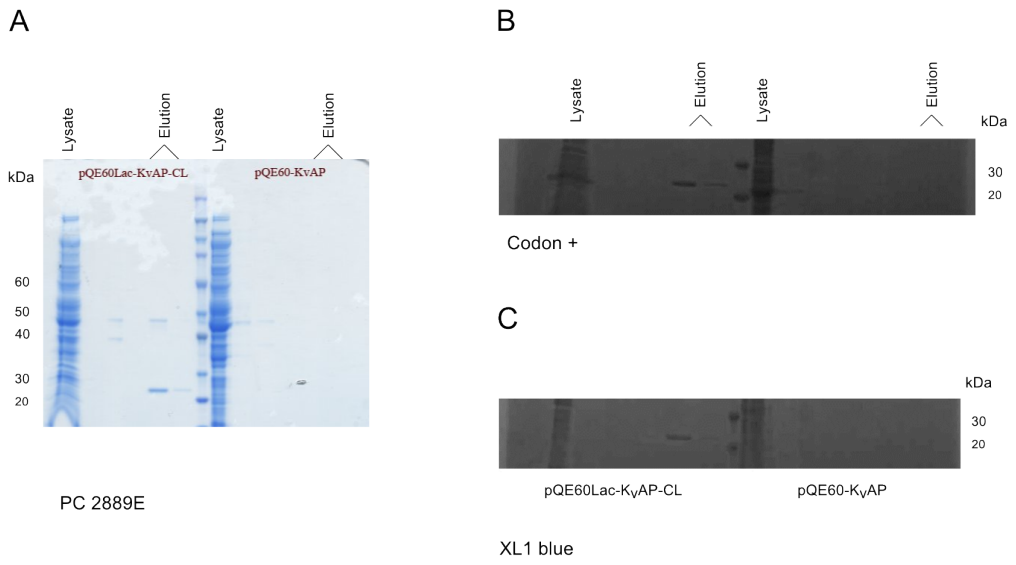


Figure 2.9: SDS-PAGE gels of the three strains, PC 2889E (panel A), Codon + (panel B) and XL1 blue (panel C) grown at 37°C and purified through cobalt TALON resin. Lane 1-6: pQE60Lac-K$_v$AP(Δ13)-CL purification, lane 7: Marker, lane 8-11: pQE60-K$_v$AP purification. Lanes 5, 6, 11, 12: Elution of the protein from the column. On the left hand side, the weight [kDa] of the marker bands are annotated. Arrow marks the K$_v$AP-CL.

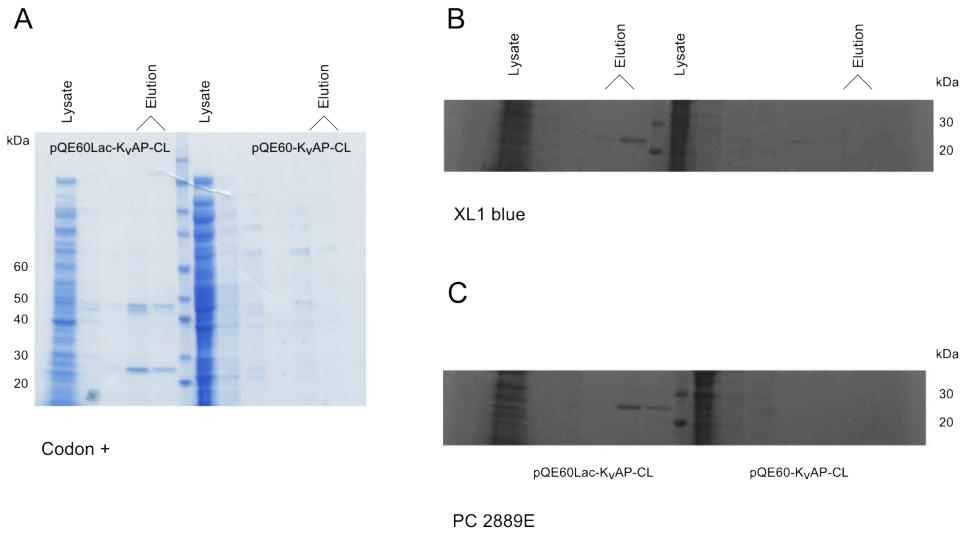


Figure 2.10: SDS-PAGE gels of the three strains, Codon + (panel A), XL1 blue (panel B) and PC2889E (panel C) grown at 28°C purification through cobalt TALON resin. Lane 1-6: pQE60Lac-K$_v$AP(ΔB13)-CL purification, lane 7: marker, lane 8-13: pQE60-K$_v$AP. Lanes 5, 6, 12, 13: Elution of the protein from the column. On the left hand side, the weight [kDa] of the marker bands are annotated. Arrow marks the K$_v$AP-CL.

2.4.2.1 Confirmation of K$_v$AP-CL expression

At this stage of the experiments, at least two protein bands, one at 24 kDa and one at 45 kDa are present on the last cobalt TALON purification steps on SDS-PAGE gels. Under denaturing conditions, K$_v$AP(ΔB13)-CL should run in the gel as a monomer. The size of the protein is 32 kDa and considering that molecular masses on gels are approximate, the 24 kDa band is quite likely to be the monomeric form of the channel. The 45 kDa band could be either the dimeric form or a contaminant. Performing a Western Blot will confirm if the ion channel is produced and the oligomeric form in which it runs.

On Figure 2.12, left, we can see the confirmation that the 24 kDa protein band the monomeric ion channel while the 45 kDa is a contaminant. When the sample boiling

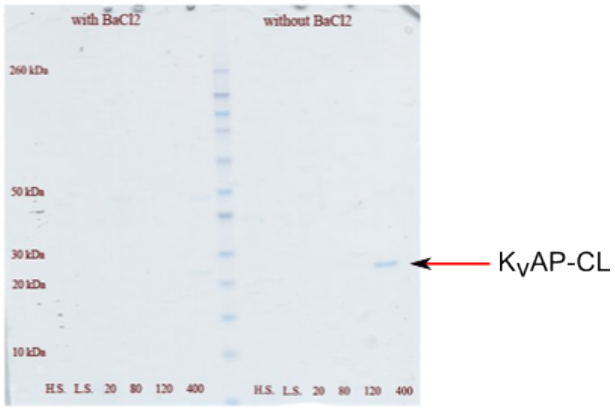


Figure 2.11: PC 2889E pQE60Lac-K_vAP(ΔB13)-CL grown at 37°C with or without $BaCl_2$ purification through cobalt TALON resin. Lane 1-6: purification of the culture with $BaCl_2$, lane 7: marker, lane 8-13: purification of the culture without $BaCl_2$. Lane 5, 6, 12: Elution of the protein from the column.

time prior to the loading in the gel is increased, K_vAP(ΔB13)-CL starts aggregating (more than 5 min) and a dimeric band at 45 kDa starts appearing on the gel, while the monomeric band signal decreases. The protein expression has been confirmed and for the sake of simplifying the analysis, the protein sample was never boiled prior to loading in a gel.

2.4.3 Optimisation of IMAC purification

Different purification trials were conducted to improve the purification purity and yield.

Once the cells were harvested after 4 hours of culture, the pellet was frozen at -80°C (Figure 2.2). After resolubilisation and cell lysis, the K_vAP-CL was either directly extracted by incubation at 20 °C with 40 mM *n*-decyl-β-D-maltoside (DM) for 3 hours, or after the membrane fraction was isolated. The membrane fraction was also frozen at -20°C and -80°C to test if the freezing process would affect the yield

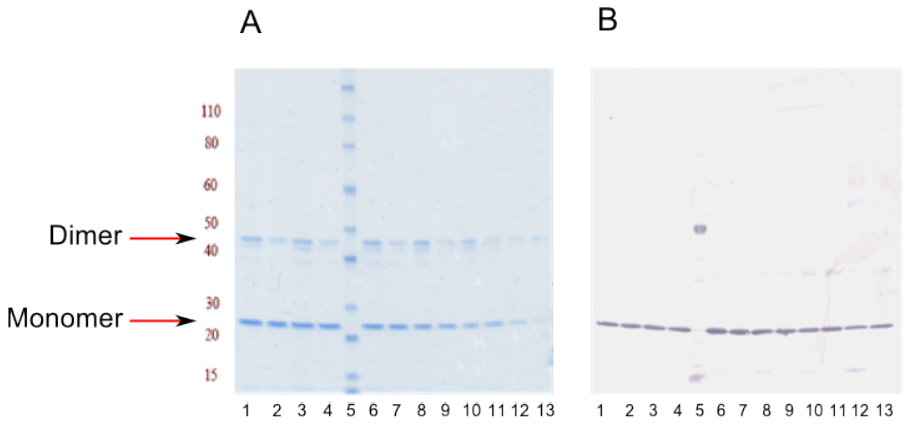


Figure 2.12: K_vAP(ΔB13)-CL purified through cobalt TALON resin. Left: SDS-PAGE gel, right: membrane of the Western blot. The two antibodies used were Anti-His (C-term)-AP Antibody (Invitrogen) and Novex AP Chromogenic Substrate (BCIP/NBT). Lane 1-2: sample unboiled. Lanes 3-4: samples boiled 1 min at 90°C. Lane 5: Marker. Lane 6-7: samples boiled 5 min at 90°C. Lanes 8-9: Samples boiled 10 min at 90°C. Lanes 10-11: Samples boiled 15 min at 90°C. Lanes 12-13: Samples boiled 30 min at 90°C.

(Figure 2.14). The K_vAP-CL extraction was also performed at 20 and 4°C, with different concentrations of the detergent (20, 40, 60 mM DM) (Figure 2.13).

Isolating the membrane fraction improves the protein yield but not its purity (Figure 2.14). Different concentrations of detergent were tried during the extraction step, 20, 40 and 60 mM DM. Figure 2.13 shows no significance between protein bands, therefore the 40 mM concentration, as suggested in the article of (83) was kept. The temperature at which the extraction was performed was also altered, 4°C to see if this could improve the ion channel yield. Despite the fact that proteins are more stable at lower temperature than at 20°C, the transfer of K_vAP(ΔB13)-CL into detergent micelles is more efficient at 20°C.

The cell slurry was then spun and the supernatant was rotated with the cobalt TALON resin for either 30 or 90 min to enhance the protein yield. The resin was then

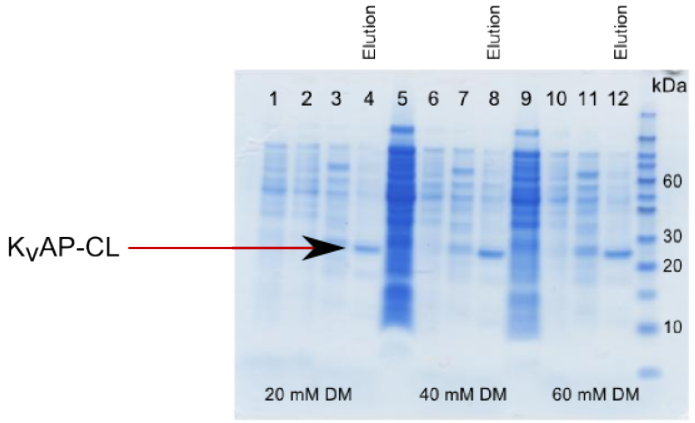


Figure 2.13: Purification of K_vAP(ΔB13)-CL samples through cobalt TALON resin. Lanes 1-4: Protein extracted with 20 mM DM. Lanes 5-8: Protein extracted with 40 mM DM. Lanes 9-12: Protein extracted with 60 mM DM. Lane 13: Marker (500 ml culture each)

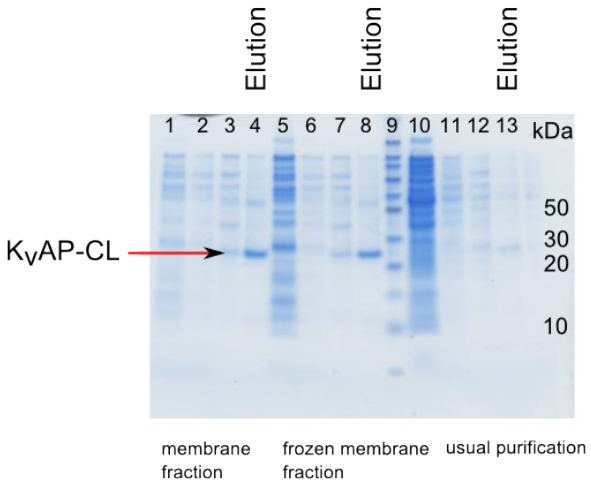


Figure 2.14: Purification of K_vAP(ΔB13)-CL samples through cobalt TALON resin. Lanes 1-4: Protein isolated from membrane fraction. Lanes 5-8: Protein isolated from membrane fraction frozen at -80°C. Lanes 10-14: Protein isolated from a usual purification. Lane 9: Marker. (500 ml culture each)

sequentially washed to remove contaminants and the ion channel was eluted with 400 mM imidazole. Washing the resin with high salt followed by an imidazole gradient in Column buffer gives the best results.

The 6xHis tag was then cleaved through a 12 hours reaction with the serine protease thrombin at a concentration of 1.0 unit per 3 mg of channel. This step was necessary for the latter purification through by FPLC. The 6xHis tag hinders separation of the oligomeric forms, and the protein aggregates and is eluted from the column at 8 ml instead of 12 ml (as shown in Figure 2.21). The efficiency of the reaction was tested by SDS-PAGE gel and by Western blot (Figure 2.15).

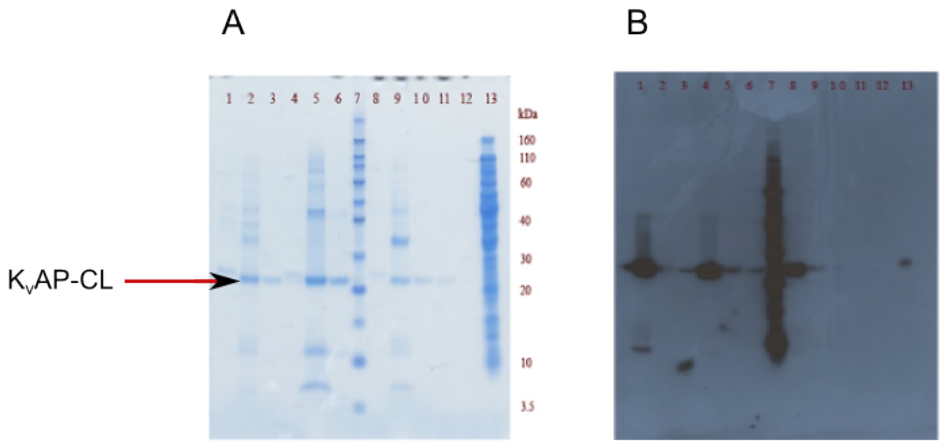


Figure 2.15: Thrombin cleavage of K$_v$AP(ΔB13)-CL. Panel A: SDS-PAGE gel. Panel B: Western blot. Lanes 1, 4. 8: Protein eluted from the cobalt TALON resin. Lanes 2, 5, 9: Concentrated fractions of the elution and thrombin protease. Lanes 3, 6, 11: Overnight reaction after removal of the endoprotease. Lane 7: Marker.

Two different strategies were used to get rid of the remaining thrombin. The mixture was passed through a benzamidine-agarose and cobalt Talon resin. The first resin binds to serine proteases including thrombin, the second resin binds to free 6xHis tags and uncleaved ion channels, letting the flow through with the untagged

ion channel. This strategy is quicker and makes the use of the different sizes of the ion channel and the thrombin, the tetramer is around 128 kDa and the enzyme is 37 kDa. Concentrating the mixture through a 50 kDa cutoff membrane only retains the tetramer and dimer of K_vAP-CL.

2.4.4 FPLC

The ion channel was then passed through a size-exclusion column (Superdex 200 10/300) connected to an Akta Prime FPLC (GE Healthcare). The tetramer, dimer and monomer forms of K_vAP-CL were eluted at approximately 12, 13.5 and 16 ml, in accordance with the reference chromatogram (Instructions "Superdex 75 10/300 GL and and Superdex 200 10/300 GL") of the Superdex 200 10/300 GL for proteins of this expected masses (they should come off the column at approximately 12-15 ml). A low flow rate, 0.15-0.2 ml/min, was required to clearly separate these fractions (Figure 2.17). Fractions were collected and analysed by Blue native-PAGE gel, as shown in Figures 2.19 and 2.20.

Despite the various conditions tested, we could not successfully remove the contaminant. However, size exclusion could separate the oligomeric forms of the protein. Using this technique, we were able to retain the tetrameric form, practically pure (Figure 2.16).

In order to improve tetramer yield, another detergent was trialled. When the MacKinnon group crystallized K_vAP, they used the detergent octyl-β-glucoside during size exclusion. In order to see if it favours the tetrameric form, this detergent was tested and U.V. traces were compared (Figures 2.18 and 2.19). Unfortunately, as seen in Figure 2.18, no increase of the tetrameric peak was seen.

In order to check the oligomeric form of the collected fractions after passage

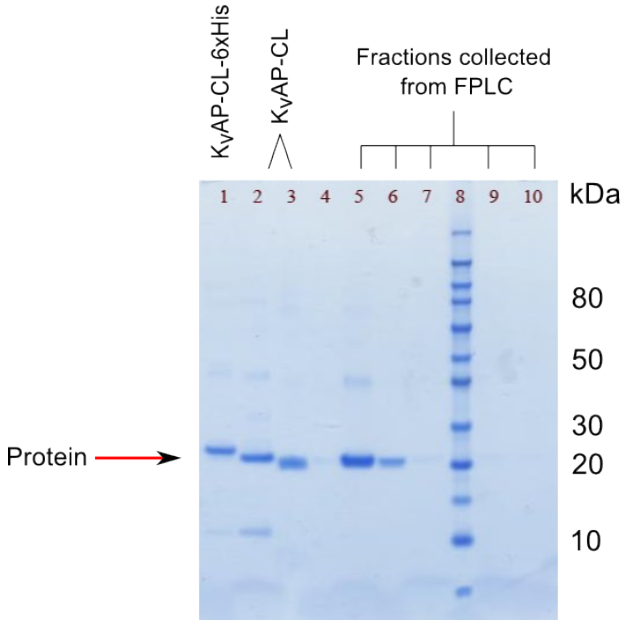


Figure 2.16: SDS-PAGE gel of K_vAP-CL purification. Lane 1: Elution from the cobalt resin. Lane 2: K_vAP-CL reacted with thrombin. Lane 3: K_vAP-CL concentrated. Lane 5-7, 9-10: Fractions collected from the size exclusion. Lane 8: Marker.

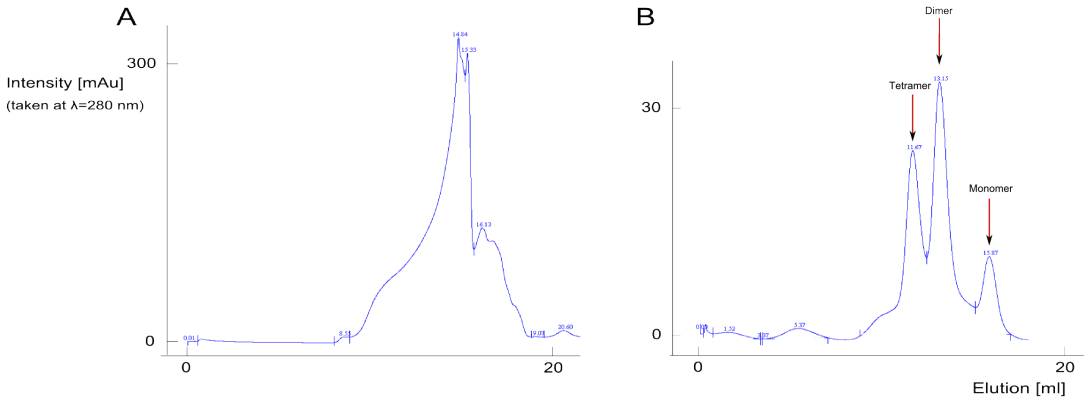


Figure 2.17: Protein elution profile from size-exclusion chromatograph analysis separation of K_vAP-CL. Panel A: Flowrate of 0.5 ml/min does not allow a separation of the oligomeric species. Panel B: A slower flowrate (0.2 ml/min), the tetramer, dimer and monomer peaks come out at 12, 13.2 and 15.9 ml respectively (red arrows).

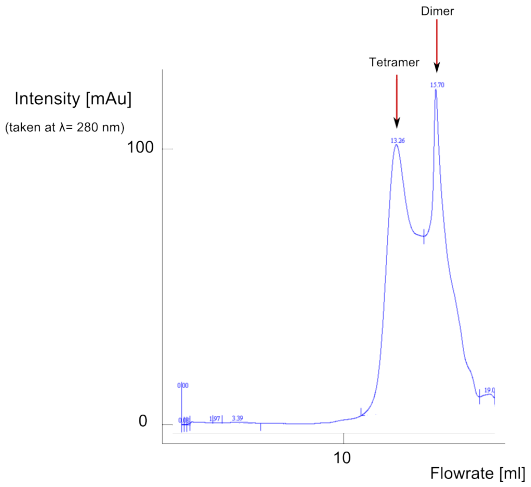


Figure 2.18: Protein elution profile from size-exclusion chromatograph analysis separation of K_vAP-L121C-CL in 20 mM Tris, 100 mM KCl, 20 mM octyl-β-glucoside pH 8.0 (Sephadex 200 10/300 column and flowrate 0.5 ml/min).

through the size-exclusion column, a Blue native-PAGE gel was performed (Figure 2.20). Under native conditions, a less stringent detergent than SDS is used as a charge-shift molecule such as proteins will run in the polyacrylamide gel under their native oligomeric form. The Coomassie G-250 binds to proteins without denaturation and for revelation as well. Unfortunately, every protein reacts differently with the charge-shift, especially membrane proteins, which causes a 15 % error in the weight resolution, according to the company's manual. In addition, other proteins were reported to show a molecular size which does not correspond to theirs (up to 4 times the expected mass).

Figure 2.20 shows different bands corresponding to sizes of 210 kDa, (lane 5, fractions 19-21 and lane 6, fractions 23-26) and 80 kDa (lane 6, fractions 23-26). The molecular masses of the tetramer and dimer are 128 and 64 kDa respectively. These observations are in good agreement with the UV-spectrum of the FPLC chro-

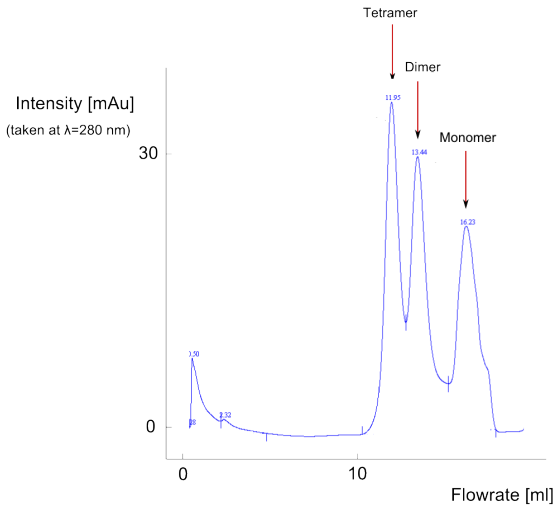


Figure 2.19: Protein elution profile from size-exclusion chromatograph analysis separation of K_vAP-CL (flowrate 0.5 ml/min). The tetramer, dimer and monomer peaks come out at 12, 13.4 and 16.2 ml respectively.

matogram (Figure 2.19).

Having successfully produced and purified K_vAP-CL, the next step was to determined if this protein was functional. Therefore, after reconstitution, the ion channel electrical behaviour was tested in planar lipid bilayer.

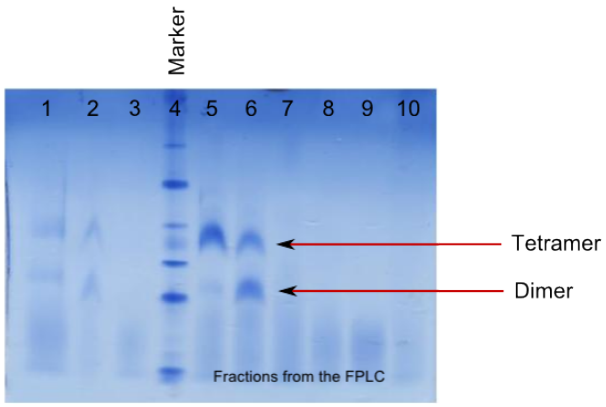


Figure 2.20: Blue native-PAGE gel of FPLC purification (FPLC 4 picture) of K_vAP-CL. Lane 1: Elution of the cobalt TALON resin. Lane 2, 3: K_vAP-CL cleaved off by thrombin. Lane 4: Marker. Lane 5: Fractions 19-21. Lane 6: Fractions 23-26. Lane 7: Fractions 27-32. Lane 8: Fractions 36-39. Lane 9: Fractions 40-43. Lane 10: Fractions 45-54.

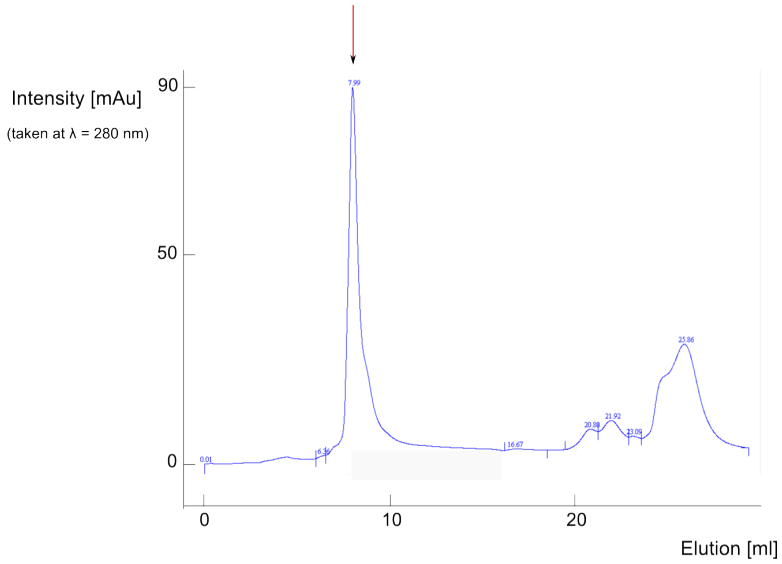


Figure 2.21: Protein elution profile from size-exclusion chromatograph analysis separation of K_vAP-CL-6xHis. The aggregate peak comes out at 8 ml (red arrow) while the small peaks coming out at 20-26 ml represent degradations products. The Y axis represents the U.V. scale [mAu] and the X axis the elution volume [ml].

2.4.5 Functional analysis of purified protein

K_vAP(ΔB13)-CL was reconstituted into (3:1) POPE:POPG lipid vesicles and applied to a planar bilayer using the apparatus and experimental conditions in (83). The hole separating both chambers was painted in a solution of 10 % (v/v) of hexadecane in *n*-pentane on both sides. The experiments were conducted in 150 mM KCl, 10 mM HEPES pH 7.0 and the planar bilayer was formed using the same lipid composition as the vesicles used to reconstitute the channel, (3:1) POPE:POPG (Figures 2.22, 2.23, 2.24).

One of the major challenges in this assay is the incorporation of the ion channel in the bilayer. The most efficient method appeared to be through lipid bilayer breakage and reformation of the bilayer by applying either an electrical pulse and then raising up and down the buffer levels in both chambers.

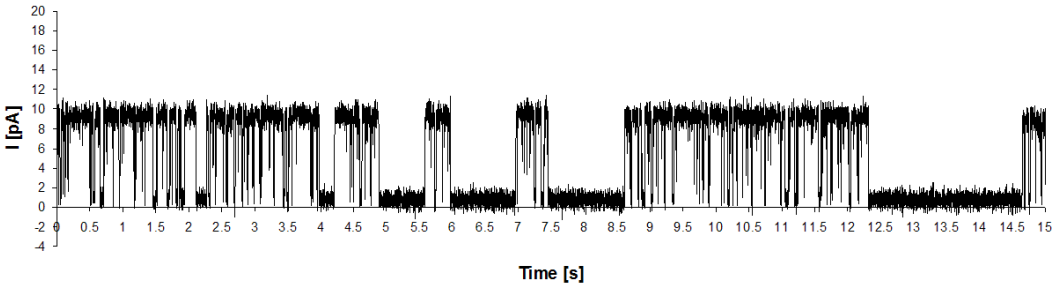


Figure 2.22: K_vAP(ΔB13)-CL reconstituted in (3:1) POPE:POPG vesicles at + 100 mV in 150 mM KCl, 10 mM HEPES pH 7.0.

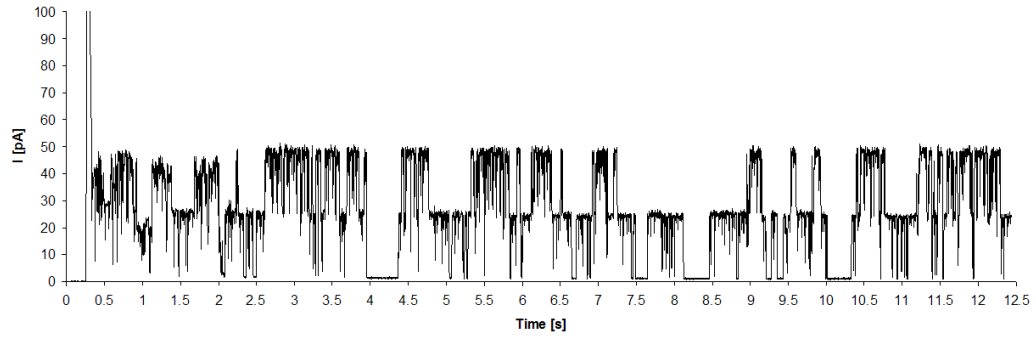


Figure 2.23: K_vAP(ΔB13)-CL reconstituted in (3:1) POPE:POPG vesicles at +100 mV in 150 mM KCl, 10 mM HEPES pH 7.0.

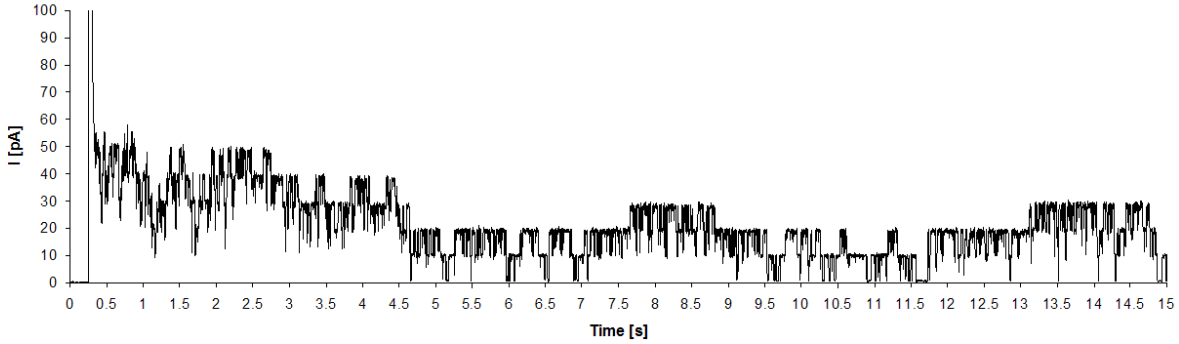


Figure 2.24: K_vAP(ΔB13)-CL reconstituted in (3:1) POPE:POPG vesicles at +100 mV in 150 mM KCl, 10 mM HEPES pH 7.0.

In Table 2.3, experimental values are compared with the literature and are in reasonable agreement. Experiments were only performed once, to check the ion channel functionality and many factors may affect the ion channel single conduction, such as

Voltage [mV]	Single channel currents of recordings [pA]	Single channel currents of (83) [pA]	Single channel currents of (33) [pA]
100	9	17.0	15.0
125	23	21.3	18.8
140	24	23.8	21.0
150	25	25.5	22.5

Table 2.3: Comparison of single channel currents between experimental values (single measurements) and the litterature

the curvature of the lipid membrane, or the presence of the agarose layer.

2.4.6 Development and optimisation of fluorescent labelling

As a preliminary attempt, two mutants $K_vAP(\Delta B13)$-Y59C-CL, and $K_vAP(\Delta B13)$-A111C-CL were incubated with TMR5M after cobalt TALON purification. Different conditions were varied such as the label/protein ratio, the time of reaction, the addition of reducing agent such as TCEP, and the buffer composition, as shown in Table 2.4.

On each trial, samples were run on SDS-PAGE and visualized under UV light prior to Commassie staining. TMR5M presence in the gel is then detected and once the gel has been stained by Commassie, protein bands become visible while the dye fluorescence is not apparent anymore (95). No fluorescent protein was detected as shown on SDS-PAGE gel (Figure 2.25); the fluorescent label is running as a diffuse band at the bottom of the gel, while the protein bands do not show any fluorescence. As a negative control, TMR5M was loaded alone in the gel as well (lanes 10-12)

Oxidation is likely the cause of reaction failure. Therefore, conditions were mod-

Mutant tested	Label/protein ratio [mM]	Conditions of reactions	Other components	Quenching of the reaction
Y59C/A111C	20x	overnight, 20°C	-	-
Y59C/A111C	20x	overnight, 4°C	2 mM TCEP	-
Y59C/A111C	50x	30 min, 20°C	-	-
Y59C/A111C	10x	15 min reaction in the dark	Phosphate/Tris buffer, 1 mM DTT	50 mM 2β-ME

Table 2.4: Labelling conditions tested with K_vAP(ΔB13)-Y59C-CL, and K_vAP(ΔB13)-A111C-CL after IMAC purification.

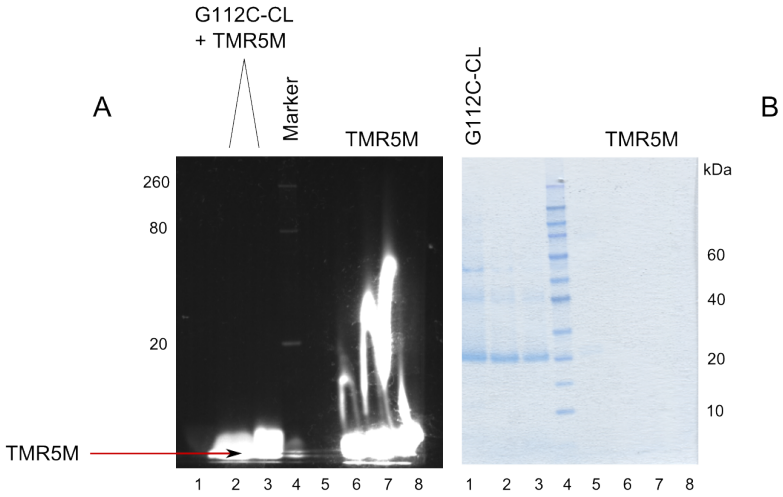


Figure 2.25: SDS-PAGE gel imaged under U.V. light (365/302 nm, acquisition time 0.1 sec) prior (panel A) and after (panel B) Coomassie staining. K_vAP-G112C-CL was loaded in lane 1, with TMR5M in Tris buffer in lane 2, with TMR5M in Phosphate buffer in lane 3. The marker is present in lane 4 and TMR5M alone was loaded in lanes 6-8. 20, 80 and 260 kDa bands in the Marker are fluorescent.

ified in order to avoid any cysteine degradation. Addition of free dye during the detergent extraction was first tried. Reduction with DTT and concentration of the sample before or after the extraction were attempted too. As previously, no fluorescent bands corresponding to proteins could be detected on SDS-PAGE gels. Since DTT could compete with the thiol during the labelling reaction, dialysis (4 hours at

Sample	Label/protein ratio added upon cell lysis	MMTS/protein ratio added upon cell lysis	Addition of 10 mM EDTA, upon cell lysis	2β-ME added with cobalt TALON resin	Label/protein ratio added upon cobalt TALON resin
Y59C	30x	-	-	-	-
Y59C	-	4000	-	5 mM, overnight at 4°C	10x
Y59C	-	4000	yes	7.5 mM, overnight	10x
Y59C	-	4000	yes	10 mM, overnight at 4°C	10x

Table 2.5: Labelling conditions tested with K_vAP(ΔB13)-Y59C-CL after IMAC purification with the use of a protective group.

4°C) was followed by the addition of TMR5M (to K_vAP-G112C-CL). Unfortunately, no labelling reaction was detected (not shown)

In the next set of trials, a protective group was used at the beginning of the purification to avoid or minimise any potential oxidation reaction. MMTS (methyl methanethiosulfonate) protects thiol function by reversible methylthiolation (47). Reductive agents can reverse the reaction and leave the thiol group unprotected. The ratio of MMTS and TMR5M added while the *E. coli* cells are lysed is based on yield estimations of previous purifications. Prior to elution, 2β-ME was added to the cobalt resin for overnight reaction. Of all the reducing agents, only 2β-ME is compatible with the cobalt TALON resin at a maximum concentration of 10 mM. TMR5M was added to the resin and incubated for 4 min, before the protein was eluted from the resin (Table 2.5). As previously, no labelling reaction could be detected by SDS-PAGE gel.

So far, no reaction was detected on any of the voltage sensor sites (meant to lie in the protein core) or also on the control on helix S2. Therefore, a control reaction between the cysteine and a PEG-maleimide compound was conducted. The PEG-maleimide is a molecule of 5 kDa molecular weight made of a long PEG chain attached to a maleimide group. Due to its long chain, any protein/molecule which will have reacted with it, will show a shift of 5 kDa on a SDS-PAGE gel. This procedure quickly offers a quick check of any possible thiol-maleimide reaction. In the next attempt, MMTS was added in excess during cell lysis and PEG-maleimide was added to the protein after size-exclusion (Figure 2.26).

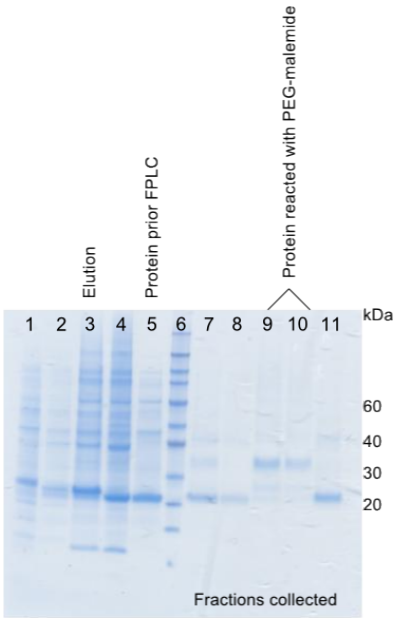


Figure 2.26: Purification of K_vAP(ΔB13)-A111C-CL. Lane 1-2: Buffers used with the cobalt TALON resin to clean the protein. Lane 3: Elution of the protein from the resin. Lane 4: Overnight reaction of the ion channel with the thrombin. Lane 5: Concentration of the protein prior the size-exclusion separation. Lane 6: Marker. Lane 7: Fractions 16-19 collected. Lane 8: Fraction 20. Lane 9: Fraction 21 reacted with PEG-maleimide. Lane 10: Fraction 22 reacted with PEG-maleimide. Lane 11: Fractions 23-25. Lane 12: Fractions 27-30.

This was the first positive result which confirmed that the thiol-maleimide reaction occurred. Therefore, any subsequent labelling reaction was performed under the same conditons. The reaction time was kept at 30 min - 1 hour in the dark at 20°C with 10x TMR5M before addition of 2β-ME (1000x concentration of TMR5M) for quenching of the reaction. Free dye was removed using a 10 kDa concentrator at 5000 rpm followed by desalting column purification before reconstitution into lipid vesicles (Figure 2.28).

Labelling of K_vAP-CL mutants was visualised by silver staining of SDS-PAGE gels. The low tetramer concentrations (around 0.02 mg/ml after size-exclusion) were not visible with Commassie staining and the higher sensitivity of silver staining (5-10 ng vs 100 ng for Commassie) had to be used. More protein were then produced to improve both the labelling efficency and detection.

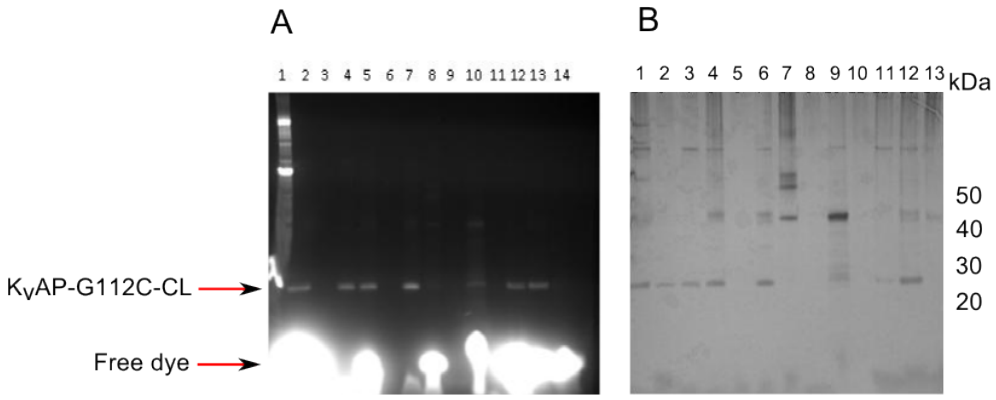


Figure 2.27: On the left, SDS-PAGE gel imaged under U.V. light (365/302 nm, acquisition time 2 sec) prior Coomassie staining. Some bands in the Marker are fluorescent. On the right, of K_vAP(ΔB13)-G112C-CL silver stained.

A negative control was performed with the cysteine-free mutant K_vAP(ΔB13)-CL. Figure 2.29 shows a fluorescent band corresponding to the ion channel in the sample taken after the reaction. After dye removal through the desalting column, K_vAP(ΔB13)-CL band appears without fluorescence confirming the specificity of the

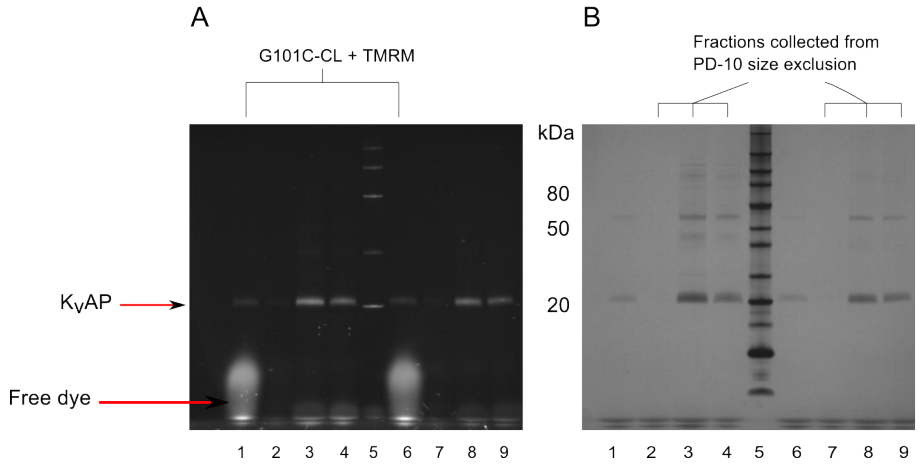


Figure 2.28: SDS-PAGE gel imaged under U.V. light (365/302 nm, acquisition time 1 sec) prior (panel A) staining and after (panel B) Coomassie staining. Sample K_vAP-G101C-CL after FPLC has been reacted with TMR5M (lane 1 and 6), and passed through the PD-10 desalting column to remove the free dye (lanes 2-4 and 7-9). Marker is on lane 4 (fluorescent bands at 20, 80 and 260 kDa).

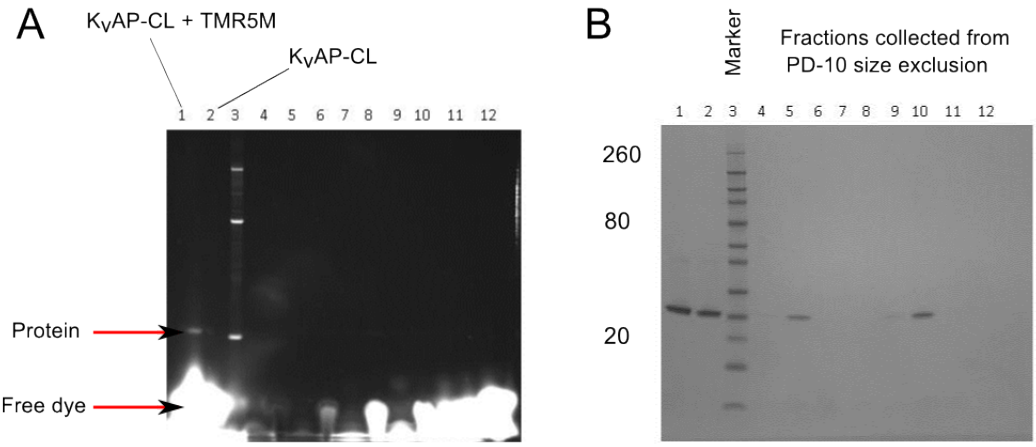


Figure 2.29: On the left side, SDS-PAGE gel of K_vAP(ΔB13)-CL after reaction with TMR5M imaged under U.V light prior staining (365/302 nm, acquisition time 0.4 sec). Lane 1: K_vAP(ΔB13)-CL + TMR5M. Lane 2: K_vAP(ΔB13)-CL prior to labelling. Lane 3: Marker. Lanes 4-12: Fractions collected after the passage through PD-10 desalting column to remove the free dye. On the right side, gel after Coomassie staining. The protein of interest appears at 24 kDa.

reaction. Free dye appears to bind to the protein non-specifically during electrophoresis (lane 1 and lanes 4-12, Figure 2.29)

2.4.7 Quantification of labelling efficiency

Absorbance measurements of labelled K_vAP-CL mutants were taken prior to reconstitution into vesicles to calculate the dye protein molar ratio, according to Equations 2.2 and 2.1 (Table 2.6). Unfortunately, the low protein yield limits a thorough quantification of labelling efficiency. Two instruments were used, a Nanodrop (Thermo Scientific) and a spectrophotometer (Varian, 50Bio UV-Visible). Due to diluted samples, no significant peaks could be detected at λ_{280} or λ_{575} with the spectrophotometer and the Nanodrop (detection limit: 0.1 Abs, corresponding to 0.1 mg/ml). Ellman's reagent was also used to test the presence of a reactive cysteine, but due to the same issue, the results were inconclusive.

From these results, I conclude that labelling of K_vAP-CL mutants is successful but incomplete. Reaction time was varied without any effect on the reaction success, and the dye concentration was kept the same (10x the protein). Every precaution was taken to preserve the cysteine reactivity such as the use of a protective group until the last moment before the labelling reaction. Unfortunately, the pH of the solution could not be raised without the risk of compromising the protein integrity (cysteine $pK_a = 8.0$). The reaction time was kept short (30 min -1 hour) in order to prevent any cross reaction with amino groups. Free dye was also washed out at several times during concentration and prior to reconstitution in order to minimise its presence in the final step.

Mutants	Protein concentration [M]	Protein quantity [mg]	mol_{prot}/mol_{dye}
K_vAP-L121C-CL	4.85 10^{-6}	124	0.54
K_vAP-G101C-CL	6.2 10^{-8}	21.3	1.96
K_vAP-A111C-CL	inconclusive	inconclusive	inconclusive
K_vAP-L121C-CL	4.18 10^{-7}	11	0.99

Table 2.6: Calculated protein/dye ratio for mutants of K_vAP-CL. Measures taken with the Nanodrop.

Labelled and unlabelled samples were also sent for Mass-spec analysis. Unfortunately, results were unconclusive due to low concentrations.

2.5 Discussion

2.5.1 Expression

Tests of culture conditions were performed to optimise the production of K_vAP(ΔB13)-CL (Table 2.2). All three strains expressed well but PC2889E was chosen due to its lack of porins. Indeed they can cause contamination problems by being purified along with the ion channel of interest until the final stage and be present during electrical recordings. In (83), 10 mM $BaCl_2$ was used during the culture growth. However, in our hands $BaCl_2$ did not enhance expression, possibly due to the tighter control of expression with the pQE60lac vector used here. Moreover, removal of $BaCl_2$ has a double advantage: this toxic compound can block channels during electrical recordings.

The identity of K_vAP-CL was confirmed by Western blot (Figure 2.12) along with

a contaminant. Optimisation of the purification was carried on in order to improve the protein yield and to get rid of this contaminant.

2.5.2 Purification

The purification of a membrane protein is notoriously known as a difficult step. The expression of membrane proteins in the first place is quite low, so a large quantity of cells need to be processed. Most than all, the purification steps need to be optimised in order to minimise the loss of protein along the way.

None of the changes made from the (83) protocol increases the yield, with the exception of isolating the membrane fraction prior to IMAC purification (Figure 2.14). Typically, a 1 liter culture gave approximately 0.6 mg of purified protein (measure taken after the cobalt TALON resin). After purification through cobalt resin, the 6xHis tag was enzymatically cleaved, which was an essential step to separate the oligomeric forms (Figure 2.21). Indeed, the 6xHis tag causes K_vAP(ΔB13)-CL to precipitate during size exclusion. This is not uncommon with this type of tag (16). Once the enzymatic reaction was complete, the mixture was filtrated through a 50 kDa cutoff membrane, in order to keep the tetrameric and dimeric forms of the protein (128 and 64 kDa respectively) for size-exclusion.

2.5.3 Size-exclusion

The size-exclusion column separates compounds according to their sizes. In order to be able to see the oligomeric species of the protein, the flow rate should be kept very slow. Even with 0.2 ml/min (minimum flowrate is 0.1 ml/min), the tetrameric, dimeric and monomeric peaks could not be completely separated (Figure 2.17). In an attempt to increase the tetramer yield, another detergent, octyl-β-glucoside (β-OG)

at a concentration of 30 mM was trialled (Figure 2.18). Unfortunately, it did not favour the tetrameric form.

2.5.4 Functional analysis of purified protein

The single channel traces confirm that the present purification lead to functional K_vAP-CL. This step is important, especially before undertaking any covalent modification of the ion channel.

Only a couple of recordings were taken, since we were only interested at this stage to confirm the presence of the channel (Figures 2.22, 2.23, 2.24).

K_vAP-CL conductances are typically 170 pS and 150 ± 26 pS respectively, (33, 83). No open probabilites were reported. In Table 2.3, single channel currents were compared with the reported conductance. Apart from one value, they are in good agreement with the literature. Measurements of ion channel conductance are approximate and a small discrepancy between reported values is not unexpected.

2.5.5 Development and optimisation of fluorescent labelling

Labelling was the most challenging part of the preparative process. A new protocol had to be established and many different conditions had to be tested.

2.5.5.1 Reducing agents

Reaction conditions were varied including the label/protein ratio, the time of reaction, the buffer and the addition of reducing agent such as TCEP. From the moment the *E. coli* cells are lysed, free cysteines can react and oxidize. Therefore, the addition of TCEP prior to the labelling reaction was used. Several reducing agents, DTT, 2β-ME and TCEP, were explored.

DTT is recycled at the end of the reaction into a stable cyclic disulfide and is quickly hydrolysed in buffer in the absence of metal chelates. The mechanism of disulfide reduction by DTT (22) operates according to the reaction shown in Figure 2.30.

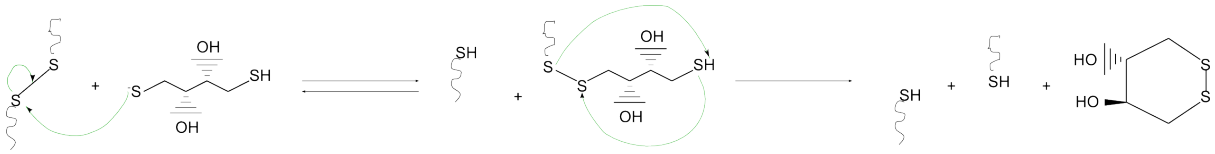


Figure 2.30: Chemical reaction between DTT and a disulfide bond.

Nevertheless, its removal is crucial for labelling success reaction (40). The presence of any reducing agent will compete with the free cysteine for the labelling reaction. Dialysis is one of the most efficient way to separate consitituents (74) and was used in some of the tests.

Finally, 10 mM DTT was reacted with the purified channel prior FPLC, for 1 hour at 0°C, prior its separation from the sample through size exclusion. The fluorescent label was then immediately added to the collected fractions.

2.5.5.2 Bufffer

Ideally, the thiol-maleimide reaction is optimal at pH between 6.5 and 7.5; when the solution becomes more alkaline, at pH greater than 8.5, the maleimide group can also react as with primary amines, such as the ones which are on the Tris molecule. The proteins are maintained at pH 8.0 through every purification step, since K_vAP(ΔB13)-CL precipitates at pH lower than this value. Therefore, at the working pH range, a Tris buffer may react with the maleimide. Phosphate buffer

will not compete with the thiol function. The concentration of the two salts was calculated such as to share the same ionic strength (106.65 mol/L) as 20 mM Tris, 100 mM KCl buffer. Both buffers were degassed prior use in order to reduce dissolved oxygen (Table 2.4). Furthermore on this trial, the TMR5M dye stock solution were first solubilised in DMF (dimethylformamide), instead of DMSO (dimethyl sulfoxide), under a N_2 atmosphere. DMSO promotes thiol oxidation (98) despite that it is reported as the choice solvent by the manufacturer, DMF was used instead.

As previously, the samples were run on SDS-PAGE gel and visualized under UV light prior Coomassie staining. No labelling reaction was detected (Figure 2.25). Since every preparative step has been conducted in Tris buffer without any problem, it was kept for the subsequent labelling reactions.

2.5.5.3 Protective group and PEG-maleimide

In view of the problems we were encountering with the reactivity, we firslty decided to use a protective group, straight after the cell lysis (Figure 2.31). Caution was taken to make sure that any incompatible reagent with the cobalt TALON resin was used. Then, we tested the cysteine reactivity by reaction with PEG-maleimide.This procedure quickly offers a quick check of any possible thiol-maleimide reaction. A clear shift was seen for the fractions which have been let with the PEG-maleimide compound and the reaction looks complete (Figure 2.26). Moreover, the negative control (with TMR5M and the cysteine less version of K_vAP, Figure 2.29) confirms that the thiol maleimide reaction happens and the gel shif is not due to any cross reaction.



Figure 2.31: Protection reaction of the MMTS reagent with a free thiol group.

2.5.5.4 Important considerations for labelling

The problems encountered draw attention to some critical aspects of any labelling protocol, the importance of working at high concentration, both for reasons of completion of the reaction and detection of the products. It is possible that many of the previous labelling trials failed mainly because of the ion channel low concentration. Even if the reaction would have been completed, detecting quantities on the order of 0.02-0.5 mg/ml is tricky. Therefore producing proteins in enough quantities remains one of the most challenging part of the procedure. Furthermore, the purity of the ion channel is equally important and was not considered with enough care during the first trials. One of the reasons for successful labelling is the effective use of size-exclusion.

An important step as well for further fluorescence experiments is to remove free dye, and concentrating the sample was thus trialled. However, a pink-red coloration on the membrane appeared during the centrifugation which indicates thatan free dye interacts and sticks to it. Concerns were raised that this extended interaction with the sticked dye to the membrane, may be detrimental for protein labelling and functionality. So another approach was considered: the samples were passed through a desalting column (PD-10, GE Healthcare) before being briefly concentrated. Figure 2.28, first fractions collected at the bottom of the desalting column contain the protein and far less free dye.

The removal of the dye through this method is not complete. However, this step is followed by the reconstitution of the channel in lipid-detergent mixed micelles, by sonication followed by dialysis against 15l, which should washes the free dye out. If by example, 10^{-7} moles of dyes have been used for labelling and we only consider the extended dialysis for the dyes removal, at the end of the processus, the dye concentration inside the dialysis cassette would have passed from 5 10^{-5} M to 64 10^{-19} M.

2.5.6 Quantification of the fluorescence

The protein-to-dye ratio of the samples was assessed by the standardized method of absorbance measurements (Table 2.6). According to these results, the labelling reaction was unfortunately incomplete; it only occured on one of the sites, without any significant variation between mutants. However, the channel was present in a very small quantity at the end of the purification process (the typical absorbance range of purified labelled tetramer K_vAP-CL mutant was around 0.05 [AU]), which made the determination of the protein-to-dye ratio challenging. The unstained SDS-PAGE gels confirmed that the labelling reaction has occured though. After Coomassie staining, no fluorescence bands could be anymore detected, probably due to the absorption of λ_{543} and λ_{575} (λ_{ex}^{TMR5M} and λ_{em}^{TMR5M} respectively) by commassie molecules.

As emphasised previously, the purity and concentration of the sample plays a major role in the labelling reaction success. However, other factors have to be taken into account. Nonetheless, the accessibility of cysteine may explain its partial reactivity towards the maleimide group. The S3b-S4 helices are buried inside the protein, surrounded by detergent molecules to solubilise it. Dye molecules may have difficulties in accessing thiol sites, despite the reaction high specificity. After reaction

quenching, the removal of free TMR5M through size exclusion and concentration was problematic. This may indicate that dye molecules would strongly interact with the ion channel through hydrophobic interactions with the detergent.

2.6 Conclusion

The ion channel was successfully produced and purified. An experimental protocol was established and the quality of the generated samples was checked by electrical recording with the planar lipid bilayer method.

18 single cysteine mutants were generated. After significant effort, positive results confirmed that the labelling reaction was working, unfortunately only partially. Regrettably, labelling the protein in detergent presence is a necessity, new approches thus had to be tried out. Another untested parameter, the temperature could be investigated in order to improve the protein-to-dye ratio. The characterisation of the labelling reaction along with the quantification of the protein was troublesome, due to low concentration of the sample. Therefore, another set of experiments was designed to offer complementary knowledge on the labelled protein (Chapter 3).

Chapter 3

Photobleaching Analysis of Labelled K_vAP-CL

3.1 Introduction

At the end of Chapter 2, the results of protein-to-dye ratio by the standardized method of absorbance measurements were unsatisfactory. The SDS-PAGE gels definitively show labelling but limited evidence were provided by the absorbance experiments, due to the ion channel low concentration. Moreover, this macroscopic measure does not give us information on the different labelled populations of the channel. Furthermore, the channel has been characterised in a lipid environement and knowledge on the accessibillity of each labelling site in detergent micelle is lacking. Even if the channel is a homotetramer with a four-fold symmetry, we cannot assume that each labelling site will have the same accessibility. Even such partially labelled channels would still be useful for single molecule studies but a better assay for determining the number of dyes bond to each channel would be advantageous. Therefore, com-

plementary experiments were done to assess the dye to protein ratio.

In 2007, Ulbrich and Isacoff published an article where they presented a new approach to determine the degree of labelling in glutamate-gated NMDA receptors fused to GFP proteins (100). After expression of these constructs in *Xenopus laevis*, they used TIRF microscopy to image areas of oocytes membranes resting on coverslips. The density of labelled NMDA receptors was kept low, so as to keep receptors at a distance further apart than the diffraction limit. By continuous illumination, they photobleached the GFP protein carried by each monomer on the surface. The examination of each step in the intensity trace corresponding to a photobleaching coming from each fluorescent spot revealed the number of GFP proteins present in the complex and thereby the subunit stoichiometry of the multimeric channel. By counting the photobleaching discrete steps in every fluorescent traces, histograms of labelled populations can be drawn, which give access to more information than a macroscopic measurement. In parallel, this approach was reported for the study of β-barrel pore-forming toxin, the leukocidin. Proteins were produced by *in vitro* transcription and translation (IVTT), purified and labelled with a malemide dye and adsorbed on coverslips before being photobleached (28).

The same methodology can be applied to labelled K_vAP-CL (K_vAP-C247S) reconstituted into vesicles, to supplement the protein-dye ratio information and to estimate the efficacy of labelling. However, this approach has its own limitations. Firstly, the protein may have degraded during the freezing-thawing process, the dye may have bleached prior to the experiment or become cleaved from the protein. In all these cases, the labelling reaction would be underestimated. Secondly, the results will intrinsically be influenced by the probability of detecting a single fluorophore. Furthermore depending on the temporal resolution of the experiment, there is a small

probability that two dyes can bleach at a very small time interval which will result on a single step in the fluorescence intensity vs time plot and miss-counting of the steps.

This analysis was performed using two softwares. The first approach presented in this chapter, involves the use of software developed in 2007 by G. I. Mashanov and J. E. Molloy, GMimPro (65). It uses two algorithms, SFDA (single fluorophore detection algorithm) and ASPT (automatic single particle tracking) which track static or moving fluorescent single particles and output their fluorescent intensity and position in time.

The second software written in-house through the MATLAB interface, by Dr. Matthew Baker (article under review). The Photobleaching Analysis Frequency Code (PAFC) detects and analyses the photobleaching intensity through time of static fluorophores.

3.1.1 First method: GMimPro

3.1.1.1 Single fluorophore detection algorithm (SFDA)

At first, the intensity at each pixel is lowpass filtered through to reduce the background noise. This filtration step is performed by averaging the pixel intensity over its surrounding area, which has been determined by the diffraction limited size of the fluorophore (parameter entered by the user). The intensity at each pixel is lowpass filtered to reduce the background noise. The next step is to identify signals arising from single fluorophores and separate them from the noise. The identification of a single fluorophore is based on one of their defining characteristics: a step decrease of their fluorescence intensity while they photobleach under constant illumination. An

edge detection algorithm is then used which calculates for every pixel the derivative of the intensity. All intensity transitions (rise or drop masks) are stored with their corresponding times in two different arrays, one for the decreasing transitions and one for the increasing ones. From these arrays, the centroid position (x, y) of each fluorophore is also determined by Gaussian fitting. Once the fluorophore position has been determined, the processed data stored in masks is superimposed upon the original lowpass filtered intensity, in order to identify any multiple photobleaching events in the trace (Ms-test). The next phase is to check that each putative detected spot has a size corresponding to the diffraction limit and emits a constant number of photons through time. In this testing process, a parameter (I) is used as a thresholding parameter to discriminate any false objects. If the potential fluorophore intensity signal is statiscally significant from the background fluorescence, the candidate is kept.

$$I(x,y) = \frac{g_{high}(x,y) - g_{low}(x,y)}{\sqrt{v_{high}(x,y) + v_{low}(x,y)}} \tag{3.1}$$

- g_{high}(x,y): Pixel intensity corresponding to the local mean of pixels in a surrounding area during interval of high fluorescence (putative fluorophore signal)
- g_{low}(x,y): Pixel intensity corresponding to the local mean of pixels in a surrounding area during interval of low fluorescence (background intensity)
- v_{high}(x,y): Variance of the signal during interval of high fluorescence
- v_{low}(x,y): Variance of the signal during interval of low fluorescence.

3.1.2 Second method: Photobleaching analysis frequency code (PAFC)

3.1.2.1 Chung-Kennedy filter

The analysis of the data uses the non-linear Chung-Kennedy filter (21). The aim of this filter is to distinguish photobleaching discrete steps from noisy jump transients, without the need of any preconceived model of the signal. The main advantage of this type of filter is the preservation of the edge of the step, which would be lost through linear filtering. The Chung-Kennedy filter principle is to run across the data with too adjacent windows (portion of data), point by point. The mean and the variance of each window are calculated and the filtered output is their weighted means. When one of the two windows encounters a step, its variance becomes larger than the one from the other window. Due to the weighting coefficients, the output data only retains the mean of the window with the smallest variance (the one not spanning the step), which enables the conservation of the edge of the step (no loss through averaging) (55).

3.1.2.2 The pairwise difference distribution function

The pairwise difference function of the filtered intensity trace is calculated using the formula below:

$$\Delta I_{ij} = I(t_i) - I(t_j) \tag{3.2}$$

- if $t_i > t_j$
- I (t_i) = Intensity at time t_i

- I (t_j) = Intensity at time t_j

It can be represented as the distance between every points in a single trace.

3.1.2.3 Photobleaching analysis frequency code

A batch of movies in TIFF format recorded under the same experimental conditions are analysed by the algorithm as a group, using the MATLAB (Mathworks, US) software. The code assumes that the density of bright spots is sufficiently low to allow the single resolution of each one of them. The first 50 brightest spots are considered for analysis in order of decreasing intensity. The code works by following these steps:

Detection of fluorophores Each pixel of the first 50 frames is scanned and a mean is calculated to form a new image. This new image is scanned to find bright spots which may correspond to labelled proteins. The bright spots size is defined by selecting 3x3 pixels areas at the spot location until the specific signal reaches twice the noise intensity. Any bright spot whose signal to noise ratio fails to match this criteria is automatically eliminated. Only spots whose intensity maxima happens within the first 50 frames are considered. At each bright spot location, the noise is defined as the standard deviation of the signal during the last 50 frames of the recording and the signal as the mean of the first 50 frames substracted from the last 50 frames. Photobleaching traces (intensity versus time) are plotted by taking the maximum pixel within the 3x3 pixels area, at each single frame.

Filtration and pairwise difference density function:

The data is then filtered using the Chung-Kennedy filter and the pairwise differ-

ence density function is calculated for each single trace.

Fourier transform The Fourier transform of the probability density function, also known as the empirical characteristic function (ECF) is calculated from the pairwise difference density function. In the frequency domain, only a couple of coefficients in the power spectrum (calculated from the ECF) represent periodicity. The largest peak, the dominant frequency, is selected as a single photobleaching step (or increment size). Stoichiometry histograms are calculated by substracting the signal intensity of the last 50 frames to the first 50 frames and dividing it by the found increment size.

The experiments and control were carried on a cover-slip surface where the samples and the control were dried out prior to recordings.

3.2 Material and methods

3.2.1 Plasma cleaning

Prior to all experiments, coverslips (Menzel-Gläzer, 24 x 40 mm) were plasma-cleaned using a Plasma System FEMTO, Diener Electronic (1.5 bar O_2, 950/1000 power for 7.5 min). This procedure involves the use of an energetic plasma created by ionization of O_2 through a high frequency field (from kHz to MHz). The cleaning action is carried in two steps. The UV photons released by the activation of the gas break organic bonds of contaminants present at the coverslip surface while the radical oxygen species react with the same species to form H_2O, CO, CO_2, which will be evacuated by the vacuum pump. The cleaning capacity of the ionized gas exceeds any other methods involving liquid. The plasma can access micrometric crevices,

irregularities on the solid surface which would be hardly accessible for a liquid. The plasma-cleaning treatment not only removes dirt on the surface but also changes the properties of the surface of the treated material. Plasma O_2 will promote surface oxidation and hydroxylation and make the coverslip surface hydrophilic, on top of decreasing the intrinsic background fluorescence.

3.2.2 Sample preparation and recordings

Samples were thawed at 20°C and diluted into 150 mM KCl, 10 mM HEPES, 5 mM DM (n-decyl-β-D-maltoside) pH 7.0 to a nanomolar concentration. A DNA duplex control labelled with four Cy3 dyes was treated the same way but diluted in MilliQ water (Resistivity : 18.2 MΩcm) (see A.3). Samples were briefly vortexed and 2 μl was pipetted onto the coverslip surface and air dried, to a concentration that would allow fluorescent spots to be separated by many multiples of the diffraction limit. They were imaged by TIRF microscopy for 25 seconds and recorded in TIFF file format. Once a movie was taken, the field of view was moved to a neighboring area to start a new recording. The illumination of the cameras field of view was controlled by a laser shutter placed on the laser path which would open only after the start of the recording, while the microscope iris diaphragm aperture would restrict the illumination area to the cameras field of view. These two measures were necessary to capture the whole emission light from the samples. Indeed photobleaching prior to recording can occur if the samples have been already illuminated, such as the illumination begins before the camera switches on (loss of the first frames) or if the cameras field of view is shifted to an area which has been already illuminated during a previous recording.

3.2.3 Analysis

Each recording was checked manually; if they presented a too high density of fluorescence spots to permit a good resolution of individual spots, they would be discarded. For GMimPro analysis, movies were first converted into RAW data files with the same software, and then converted to GMV files using GMimPro. The SFDA module was applied using Ms-test at a threshold of 20, a spatial filter of 5x5, FWHM of 224 nm (fitting limit of 1 pixel corresponding to 0.4 μm). Every intensity decay plot was saved in text and bitmap formats, excluding plots whose maximal intensity was under 80 counts/pixels. Since the selected traces show a variation in their signal to noise ratio, an arbitrary limit was chosen to discard the noisier traces. The number of photobleaching steps was also assessed manually and recorded as well as the programs fitting. A minimum of 50 datapoints were collected corresponding to 2500 ms and normalized distributions of photobleaching steps were generated in Excel format. The same batch of recordings was analysed similarly to the GMimPro approach, through the Matlab interface, by the PAFC method.

3.2.4 TIRF microscopy setup

The experiment was carried with an inverted objective microscope, installed on an anti-vibration table. The sample was dried on a coverslip surface mounted on an oil immersion objective lens of 60x magnification (N.A.: 1.4). The light coming out of a 532 nm continuous wave laser was collimated and focused off axis at the back aperture of the objective lens, creating an evanescent wave at the coverslip surface. The emitted fluorescence light was collected by the same objective and passed through a dichroic band multiset (400-535-635) (Horiba Scientific) and an emitter single band

dielectric filter (bandpass: 570-600 nm) (Horiba Scientific), before being recorded by a cooled EMCCD (Electron Multiplying Charge Couple Device) camera (iXon + Andor). Exposure to the laser was controlled through a shutter placed on the laser beam path which opened approximately 1 sec after the recording commenced. Unless otherwise stated, 500 frames at 50 msec were collected on the 128 x 128 frames camera and converted into 16 bits Tagged Image File Format (TIFF) image stack.

3.3 Results

3.3.1 GMimPro analysis

Before using this software, controls using both simulations and real data were employed in order to check the softwares ability to carry such analysis. Three simulations and a sample with four bound labels (curtesy of Dr Matthew Baker) were analysed with GMimPro.

3.3.1.1 Control: simulation with four photobleaching steps

As a positive control, two simulations of 20 fluorescent spots ("Noisy simulation in 4 steps", "Clean simulation in 4 steps") each decaying in four discrete steps were generated and run with Ms-test. Different thresholds were explored to find an appropriate one to use for the tested samples (Table 3.1), under the Ms-test mode.

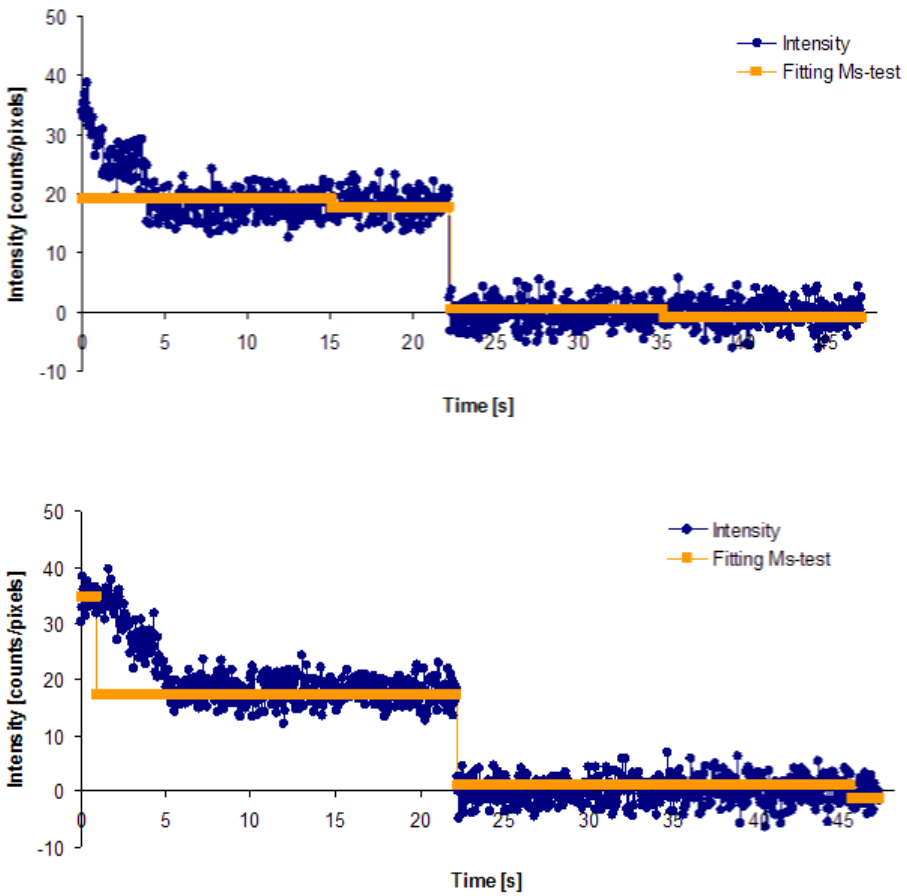


Figure 3.1: Photobleaching traces of 20 spots-4 photobleaching steps-noisy simulation, analysed by GMimPro at a threshold of 20, Ms-test. The raw data is marked in blue and the programs fitting in orange colour.

Examples of photobleaching steps are presented in Figures 3.1 and 3.2 and the Bar-graph 3.3 summarises the results found for these two controls. Results are hugely dependent on the chosen threshold (Equation 3.1) and the "mode" the program is in; "Drop" being the default one, and "Ms-test" which selects spots disappearing in a sequence of separate bleaching steps. When the threshold is set under 10, the Ms-test starts picking up false events and a a value of 30 or above greatly reduces the number of selected fluorescent spots. As a compromise, a threshold of 20 was chosen to carry

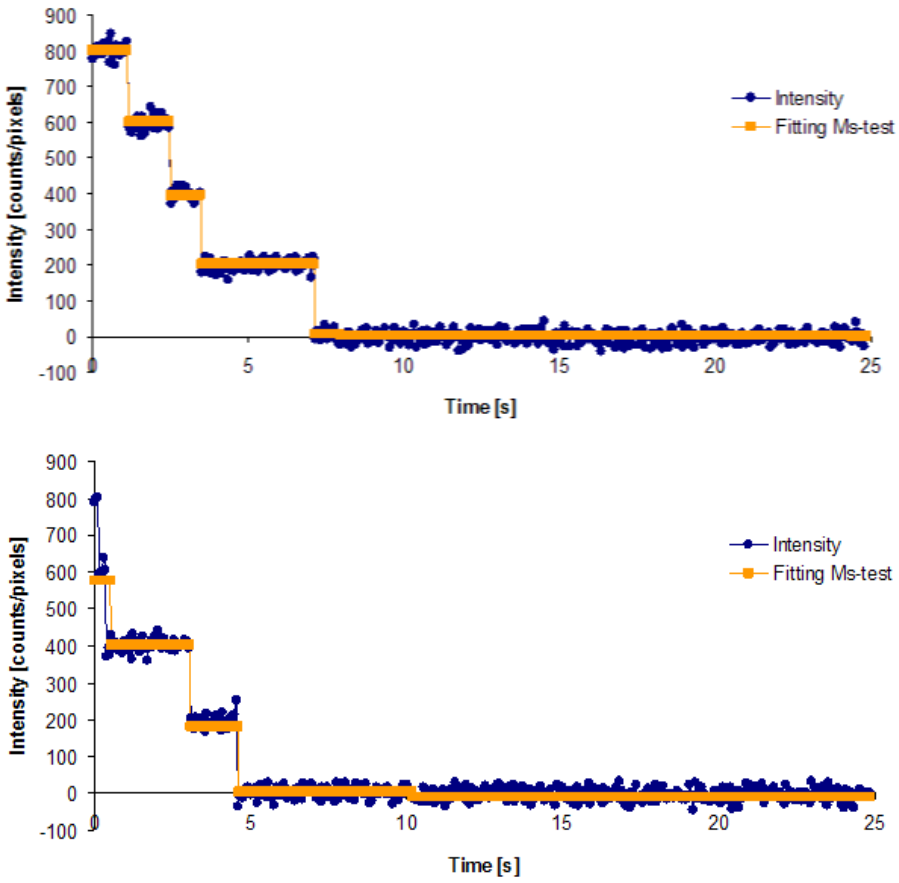


Figure 3.2: Photobleaching traces of 20 spots-4 photobleaching steps-clean simulation, analysed by GMimPro at a threshold of 20, Ms-test. The raw data is marked in blue and the programs fitting in orange colour.

the analysis of the samples.

3.3.1.2 Control: simulation with one photobleaching step

The Spot Simulator plugin (developed in the laboratory of Dr Mark Wallace) of ImageJ was used to generate a simulation of 27 fluorescent spots decaying in a single

	Noisy simulation in 4 steps				Clean simulation in 4 steps			
	Drop		Ms-test		Drop		Ms-test	
	Spots	SNR	Spots	SNR	Spots	SNR	Spots	SNR
Threshold 8	20	7.9	20	10	366	1.3	22	5.9
Threshold 10	20	10	20	10	366	1.3	16	7.7
Threshold 15	20	10	18	9.9	366	1.3	16	7.7
Threshold 20	11	11	14	9.7	337	1.3	15	8.1
Threshold 30	1	5.8	2	8.7	28	2.1	15	8.1
Threshold 35	0	5.8	2	8.7	18	2.5	15	8.1

Table 3.1: GMimPro conditions tested on the two simulations (20 fluorescent spots). The number of detected spots and the signal to noise ratio (SNR) calculated are shown.

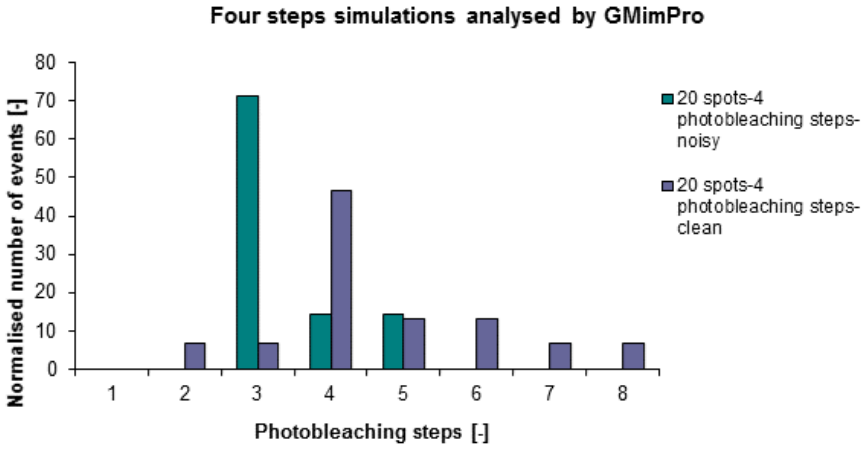


Figure 3.3: Bargraph of the photobleaching steps of the two four steps simulations determined by GMimPro at a threshold of 20, Ms-test. Each movie shows 20 fluorescent spots, each one photobleaching in 4 discrete steps.

step. The conditions (time step, noise baseline, spot peak intensity, etc) were adjusted such as the resulting recording displays fluorescent spot intensity decays similar to the recorded ones. The photobleaching traces with the fitting generated by the program are presented (Figures 3.4, 3.5), as well as a Bar-graph 3.6 which summarises the

GMimPro analysis.

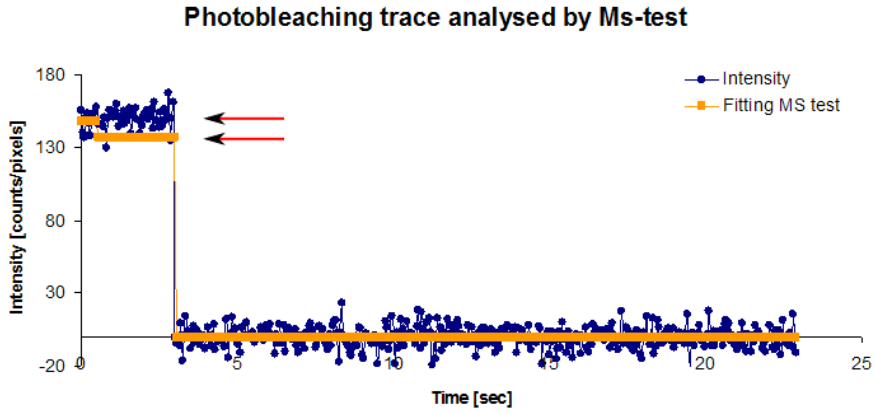


Figure 3.4: Light intensity decrease over time of one of the spots in the simulation movie. The light intensity is marked in blue while GMimPros fitting in Ms-test, threshold 20, of the trace is in orange.

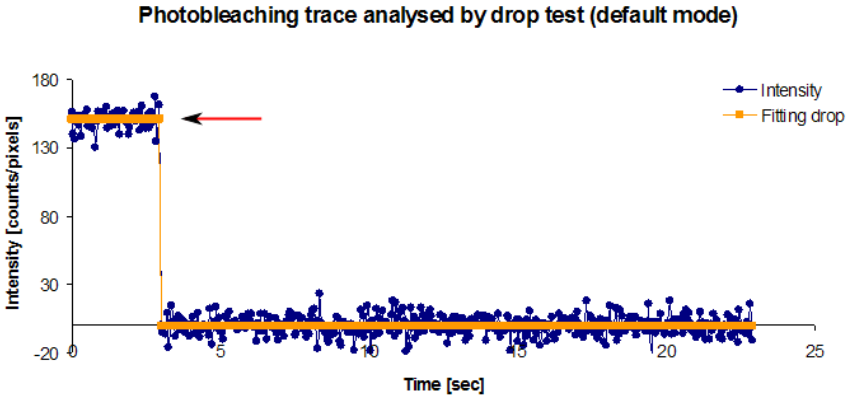


Figure 3.5: Light intensity decrease over time of one of the spots in the simulation movie. The light intensity is marked in blue while GMimPros fitting in drop, threshold 20, of the trace is in orange.

By comparing Figures 3.4 and 3.5, we can notice that the fitting finds an additional step on the Ms-test. It clearly shows that the Ms-test mode fits at least 2 decaying

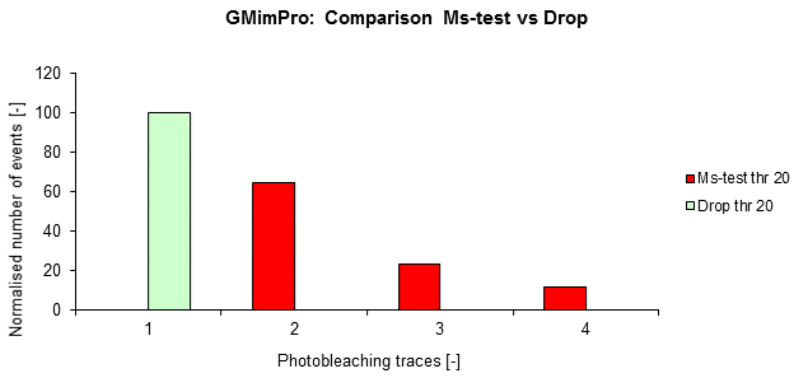


Figure 3.6: Histogram of the counted photobleaching steps of the simulation movie analysed by GMimPro software under two conditions: the Ms-test and the drop test.

steps with the trace, but cannot fit one step by itself. Therefore, the Ms-test will find additional discrete steps to the fitting of the data and cannot distinguish between a single discrete decay in the raw data which greatly limits the ability of the program.

3.3.1.3 Control: four Cy3 labelled DNA sample

The photobleaching traces of pieces of DNA carrying four Cy3 dyes (see Appendix **??**) were recorded similarly as the samples (Figure 3.7). The labelled DNA was diluted in MilliQ water, dried on plasma-cleaned coverslips and recorded with the same settings as the samples. This provides us with a positive, real sample control of the photobleaching of 4 dyes (such as a tetramer) (Bar graph 3.8).

The distribution does not look as the one we should expect from a 4 Cy3 labelled sample. The maximum should be located at 4 with a deacreasing trend towards lower stoichiometry. The shape of the Bar-graph 3.8 indicates a poor step detection probability, or low labelling or prephotobeaching. Provided that the control stoichiometry

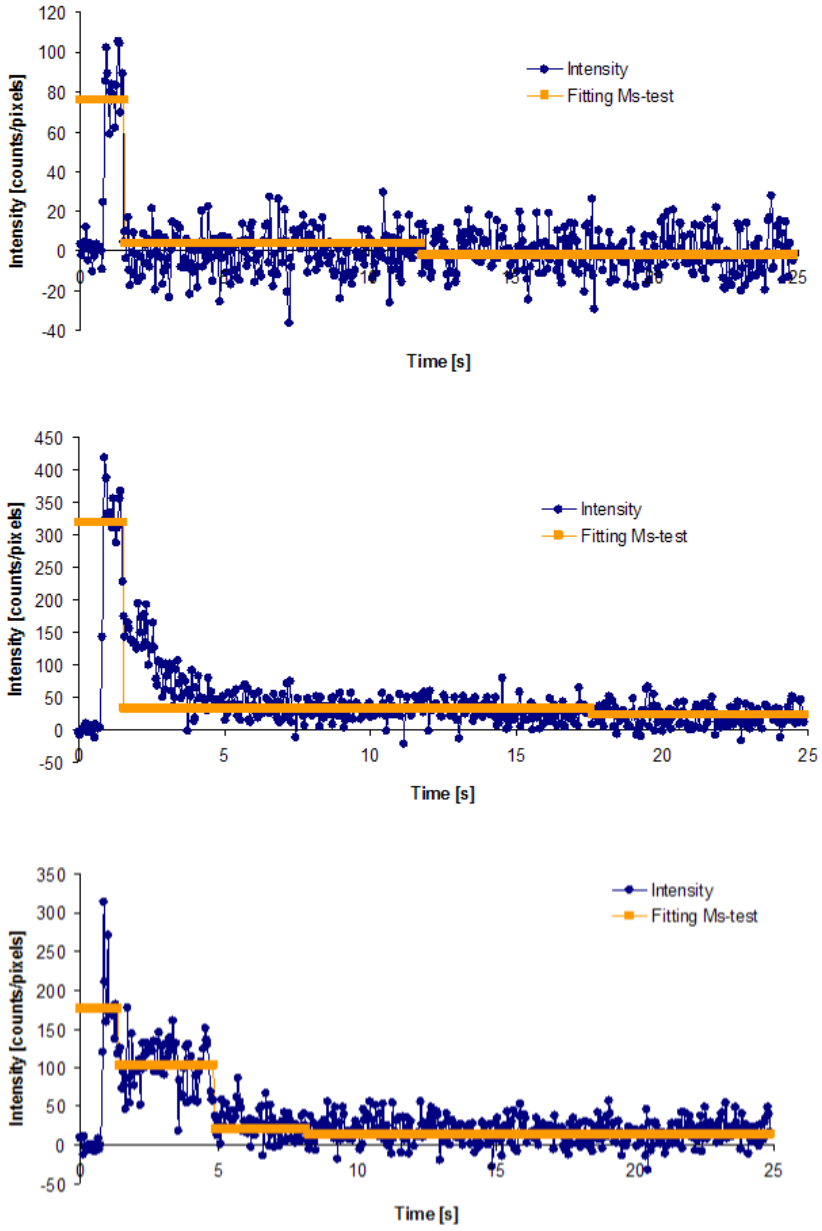


Figure 3.7: Three examples of photobleaching traces of the DNA carrying four Cy3 dyes. The decreasing fluorescent light is represented in blue and the GMimPros fitting (Ms-test, threshold 20) is shown in orange.

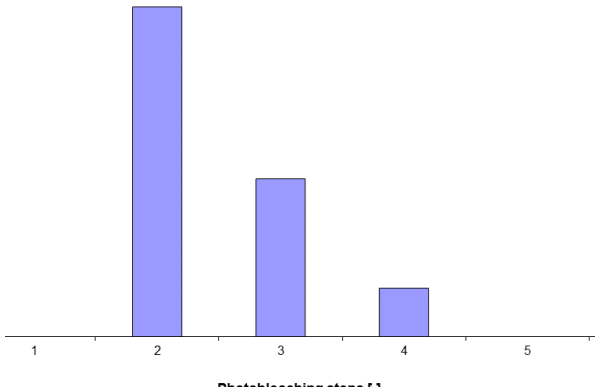


Figure 3.8: Histogram of the counted photobleaching steps of the positive control, the DNA carrying four Cy3 dyes (curtesy of Dr Matthew Baker), analysed by GMimPro.

integrity is not compromised, a low signal to noise or algorithm limitations account for this result.

3.3.1.4 Labelled K_vAP-CL

The reconstitued labelled channel was diluted in 5 mM DM (n-decyl-β-D-maltoside) to disrupt the lipid vesicles and homogenise the solution. Indeed, the number of channels incorporated into lipid vesicles during the reconstitution varies greatly; some vesicles will be channel free and others will contain one or more channels (68). The exact number of incorporated channels per vesicle cannot be controlled during this step. The probability of resolving individual fluorescent spots will be higher if the fluorescent samples are evenly distributed on the surface. Therefore, the sample was first diluted into a detergent solution and dried onto a plasma-cleaned coverslip. The use of plasma-cleaned coverslips was crucial for success: it not only reduces the intrinsic fluorescent background, but also makes the coverslip surface hydrophilic, allowing the sample to evenly spread on the surface for a better dye spatial separation.

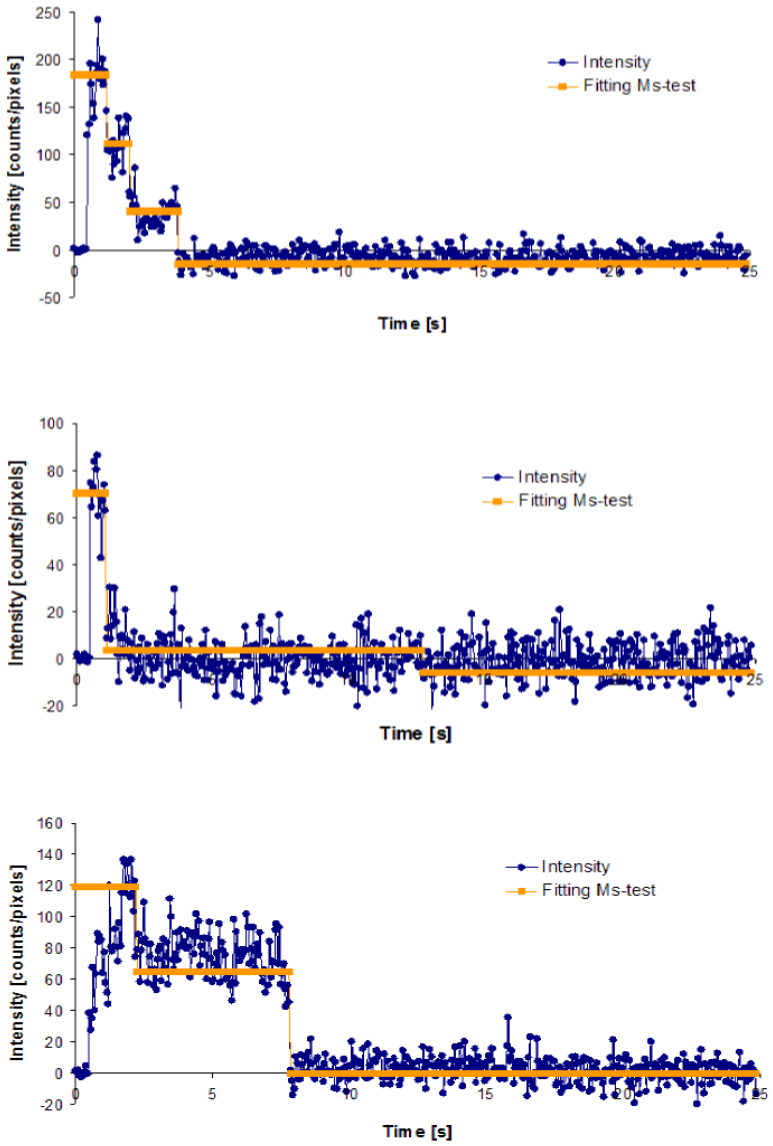


Figure 3.9: Three examples of photobleaching traces of K_vAP-G101C-CL sample. The decreasing fluorescent light is represented in blue and the GMimPros fitting (Ms-test, threshold 20) is shown in red.

Prior to every experiment, the buffer (with detergent) purity was checked by taking a recording with the EMCCD camera. Fluorescent contaminations arising from air or contact with plastic tips occur quickly and it was necessary to use fresh

stocks, and control their purity quite regularly.

Different TMR5M labelled mutants were analysed with the GMimPro software: G101C, A111C, G112C, and L121C. The first three were purified and labelled at the same time with the same protocol. The L121C-CL mutants underwent different purification and labelling protocol. L121C-CL purification 1 and 2 went through the same purification protocol but purification 2 was subjected to additional rounds of IMAC chromatography.

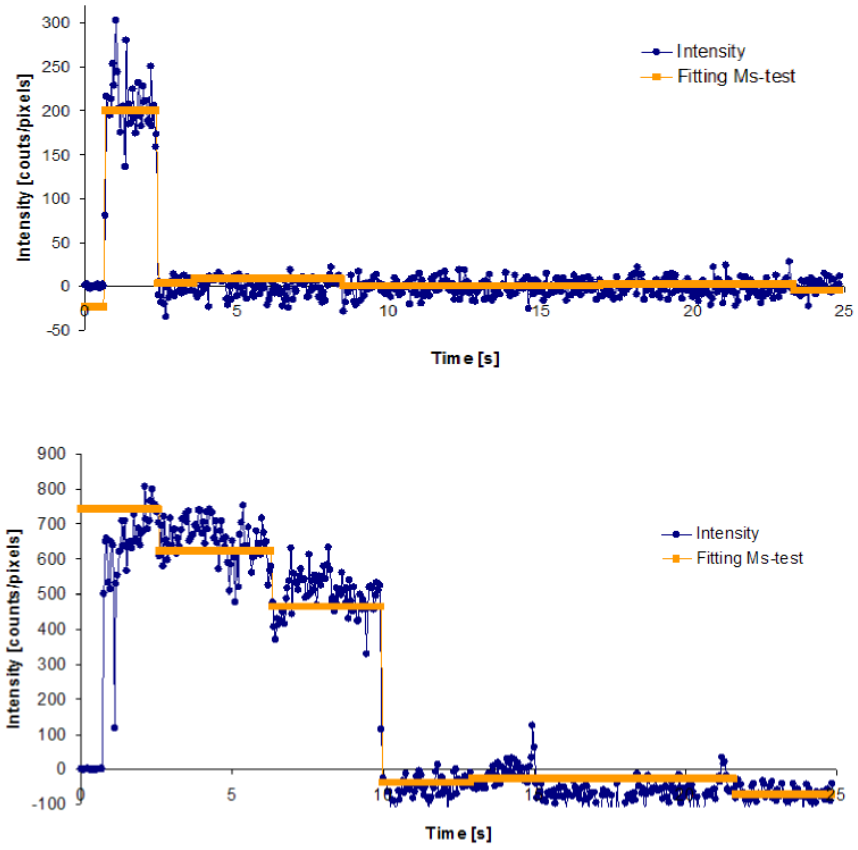


Figure 3.10: Two examples of photobleaching traces of K_vAP-L121C-CL 3nd cycle label sample. The decreasing fluorescent light is represented in blue and the GMimPros fitting (Ms-test, threshold 20) is shown in red.

The L121C-CL cycle samples were initially purified and prepared together. After

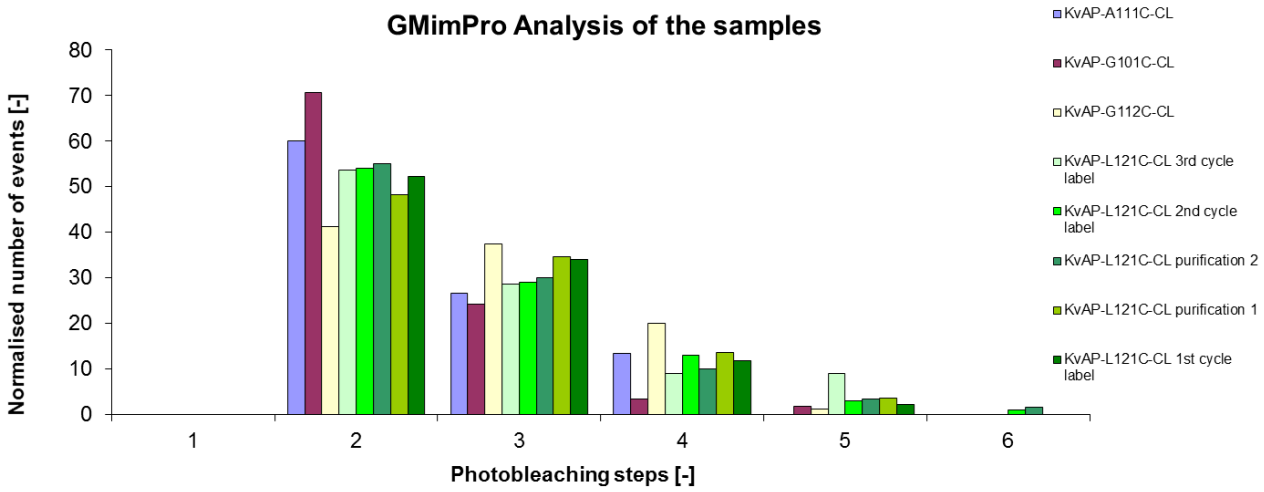


Figure 3.11: Bar graph of the counted photobleaching steps of the samples analysed by GMimPro software (Ms-test, threshold 20).

labelling, the sample was split into three fractions. One was used for a second labelling reaction (after dye purification) ("L121C-CL 2nd cycle label") and another fraction was used for two consecutive labelling reactions ("L121C-CL 3nd cycle label"). The movies were then analysed with GMimPro and Bar-graph 3.11 summarises the results.

On the Bar-graph 3.11, each sample follows the same trend as seen for Bar-graph 3.8: a gradual diminution of the poplulation with the number of photobleaching steps. The predominant labelling stoichiometry was two for every samples; only the difference between the peaks at 2 and 3 stoichiometry for G112C-CL is not as pronounced as for the others. Complete labelling of the protein (four steps) was only found to occur between 10 and 20 % of the cases and 5 or 6 photobleaching steps were also present.

3.3.2 Photobleaching analysis frequency code

3.3.2.1 Controls

The two simulated movies with photobleaching traces decaying in four steps (curtesy of Dr Matthew Baker) were analysed with the in-house software. The positive real control, the DNA labelled with four Cy3 and a negative control, the unlabelled K_vAP-CL were analysed in the same way. The histograms of the four controls are presented in Figure 3.13 with the Table 3.2 resuming the statistical values of the lognormal fit. Some of the photobleaching traces are presented in Figure 3.12.

In both simulations, the software was able to detect four discrete steps in 19 out of the 20 spots presents. Both movies give a similar result, their calculated stoichiometry falls between 4 and 3 (medians 4.1 for the 20 spots 4 photobleaching steps - clean, and 3.48 for 20 spots 4 photobleaching steps - noisy), a discrepancy of 2.5 and 13 % from the real value (Figure 3.13). GMimPro analysis finds the predominant step on 4 (close to 50 % of the population) and 3 (70 % of the population) for the clean and noisy traces respectively. Therefore the in-house program seems to be more robust while handling different sets of data; there is a variation but the addition of extra noise does not seem to skew the analysis.

Regarding the four Cy3 labelled DNA control (curtesy of Dr Matthew Baker), the measured stoichiometry has a median of 4.97 $\pm$ 0.17, which is an overestimation by one. The negative control, performed on unlabelled channel (K_vAP-CL) reconstituted in vesicles has a median of 3.80 $\pm$ 0.34, which indicates that fluorescence background, probably arising from contamination affects sample's data. Nevertheless, its fluorescence intensity and occurence are much lower than for the four Cy3 labelled DNA control, accounting smally on the calculated distribution (Figure 3.13). Moreover,

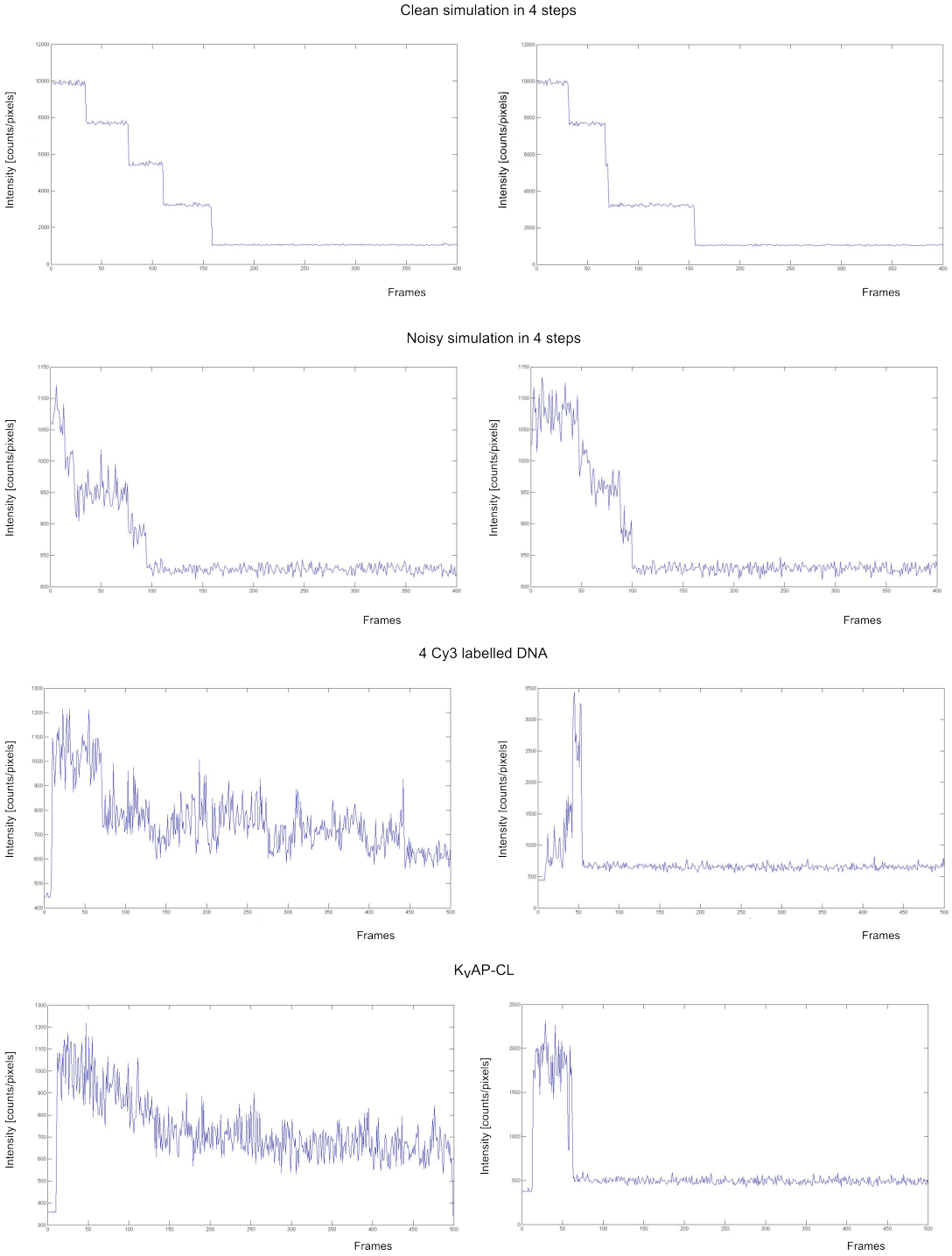


Figure 3.12: Individual photobleaching traces analysed by the Photobleaching Analysis Frequency code for the controls (camera frame rate 50 sec).

these two controls suggest that the software has the tendency to overestimate the stoichiometry.

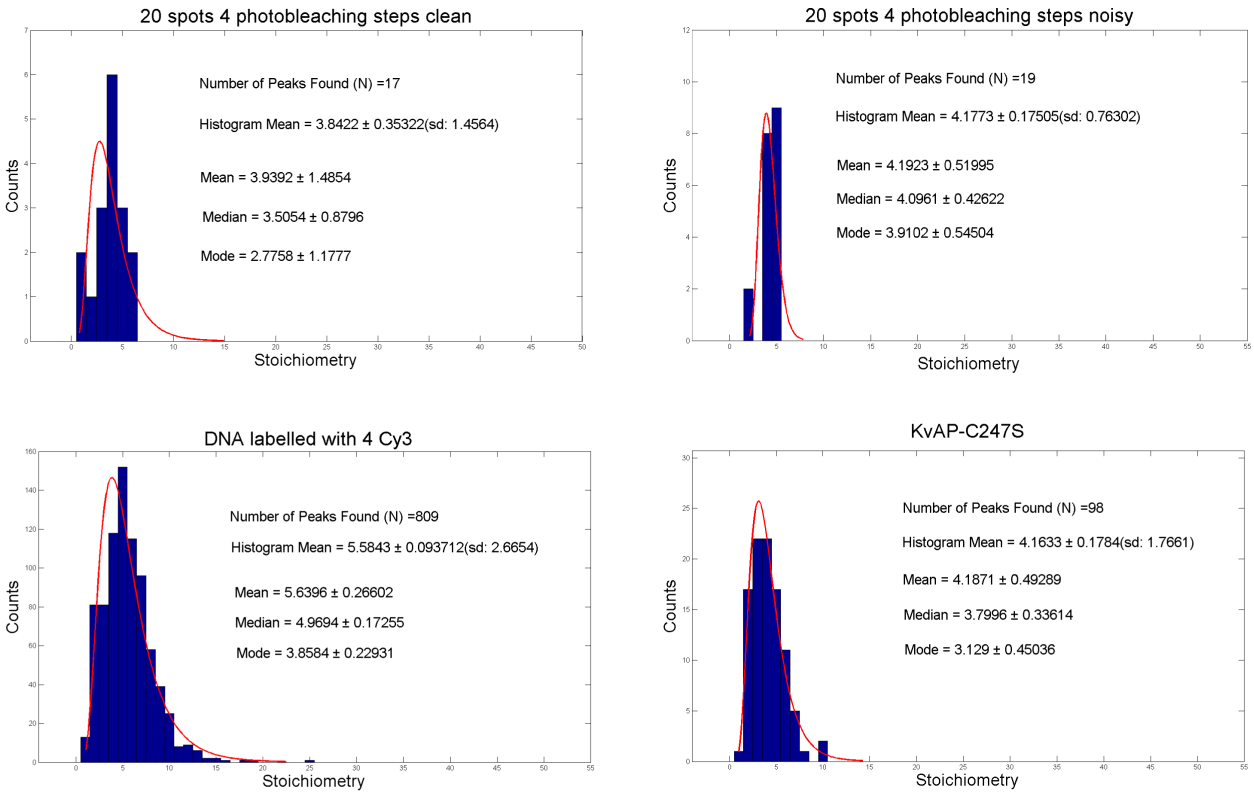


Figure 3.13: Histograms of the four controls analysed by the Photobleaching Analysis Frequency code.

Controls	Samples	Number of spots detected	Median	Error	Mean	Error	Mode	Error
Positive (simulation)	4 steps clean	19	3.51	0.88	3.94	1.49	2.78	1.18
Positive (simulation)	4 steps noisy	19	4.1	0.43	4.2	0.52	3.91	0.55
Positive	Four Cy3 labelled DNA	-	4.97	0.17	5.64	0.27	3.86	0.23
Negative	K_vAP-CL	-	3.80	0.34	4.19	0.49	3.13	0.45

Table 3.2: Statistical values and standard error calculated by PAFC for the controls.

3.3.2.2 Labelled K_vAP-CL

The labelled K_vAP-CL mutants data were analysed by the PAFC method. The program generates histogram fitted with a lognormal fit. The mean, median and mode of the fit for each sample are resumed in Table 3.3. The histograms and the examples of photobleaching traces are showed in Figures 3.14-3.16.

In this analysis, the median of mutants A111C-CL and G112C-CL results in close value. Perhaps this is not surprising because they were labelled at the same time, and both mutants are adjacent to each other, which may imply that the labelling reaction is similar on the S3b-S4 loop, and the orientation of the amino acids does not influence it greatly (Figure 3.16). However, the G101C-CL labelling efficiency seems to decrease compared to A111C-CL and G112C-CL (Figure 3.16). The labelling site is further away of the S3b-S4 loop, perhaps more embedded in the protein and less flexible, which may lead to a decreased cysteine reactivity (Figure 3.17). All median values are higher than the four available labelling sites in the protein. Poor fitting

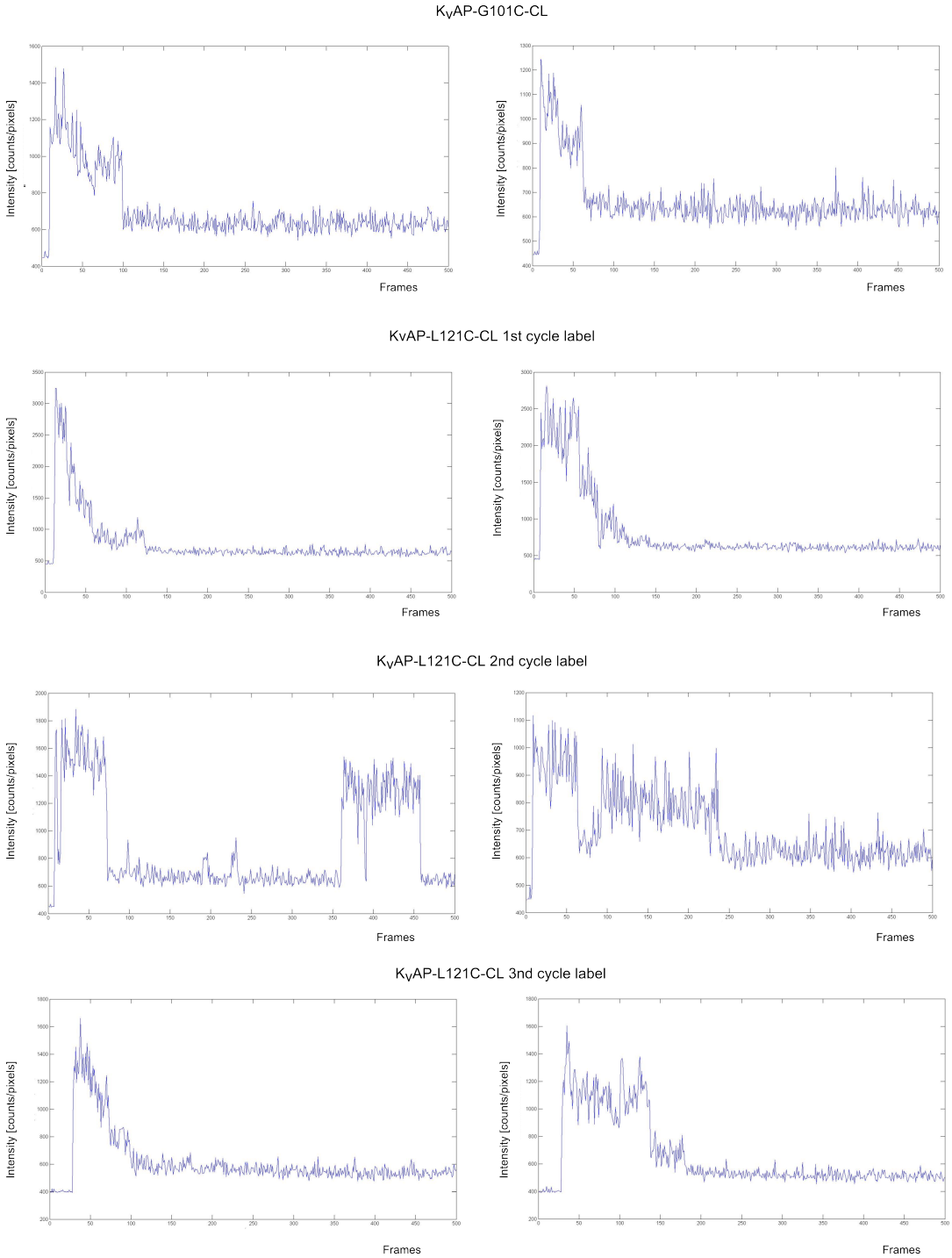


Figure 3.14: Individual photobleaching traces analysed by the Photobleaching Analysis Frequency code (camera frame rate 50 sec).

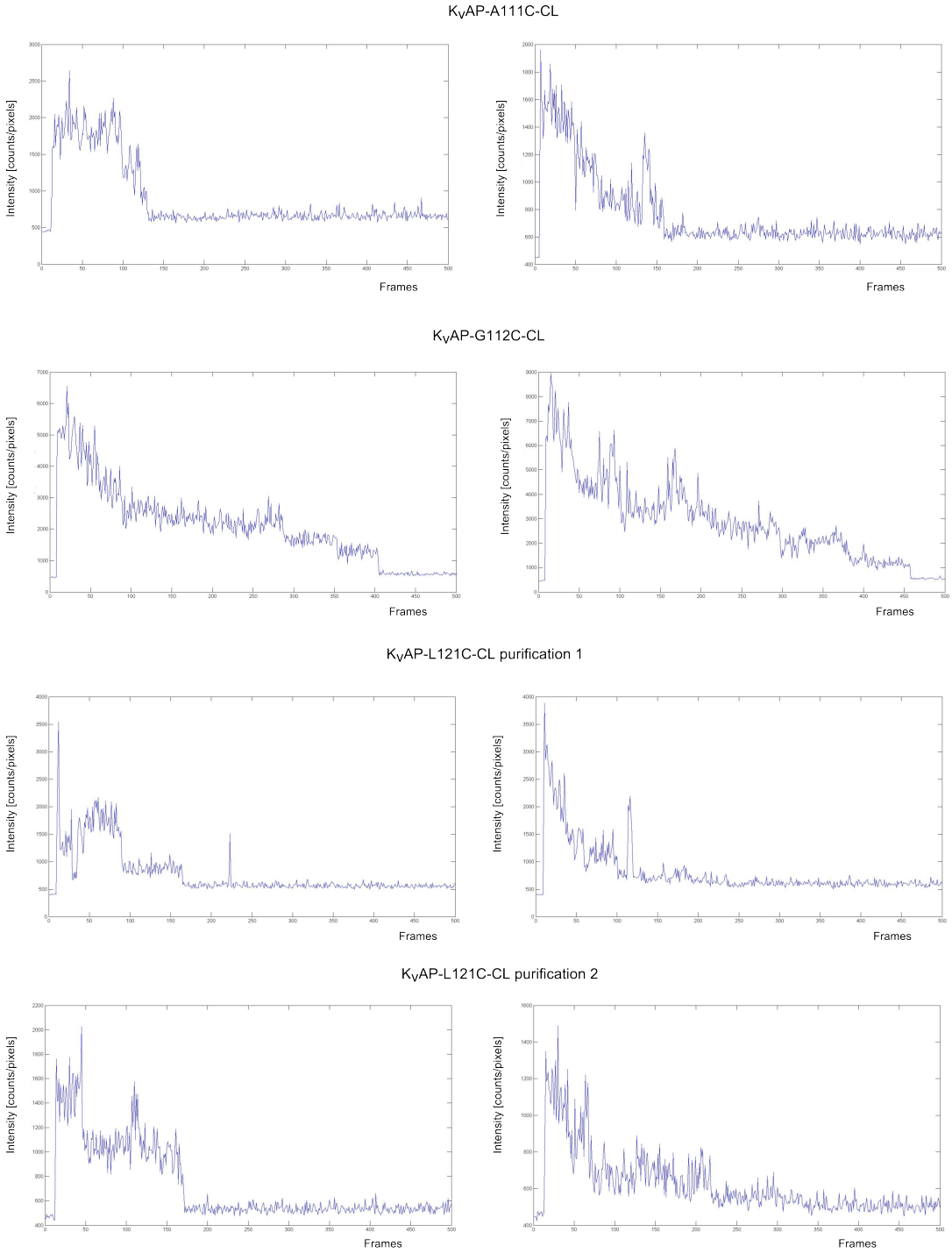


Figure 3.15: Individual photobleaching traces analysed by the Photobleaching Analysis Frequency code (camera frame rate 50 sec).

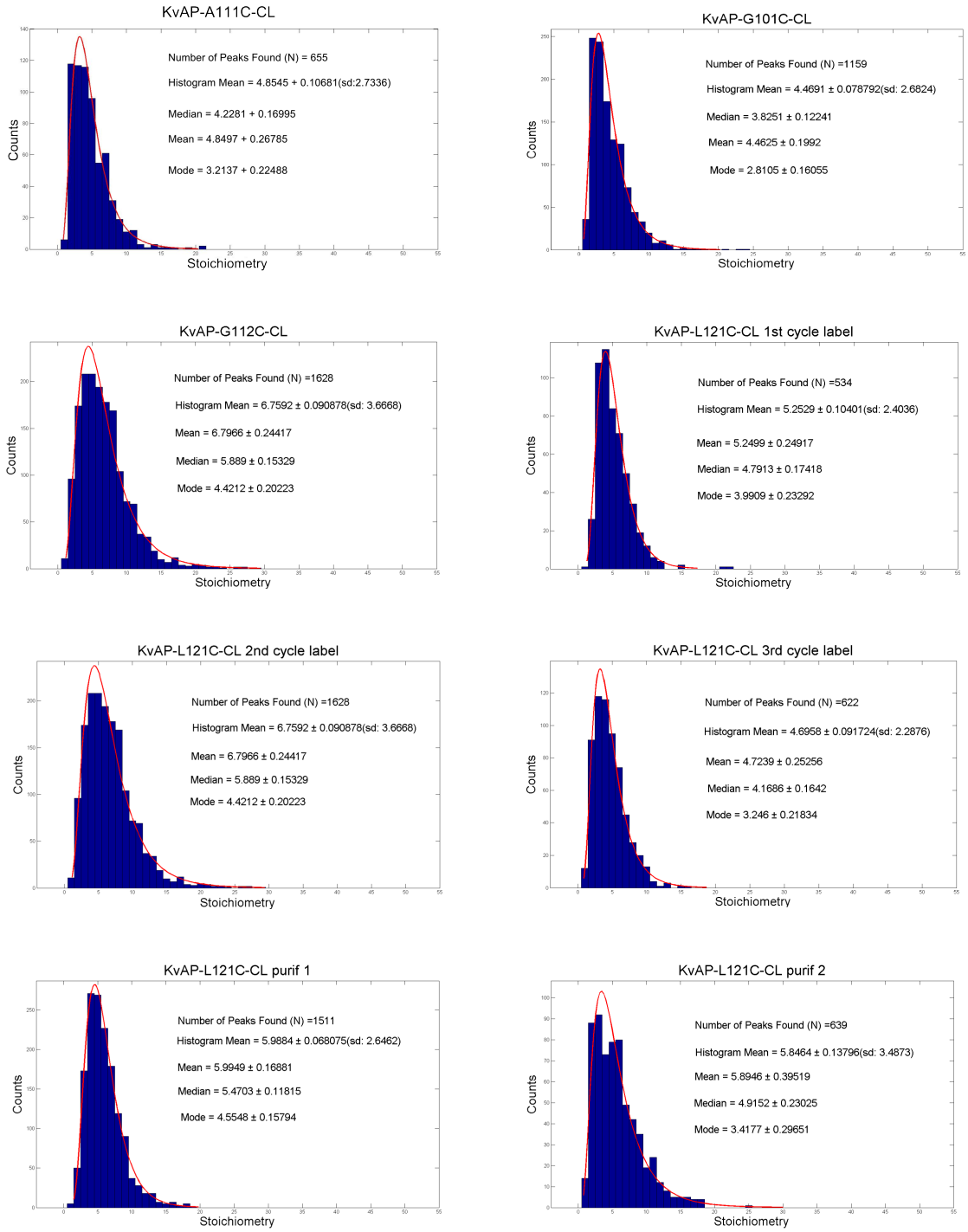


Figure 3.16: Histograms of the labelled K_vAP-CL mutants analysed with the Photobleaching Analysis Frequency Code.

of the program, over-reaction of TMR5M with the protein or presence of fluorescent contaminant are possible explanations. Therefore, a shorter labelling time reaction, a lower dye concentration or a more extensive dye purification through a larger size-exlusion column by example should be tested.

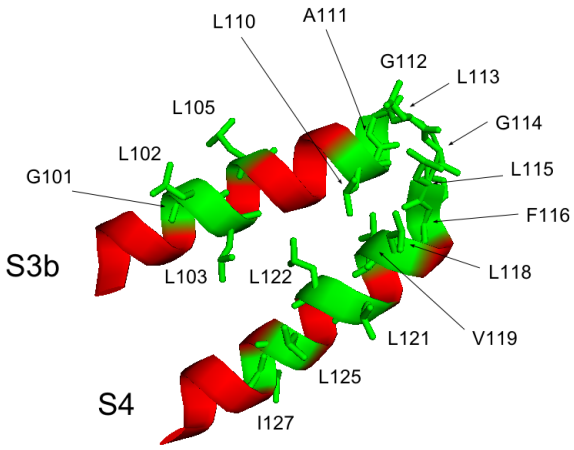


Figure 3.17: Voltage-paddle sensor of K_vAP-CL (S3b-S4 helices) with the residues which were mutated to cysteines.

The results of the three L121C-CL samples which have undergone different labelling cycles are surprising. The sample with the median closer to the ideal tetrameric stoichiometry was the sample which had undergone the most cycles of labelling, while the other two actually show larger values (Figure 3.16 and Table 3.3). Two explanations are possible: either the analysis has failed, or the additional labelling cycles do not have any effect apart from removing some free dyes uncovalently bound to the protein. At the end of the purification, each sample needed to be passed through a size exclusion column and concentrated (removal of the dye through the membrane) for a couple of hours. In addition, the labelled protein was reconstituted using a

Samples	Median	Error	Mean	Error	Mode	Error
K_vAP-A111C-CL	5.92	0.25	6.55	0.36	4.83	0.33
K_vAP-G101C-CL	5.20	0.17	5.87	0.26	4.09	0.23
K_vAP-G112C-CL	5.89	0.15	6.80	0.24	4.42	0.20
K_vAP-L121C-CL 1st cycle label	4.80	0.17	5.25	0.25	4.00	0.24
K_vAP-L121C-CL 2nd cycle label	5.89	0.15	6.80	0.24	4.42	0.20
K_vAP-L121C-CL 3nd cycle label	4.17	0.16	4.72	0.25	3.25	0.22
K_vAP-L121C-CL purification 1	5.47	0.12	5.99	0.17	4.55	0.16
K_vAP-L121C-CL purification 2	3.07	0.12	3.43	0.23	2.46	0.21

Table 3.3: Statistical values calculated by PAFC for the samples tested

large volume during dialysis. The presence of remaining dyes was easily observed by eye during the first two steps, so it seems possible that the 10x more concentrated TMR5M strongly unconvalently interacts with the protein.

3.4 Discussion

3.4.1 GMimPro analysis

Two types of simulations were analysed with GMimPro: two simulations of 20 fluorescent spots decaying in four discrete steps, each one with a different signal to noise ratio (Figures 3.1-3.2). The second type is a simulation of 27 fluorescent spots decaying in a single step (Figures 3.4-3.5).

These two types of control demonstrate that GMimPro has the tendency to underevaluate the stoichiometry. The analysis is dependent on the "mode" (Ms-test, drop

test) the software is in (Table 3.1). One of the main limitations of this analyis is the software incapacity to assess a single photobleaching step to its fit, in the Ms-test (Figures 3.4-3.5). Any tetramer carrying one fluorophore will be thus counted as a double steps, which fasifies the analysis.

The positive control (4 Cy3 dyes attached to a DNA piece, Bar-graph 3.8) presents the same distribution shape as the results (Figure 3.11) which clearly shows that any labelled K_vAP-CL population cannot be reliably assessed. Counting photobleaching events in fluorescence trace depends on the probability of detecting discrete steps by the software. This probability follows a binomial distribution. Three factors may influence it: the signal to noise ratio, the labelling and the algorithm. If the signal to noise ratio decreases, counting discrete steps becomes harder and the distribution starts skewing towards the lowest stoichiometry populations. An algorithm can be itself inefficient in detecting photobleaching events or becomes less adequate at this task with a poor signal to noise ratio too. In this specific case, a higher signal to noise ratio would give better results when analysed by GMimPro, as we can see on Bar-graph 3.3 where the simulation with less noise gives rise to a bell-shaped distribution. The 5 and 6 stoichiometries are certainly caused by samples overlabelling or free dyes, while the absence of the single step peak is due to the algorithm's failure (counted as a double step).

3.4.2 Photobleaching Analysis Frequency Code

3.4.2.1 Controls

In general, the controls give a better result with this analysis method than with GMimPro. The program has a good ability to detect photobleaching events (19 out

of 20 for each simulation movie) and results for the stoichiometry assessment does not seem to be compromise by noisier traces, on the contrary (3.51 ± 0.88 for the "clean" simulation and 4.1 ± 0.43 for the "noisy" simulation). Each distribution has a bell-shaped, as we could expect from these results. However, since the histogram distributions are all skewed to the right, the median of the lognormal fit was taken as the most representative value of the stoichiometry assessment compared to the mode and the mean. This bias indicates a tendency of the algorithm to overestimate the stoichiometry.

3.4.2.2 Labelled K_vAP-CL

The same recordings previously analysed with GMimPro were analysed with the Photobleaching Analysis Frequency Code. Each distribution has the form of a bell-shaped, which is what could be expected from a binomial distribution. The distribution is also skewed to the right which may be caused by overlabelling or presence of remaining free dyes. Nonetheless, my controls have demonstrated that the algorithm has a tendency to overestimate the labelling results. However, the first option should not be entirely ruled out, since it is difficult to completely wash away free TMR5M (Sections 2.29 and 2.5.5.4). Moreover, the results of L121C-CL 1st, 2nd and 3nd cycles can be interpreted as supporting this hypothesis: more purification schemes after labelling are needed to remove free dyes. Similarly, the purity seems to be an important factor as well. The L121C-CL purification 2 had the lowest stoichiometry, of all the samples (3) (Figure 3.16). The second one, L121C-CL purification 1 shows a higher stoichiometry of around 5.5; this confirms that the purity may affect the labelling reaction with the purest sample (L121C-CL purification 1) having a higher protein to label ratio (Table 3.3). But these results are in sharp contrast with the

dye to protein ratio calculated in Section 2.4.7. According to them, the reaction is complete and overlabelling may even have occured.

3.5 Conclusion

The Photobleaching Analysis Frequency Code has definitively proven to be a more reliable and robust software to analyse static fluorescent decaying spots through time. Both positive and negative controls give results closer to the expected one. Moreover, GMimPro is less sophisticated; only photobleaching traces with the fits are produced by the program; the experimentor has to collect all the stoichiometry fits and generate plots, using other programs such as Microsoft Excel. By contrast, the Photobleaching Analysis Frequency Code generates histogram distributions fitted with a lognormal function with the histogram mean, the mean, the median and the mode and their errors. Thus, in addition of giving a more accurate and sensitive analysis, the software is also more straightforward to use. The main issues with the GMimPro software are its inability to distinguish between 1 and 2 steps in the Ms-test mode and its reduced capacity to handle data with background noise.

When the data was analysed by PAFC, each sample produced a different stoichiometry result, something which was absent in the GMimPro analysis. Every one gives rise to a higher stoichiometry value than 4 (with the exception of K_vAP-L121C-CL purification 2), which means that the labelling reaction seems to be completed after 30 minutes and no additional steps were required to fully label the ion channel mutants. The additional fluorescent step read by the program can arise from fluorescent contamination source, despite the care taken to minimize them. Perhaps free TMR5M has not been fully removed from the sample and interacts with the

ion channel through hydrophobic forces. Another possibility would be that the ion channel is still poorly labelled and the step detection algorithm missreads the data. However, the two simulation (positive) controls generate good results, such as the four Cy3 DNA sample. The controls in general have indicated that the number of fluorescent discrete steps in the traces is overestimated by the software, though.

Chapter 4

Combined Electrical and Fluorescent Measurements of K_vAP

4.1 Introduction

4.1.1 Summary of the Chapter

This chapter describes recording simultaneous electrical and fluorescence traces from individual K_vAP molecules present in a DIB (droplet interface bilayer). The first part describes the system set-up and testing. Lipid concentration, buffer composition, osmolarity were varied to optimise the DIB working conditions and to preserve channel functionality. Single electrical traces of K_vAP were also recorded in order to confirm successful incorporation of the channel into DIB and the I/V curve was compared to the published literature. Next fluorescently labelled K_vAP diffusing in the bilayer was

imaged and its diffusion coefficient calculated and compared to that of fluorescently labelled lipids. Simultaneous fluorescent and electrical recordings were then made from K_vAP-CL (K_vAP-C247S, the cysteine mutant of the wildtype channel).

4.1.2 Droplet interface bilayer (DIB)

As described in the introductory chapter, Droplet Interface Bilayers can be used to study membrane proteins in reconstituted systems. The core principle of the technique is based on the self-assembly of lipids at oil/water interfaces. Briefly, a droplet of aqueous solution (100-300 nL) is formed in a mixture of lipids in oil solution, and then brought into contact with a well whose bottom is a hydrogel substrate (Figure 4.2). The lipid hydrophilic heads orientate themselves towards the hydrophilic phase, forming a monolayer coating the droplet and the hydrogel. When the two monolayers are brought into contact, a bilayer is formed (Figure 4.2).

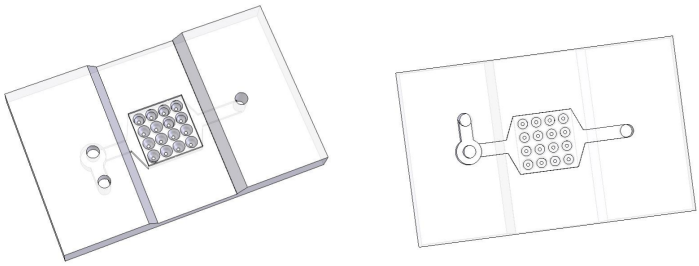


Figure 4.1: PMMA (polymethyl methacrylate) device view from the top (left) and the bottom (right). The 12 wells where the droplets make contact with the agarose gel are located in the middle of the device while the external holes are used to place the electrodes. The device makes 27, 43 and 4.20 mm in respectively in width, length and height.

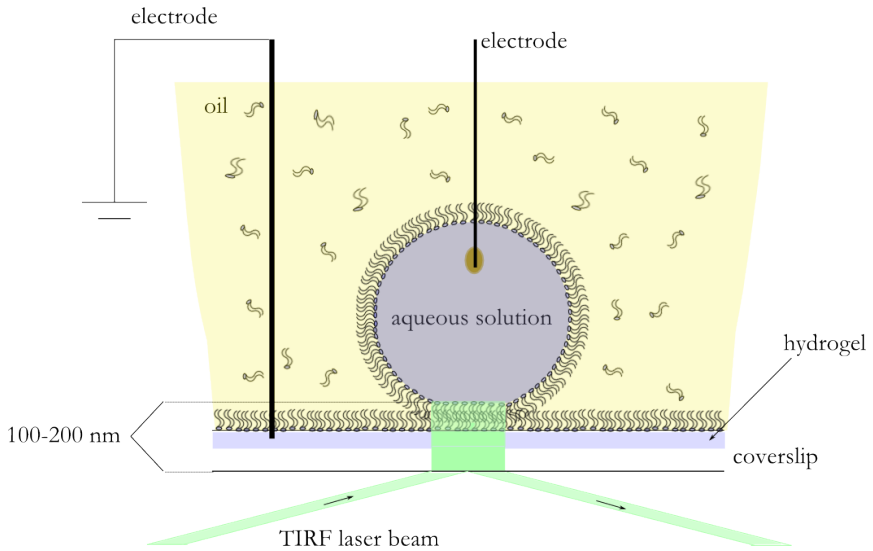


Figure 4.2: A monolayer lipid coated droplet is brought into contact with a planar monolayer sitting on an hydrogel substrate. Two electrodes, one in the droplet and one in the substrate control the voltage across the bilayer. Fluorescent molecules present in the membrane are illuminated through TIRF laser beam (in green).

A 100 μm diameter Ag/AgCl agarose-coated electrode is inserted into the droplet, controlling both the voltage and bilayer area by up and down movements. The primary advantage of this technique is its robustness: the lipid/oil solution provides enhanced stability and extended lifetime to the bilayer due to the presence of a constant reservoir of lipids in incompressible oil. Moreover, membrane proteins can be incorporated into the lipid bilayer, either directly from the droplet solution, or following deposition on the hydrogel surface. In (59), single channel traces from KcsA, $K_v1.3$ and $K_v11.1$ were recorded, following reconstitution of these channels into the bilayer. Most studies using this new technique have focussed on the β-barrel pore forming prokaryotic toxin, α-hemolysin (96, 97). This membrane protein has been used extensively for ion flux measurements in artificial membrane due to its robustness. Other studies have focused more on technique development, such as

the measurement of bilayer capacitance and surface density of membrane proteins (42, 43).

4.1.2.1 System requirements

The lipid concentration in the oil and their quality greatly influence bilayer formation; in general 10 mg/ml gives good results. Detergent plays a role in the electrical stability of the droplet. Osmotic forces across the bilayer also have to be taken into account. Ag/AgCl electrodes have to be manipulated by a high precision micromanipulator in order not to introduce any drift during the electrical recording. Moreover, the set-up has to be installed on an anti-vibration table, in a Faraday cage so as to keep mechanical and electrical noise to a minimum.

4.1.2.2 Coupling with optical imaging

One of the key aspects of this technique is the hydrogel surface that provides a flat support where optical imaging then becomes possible. By controlling the hydrogel substrate thickness (150 nm), fluorescence arising from the bilayer can be imaged by TIRF microscopy. This set-up requires laser light to be focused at the back focal plane of the objective and orientated at an angle greater than the critical angle for TIRF to occur. This can only be achieved through a high numerical aperture (NA) objective. The fluorescence light is collected by the same objective and the removal of unwanted wavelengths is made through a dichroic mirror and an emission filter (Section 4.2.10). The image is then projected onto a charge coupled device (CCD), an array of capacitors specialised into the conversion of photons into electric charges, and recorded by the camera. Ca^{2+} flux through α-hemolysin inserted in DIB has been successfully recorded (17, 45) and fluorescently labelled α-hemolysin has been

tracked in the same system (97).

4.1.3 Membrane protein incorporation via vesicle fusion with a planar lipid bilayer

Membrane protein can be delivered to lipid bilayers through vesicle fusion, a process similar to exocytosis. This process happens in two steps:

1. Swollen vesicles associate with the planar membrane tightly and irreversibly, a step called the prefusion state.

2. Fusion of the vesicle with the bilayer.

In the planar lipid bilayer technique, membrane proteins reconstituted into vesicles are introduced on one side of the bilayer and stirred. If negatively charged lipids are used, the presence of a divalent cation (typically 10-15 mM) is necessary to bring both bilayers in close contact (25). An interaction then occurs between the negatively charged lipids and the divalent cation which forms a bridge between them. This bond has two effects: reduction of the electrostatic repulsion and dehydratation of the headgroups, which diminish this interaction energy barrier (80). Any divalent cations promote the prefusion state but Ca^{2+} is the most efficient, probably due to its size which fits well the interspace between both lipids walls. However, high Ca^{2+} will also promotes vesicle aggregation. Therefore the chosen Ca^{2+} concentration should be a compromise between these two effects.

Vesicles must be swollen in order to fuse with the planar bilayer. This is normally achieved by establishing an osmotic gradient between both sides of the bilayer (the cis side where vesicles are added is hyperosmotic compared to the trans side). In this configuration, once the vesicles are tightly bound to the bilayer, water flows from

the trans side into the vesicle interior, causing swelling (5, 24). Water entry into the vesicle creates an hydrostatic pressure which drives the fusion of the two adjacent bilayers. In general, a 250 mOsm salt gradient will cause fusion of vesicles (5).

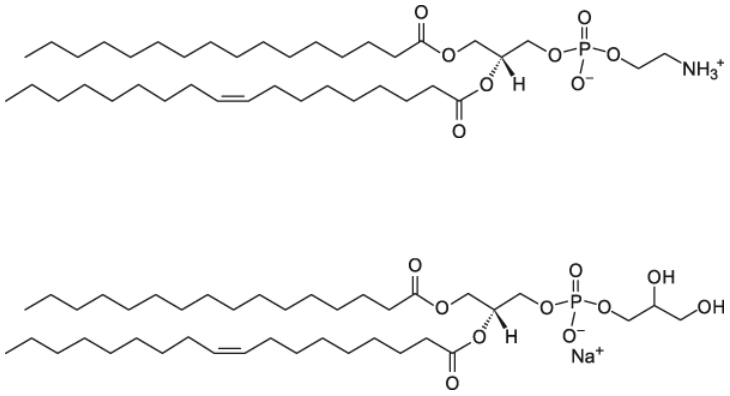
The osmotic gradient influences the fusion rate, but the osmolyte should be chosen with care since its permeability through lipid vesicle will affect the vesicle swelling. The osmolyte should be partially permeant through vesicle membrane to avoid shrinkage of vesicles but not so great to dissipate the gradient through the planar bilayer. Glycerol is a good osmolyte for this purpose; it quickly enters (along with water) the vesicle interior (glycerol and water permeability through membrane are 1.9 nm/sec, and 2 μm/sec, respectively) (5, 68).

4.1.4 Lipids

4.1.4.1 POPE and POPG

The lipidic composition found in bacteria is extremely complex. However, the primary components of this membrane are phosphatidylethanolamine and phosphatidylglycerol and its derivatives. In *E. coli*, PE (phosphatidylethanolamine), PG (phosphatidylglycerol) and cardiolipin form the most abundant lipids in the inner membrane, respectively 70 % and 25 % (79). POPE (1-plamitoyl-2oleoyl-*sn*-glycero-3-phosphoethanolamine) and POPG (1-pal-mitoyl-2 oleoyl-*sn*-glycero-3-phospho-(1'-*rac*-glycerol)) are the standard lipid composition which has been used to study K_vAP, at (3:1) ratio (83). They share the same glycerol backbone and fatty acid chains but differ in headgroup (Figure 4.3). POPE carries a zwitterionic headgroup, self assembles into multilamellar vesicles and can form negative curvature surfaces. Whereas POPG carries a negative charge (pH >5), form unilamellar vesicles and tend to as-

semble into flat surfaces (79).


O
O
O
O
O
O
O
O
O
O
O
O
H
O
O
O
O
O
O
O
O
O
O
O

4.1.4.2 DPhPC

DPhPC (1,2-diphytanoyl-*sn*-glycero-3-phosphatidylcholine) has been found to be particulary good at forming bilayers on supported surfaces (Figure 4.4). Bilayers made of DPhPC show valuable properties: a constant resistance over time, unreactivity towards pH variation, a good resistance against hydrostatic pressure. Further, the lipid is non-autoxidizable (81).

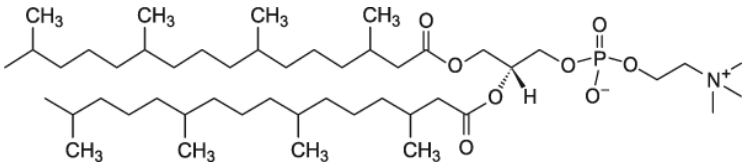


Figure 4.4: 1,2-diphytanoyl-*sn*-glycero-3-phosphatidylcholine chemical structure

4.1.4.3 TRITC-DHPE

TRITC-DHPE (N-(teramethylrhodamine-6-thiocarbamoyl)-1,2-dihexadecanoyl-*sn*-glycero-3-phosphoethanolamine, triethylammonium salt) is lipid carrying a fluorescence (TMR) probe on its head group (Figure 4.5). Its excitation and emission maxima in methanol are respectively 540 and 566 nm.

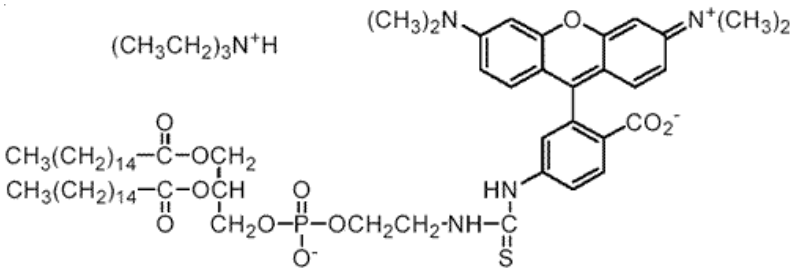


Figure 4.5: N-(teramethylrhodamine-6-thiocarbamoyl)-1,2-dihexadecanoyl-*sn*-glycero-3-phosphoethanolamine, triethylammonium salt chemical structure (adapted from Biotium website).

4.1.5 Analysis of electrical and fluorescence traces

Analysis is straightforward for single channel traces; the evolution of the current is displayed versus the time. In contrast, analysis of single fluorescence molecule needs extraction from recordings post acquisition. The camera records a sequence of frames of fluorescent particles diffusing in 2D. Each one of these snapshots of fluorescent particles needs to be linked together to form trajectories. From these trajectories, the evolution of single molecule fluorescence can be plotted versus time.

4.1.6 Particle tracking

Recordings were analysed with the ImageJ plugin Mosaic (86). ImageJ is a Java-based software developed for image processing at the National Institute of Health (NIH). This plugin detects and analyses particle trajectories moving in 2 dimensions and is based on the assumption of small feature points (compared to background variations). It can handle fast moving objects, strong intensity fluorescence variation, long time tracking and events such as occlusion, entry or exit. Moreover, the algorithm does not require any prior mathematical modeling and is self-initialising.

The plugin starts by filtering each image frame to correct from artifacts such as discretization noise and uneven illumination. Then, the plugin looks for local intensity maxima on each image in the recording. The position of each potential maximum is refined, based on the assumption that its true geometric center is located within a small offset of the local intensity maxima. In the next step, intensity moments of 0 and 2nd orders are calculated for each candidate in order to discriminate any non-particle. Single particles will give rise to an intensity momentum different from clustering or aggregation. Once every particle candidate has been checked, constructing trajectories between each frame can start by linking the detected particles on each frame to each other. This step is done by using a particle matching algorithm. Each frame is coupled with its subsequent one, and each potential particle on one frame is assigned to its closest neighbour which has not already been assigned on the other frame. An optimal set of links between particles is found; by keeping their distance to a minimum (parameter L entered by the user), through iteration the minimal trajectory between frames is kept over the other possibilities.

Five parameters are entered into the program which will dictate the output of the analysis, 3 to identify the bright particles and 2 to link the data of each frame together to build trajectories: the approximate radius [pixels] of the particle, the cutoff score [-] which discriminates the non-particle, and the percentile [%] which corresponds to the brightness of the prospective particles. Links between particles in different frames, L are then created subjected to the maximum displacement [pixel] and the link range [frames] that determines the number of subsequent frames taken into account to link frames.

4.1.7 Lateral diffusion coefficient

The lateral diffusion coefficient (D_{lat}) characterises the movements of a particle. It is a measure of how freely the particle diffuses in its media. The size of the particle, the temperature, the thickness and the components of the lipid bilayers are parameters which influence the behaviour.

The mean square displacement (MSD) of a particle moving in 2 dimensions is given by the formulae below.

$$\Delta x_i(\Delta t) = x_i(\Delta t) - x_{i-1}(\Delta t) \tag{4.1}$$

$$\Delta y_i(\Delta t) = y_i(\Delta t) - y_{i-1}(\Delta t) \tag{4.2}$$

- Δ $x_i(\Delta$ t) and Δ $y_i(\Delta$ t) represent the displacement of the particle along the x and the y axis respectively from step i to i+1. The trajectory undergone by the particle is fractioned into N steps.
- Δt: time interval [s]

For an individual step, the displacement is defined as the sum of the particle displacement on both axis:

$$r_i(\Delta t)^2 = (\Delta x_i(\Delta t))^2 + (\Delta y_i(\Delta t))^2 \tag{4.3}$$

If the sum of all steps along the particle trajectory is taken into account, the mean square displacement is:

$$MSD = \frac{1}{N}\sum_{i=1}^{N} r_i^2(\Delta t) \tag{4.4}$$

- N: number of steps

The lateral diffusion coefficient is linked to the MSD in two dimensions by:

$$MSD = 4D_{lat}\Delta t \tag{4.5}$$

- Δt: time interval

4.2 Material and Methods

Substrate buffer:

0.75 % (m/v) of low melting point agarose was diluted in ultrapure water (MilliQ filtered) and briefly vortexed. The solution was molten and used at 90°C.

Rehydratation buffer:

2 % (m/v) of low melting point agarose was diluted in 150 mM KCl, 10 mM HEPES, pH 7.0 buffer and briefly vortexed. The solution was dissolved by boiling and used at 90°C.

4.2.1 Lipid preparation for electrical recordings

(3:1) POPE (1-palmitoyl-2-oleoyl-*sn*-glycero-3-phosphoethanolamine)/ POPG (1-palmitoyl-2-oleoyl-*sn*-glycero-3-phospho-(1'-*rac*-glycerol)) in chloroform stock solution:

Lipids were purchased from Avanti Polar, in powder. Immediately after opening, each lipid was dissolved in chloroform (final concentration: 25 mg/ml) and mixed at a ratio of (3:1) POPE:POPG. 200 μl stock solutions of the mixture were aliquoted and kept at -80°C.

(3:1) POPE:POPG in hexadecane stock solution:

Once at 20°C, the stock solution was opened. The chloroform was evaporated under a gentle N_2 stream and the dried lipids were vacuum down for 1 hour. Hexadecane was added to a measured lipids concentration of 9.5 mg/ml and the mixture was thoroughly vortexed. The stock solution was kept for 1-2 days.

4.2.2 Lipid preparation for fluorescent lipids

DPhPC (1,2-diphytanoyl-*sn*-glycero-3-phosphocholine) and TRITC-DHPE (N-(6-tetramethylrhodaminethiocarbamoyl)-1,2-dihexadecanoyl-*sn*-glycero-3-phosphoethanolamine, triethylammonium salt) chloroform stock solutions were prepared as above.

Day stocks: The aliquots dissolved in chloroform were unfrozen and used only after having reached 20°C. 38 μl of DPhPC (concentration of 9.5 mg/ml in chloroform), 0.6-64 μl of TRITC-DHPE (concentrations ranging from 51 ng/ml to 0.51 mg/ml in chloroform), and 40 μl of chloroform were quickly mixed (end concentration: 0.12-0.0000012 % TRITC-DHPE/DPhPC). Chloroform was then evaporated under a gentle N_2 stream and the dried lipids were vacuum down for 1 hour. Hexadecane was then added to a measured final lipid concentration of 9.5 mg/ml. The lipids were then vigorously mixed at 70°C for two minutes.

4.2.3 DIB preparation for experiments with fluorescent lipids

The protocol is identical to the ones used for K_vAP, with a minor modifications. The rehydratation buffer contains 2.5 % of molten Agarose. The buffer used was 0.5 M KCl, 10 mM HEPES, pH 7.0.

4.2.4 Samples preparation

After thawing, the samples were diluted in 150 mM KCl, 10 mM HEPES, 2 mM $CaCl_2$, 150 mM glycerol, pH 7.0, and briefly sonicated and vortexed. The diluted and stock solutions were kept at 4°C; the diluted solutions were freshly prepared every day.

4.2.5 Plasma-cleaning of the coverslips

Prior to all experiments, coverslips (Menzel-Glzer, 24 x 40 mm) were plasma-cleaned using a Plasma System FEMTO, Diener Electronic (1.5 bar O_2, 950/1000 power for 7.5 min). This procedure involves the use of an energetic plasma created by ionization of O_2 through a high frequency field (from kHz to MHz).

4.2.6 Cleaning of PMMA (polymethyl methacrylate) and equilibration device

The devices were sonicated in 30 % (v/v) ethanol in ultrapure water for at least 20 min in cleaned glass beakers. The devices were subsequently rinsed in 10 % (v/v) isopropanol, washed in 0.01 M NaOH in ultrapure water for 10 min upon stirring, and sonicated in 30 % (v/v) ethanol for 30 min.This procedure was followed by 4 washing steps for 20 min upon stirring in ultrapure water. The protocol is a modified

version of a previously published protocol (109).

4.2.7 DIB preparation for experiments with K_vAP

140 μl of molten substrate buffer was spin-coated onto a plasma-clean coverslip at 4000 rpm for 30 seconds, by a Model WS-650MZ-23NPP/LITE (Laurell Technology Corporation). The coverslip was immediately mounted on the bottom of a PMMA (polymethyl methacrylate) device and the whole was placed on the heating stage at 40°C. The resulting dried agarose layer has a thickness less than 200 nm, so that the supported bilayer remains within the evanescent field created by the TIRF. 200 μl of molten rehydratation buffer were pipetted through the outside channels of the PMMA device, to create an agarose gel layer in the neighboring space outside the wells. This second agarose layer sits on top of the substrate agarose, allowing ions and water to diffuse to the bottom layer. Immediately afterwards, the wells were filled with 40 μl of 9.5 mg/ml lipids dissolved in hexadecane. The PMMA assembled device was then left for 30 minimum to allow lipid monolayer formation on the substrate. The device was then attached to a moving headstage on an inverted objective microscope, installed on anti-vibration table. A Ag/AgCl electrode was inserted in one of the outside channels (the grounding electrode), in direct contact with the substrate layer.

4.2.8 Droplet preparation

The diluted sample was briefly sonicated and pipetted in the same lipid mixture, 9.5 mg/ml (3:1) POPE:POPG in hexadecane, in a 1.3 nL droplet with a 2 μl pipette and kept in an equilibration tank for at least 30 min. This step was necessary to allow the monolayer formation at the water/lipid interface.

4.2.9 Electrical recordings

The droplets were pippetted into a well, and upon contact with the substrate layer, a lipid bilayer spontaneously formed between the two monolayers. Upon bilayer formation, a Ag/AgCl electrode agarose-coated tip was carefully inserted on the top of the droplet (sample electrode). Through a micromanipulator (NMN21, Narishige), fixed in a Faraday cage, the bilayer size could be changed by lowering or raising the sample electrode. Ionic currents were recorded with an Axopatch 200B amplifier (Molecular Devices) and digitized through a Digidata 1440A (Molecular Devices). The currents were analysed with the Axopatch 10.2 or the pClamp software, and filtered with a low-pass Gaussian filter (cut-off: 200 Hz).

4.2.9.1 I/V curve

The recordings showing single channel data were selected and each single channel amplitude value was saved in Excel software. Knowing that the published I/V curve of K_vAP is linear (33, 83) and at 0 mV, no current passes through the channel, a mean of the amplitude of the single channel events at 0 mV was taken as the general current offset. This current offset was subtracted to the recorded amplitude single channel events at different voltage and an I/V curve was plotted.

4.2.10 TIRF microscopy setup

The experiment was carried with an inverted objective microscope, installed on an anti-vibration laser table. The DIB was placed in a Faraday cage on a x, y directions moving headstage mounted on an oil immersion objective lens (Plan Apo TIRF 60x, 1.45 NA, Nikon) of 60x magnification. Prior to experiments, an index matched im-

mersion oil drop (Zeiss, Immersol TM) was pipetted onto the objective. Once bilayer formation was observed through a 4x objective, focus on the bilayer edge with white light was achieved by very carefully raising the 60x objective. A 532 nm continuous wave laser (Compass 215M) illuminated the bilayer and recordings were made. The laser light was collimated and focused on the back aperture of the objective lens parallel to the optical axis, creating an evanescent wave at the coverslip surface. The emitted fluorescence light was collected by the same objective and passed through a XF2055 (Horiba Scientific) dichroic mirror and a D605/55m (Chroma Technology Corp) emission filter, before being recorded by a cooled EMCCD (Electron Multiplying Charge Couple Device) camera iXon+ (DU-860E-CS0-#BV) (Andor Technology). Unless otherwise stated, 500 frames at 50 ms or 1000 frames at 20 ms were collected on the 128 x 128 frames camera and converted into 16 bits Tagged Image File Format (TIFF) bitmaps. Recordings were analysed using ImageJ software.

4.2.11 Particle tracking and lateral coefficient diffusion calculation

Trajectories of the particle tracking with the Mosaic plugin were calculated with the parameters, a particle radius of 2 [pixels], a cutoff score of 3 [-], an intensity percentile of 0.1-1 %, a maximum step length of 10 [pixels] and a link range of 1 [frames]. Tracks longer than 25 frames were selected and their x and y displacements loaded into Igor Pro software (WaveMetrics). A plot of the MSD (mean square displacement) versus time was calculated. Its derivative (taken up to the 15 first points) divided by 4 was taken as the MSD value for the particular trajectory. The lateral diffusion coefficient was calculated by averaging the MSD over all trajectories.

4.2.12 Single particle trajectories and bulk fluorescent intensity analysis

The trajectories of the particles were detected with the Mosaic plugin with the same parameters used for particle tracking. Events detected on areas outside the bilayer were discarded during the analysis. Fluorescent intensities trajectories were analysed in Excel (Microsoft). The fluorescent intensity from every detected particle at each frame was plotted against time, along the voltage steps.

In order to construct histograms, fluorescent particles were categorized according to their corresponding voltage value (voltage positive, voltage negative, voltage=0), in every automated protocol. The overall fluorescent intensity arising from every detected particle for each category was normalized and plotted as a histogram.

4.3 Results

4.3.1 DIB formation

The published functional data of K_vAP in planar lipid bilayers demonstrated electrical activity in 150 mM KCl, 10 mM HEPES, pH 7.0 upon voltage activation, (83). These results have also been successfully reproduced with the planar lipid bilayer (see Section 2.4.5). However, different conditions were required to result in a stable droplet hydrogel system, along with successful vesicle fusion. Membrane proteins can be incorporated into the lipid bilayer either through the agarose layer or through the droplet. The second solution has always seemed preferable since all previous work on vesicles incorporation has been carried on the water phase (5, 24).

The two Tables 4.1, 4.2 describe the parameters exploited in this study to optimise this experiment.

[KCl] in hydrogel layer [mM]	[KCl] in droplet [mM]	[Glycerol] in hydrogel layer [mM]	[Glycerol] in droplet [mM]	[Lipids] [mg/ml]
150	15/150	-	-	7.0
15	15/150	-	-	7.0
150	150	-	-	8.0
15	150	-	-	8.0
150	15/150	-	- /5.1	9.0
15	15/150	-	- /5.1	9.0
15	15/75/150	-	- /5.1	9.0
2000	-/15/150/2000	-	-	9.5
2000	- /15/150/1000/1500/2000	-	-	9.5
1000	1000/1500/2000	-	-	9.5
1000	800/1200/1000	-	- / 2.5	9.5
1000	800/1000/1200	2.5	- / 2.5	9.5
1000	1000/1200	2.5	- / 1.26 / 1.7 / 2.5	9.5
1000	350/1200	2.5	1.26 / 1.7 / 2.5	9.5
150	150/350	3.8	1.26 / 1.7 / 1.83 / 3.8	9.5

Table 4.1: The droplets were incubated in the lipids/oil mixture for 20 min prior the experiment. 10 mM HEPES, pH 7.0 buffer was used in the rehydratation layer, in the droplet, and in the sample (K_vAP-G112C-CL) as well.

Over the course of the experiments, it was noted that bilayers whose droplet has been incubated for 20 min were more stable than those incubated for 10 min. 20 min corresponds to the minimum incubation time to allow the formation of stable lipid monolayer on the aqueous surface. Later on, the incubation time was extended up to 30 min to give sufficient time for the experiment preparation, without any changes in the droplet success rate. An equimolar salt concentration on both sides of the bilayer also gave rise to good stability. 150 mM KCl in 10 mM HEPES pH 8.0 was chosen as the salt concentration since it was used in the published functional analysis

[KCl] in hydrogel layer [mM]	[KCl] in droplet [mM]	[$CaCl_2$] in droplet [mM]	[Glycerol] in droplet [mM]	[Lipids] [mg/ml]
50	100	2/20	-/50	7.11
50	100	2/10	25	10
50	100	2	25/50/75	10
150	150/250	2	125/250	10
50	100	-	25/59/75	10
150	150	2	125/250	10
50	100	2	100	10
100	100	2	125	10
150	150	2	100/150/200/250	10

Table 4.2: The droplets were incubated in the lipids/oil mixture for 20 min prior the experiment. 10 mM HEPES, pH 7.0 buffer was used in the rehydratation layer, in the droplet as well.

of K_vAP. 10 mg/ml of (3:1) POPE:POPG in hexadecane was kept as the standard concentration, since bilayers form and have a good stability at this concentration (60). A very small amount of $CaCl_2$ (2 mM) was added to the droplet buffer. $CaCl_2$ in 2-20 mM concentration is normally added in PLB experiments to assist vesicle fusion. However, because the presence of Ca^{2+} can interfere with the K^+ currents through the ion channel and enhance vesicle self aggregation, the concentration was kept low.

Glyercol was added last to the system and its concentration was varied from 100 mM to 300 mM (68). No major differences were observed by changing the glycerol concentration, in bilayer stability or ion channel incorporation.

Another incorporation methodology also exists using membrane proteins solubilised in detergents and diluted to the point that detergent concentration is under 10^8 molecules per ml. However, vesicle incorporation was chosen for this study because ion channels are frail and sensitive proteins; the removal of detergent through dilution (to a value below the detergent CMC) may cause protein precipitation.

4.3.2 Electrical recordings

K_vAP-CL and K_vAP-L121C-CL were successfully incorporated into the bilayer in the DIB system and recorded at the single molecule level (Figures 4.6 to 4.8). As mentionned in Section 2.1.3, the L121C mutation is thought to be a particulary well suited site to investigate the mobility of the voltage-sensor, therefore we concentrated our efforts on this particular one.

As soon as currents arising from channels were detected, the electrical traces were recorded and the voltage was manually shifted. The same protocol was applied: the voltage was increasingly stepped up and down. An observation was made in (89) that K_vAP channel exhibits a longer recovery time following a depolarizing step in POPE:POPG than in DPhPC lipids. Therefore, each voltage step was followed by a resting time where the voltage was kept at 0 mV for as long as the precedent step has lasted, in order to avoid any inactivation of the channel.

4.3.3 I/V curve

From single channel recordings (see Figures 4.6 to 4.8), an I/V curve was plotted, to confirm the channel identity and functionality (Figure 4.9). The calculated conductance of K_vAP is 240 $\pm$ 80 pS.

The two reported I/V curves in the literature are also based on single channel events from K_vAP-CL (33, 83). They were calculated on the K_vAP wild-type in (3:1) POPE:POPG decane bilayer in PLB. The two conductances, 170 pS and 150 $\pm$ 26 pS are not very far from the one presented here: 240 $\pm$ 80 pS and statistically signifiant. Three factors might explain this difference: two mutants have been used to calculate the I/V cure, the DIB was employed instead of PLB and hexadecane

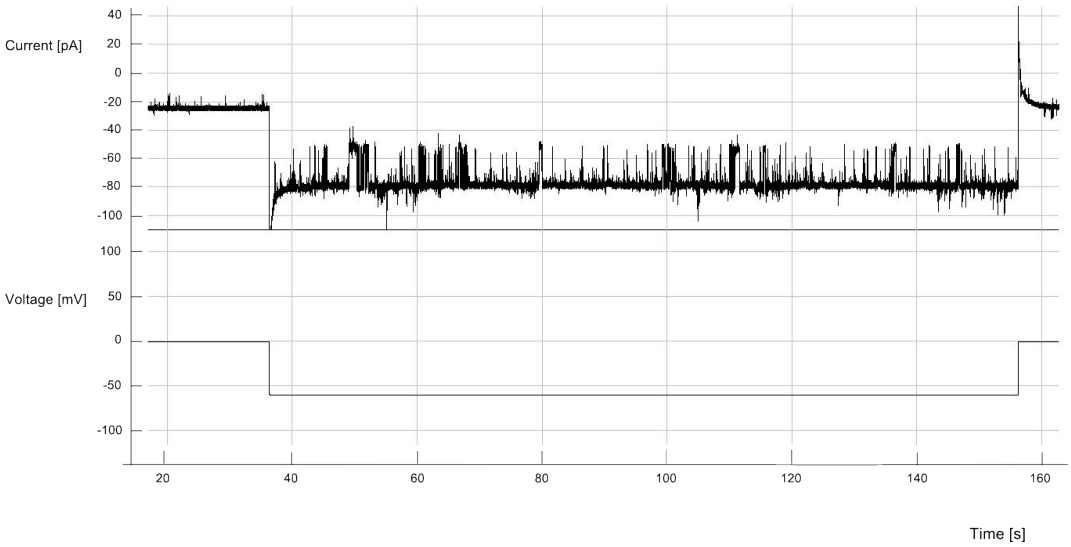


Figure 4.6: K_vAP-CL single channel events recorded with the DIB, in 150 mM KCl, 10 mM HEPES, 2 mM $CaCl_2$, 100 mM glycerol, pH=7.0, 10 mg/ml (3:1) POPE:POPG. The data was recorded at a sampling rate 20 kH, with a Bessel Filter of 2 kHz, at a gain of 2.

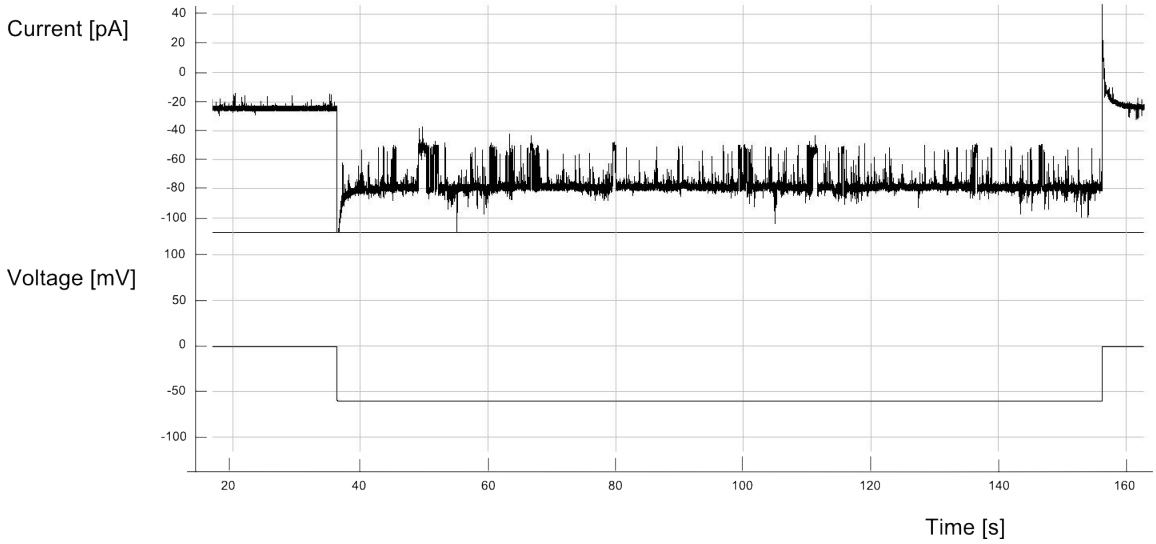


Figure 4.7: K_vAP-CL single channel events recorded with the DIB, in 150 mM KCl, 10 mM HEPES, 2 mM $CaCl_2$, pH=7.0, 10 mg/ml (3:1) POPE:POPG. The data was recorded at a sampling rate 20 kH, with a Bessel Filter of 2 kHz, at a gain of 2.

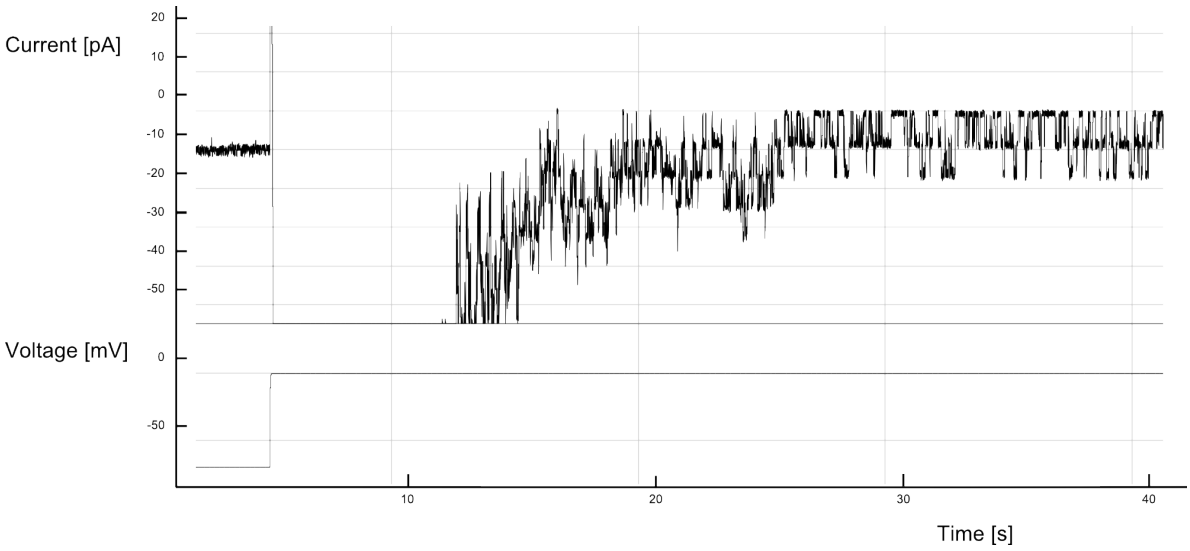


Figure 4.8: K_vAP-CL single channel events recorded with the DIB, in 150 mM KCl, 10 mM HEPES, 2 mM $CaCl_2$, 150 mM glycerol, pH=7.0, 10 mg/ml (3:1) POPE:POPG. The data was recorded at a sampling rate 20 kH, with a Bessel Filter of 2 kHz, and the voltage was shifted from -70 to 0 mV. This sample appears to show inactivation.

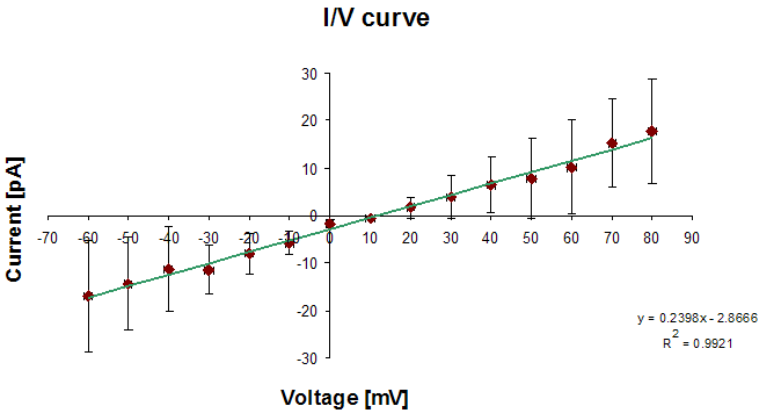


Figure 4.9: I/V curve calculated from 3 single channel traces of K_vAP-CL and K_vAP-L121C-CL mutants, in the DIB system. The lipid bilayers were formed of (3:1) POPE:POPG in hexadecane in 150 mM KCl, 10 mM HEPES, pH 7.0 buffers on both sides.

was present in the system instead of *n*-decane. Voltage K^+ channels strongly interact with their lipid environment. In particular the hexadecane remainings in the lipid bilayer (compared to the decane in the PLB) will influence the channel behaviour. One study that focused on the influence of alkanols, cholesterols and anesthetics on K_vAP unitary conductance clearly demonstrated that these molecules have a strong effect on the channel gating properties (conductance, activation, inactivation) (33).

4.3.4 Lateral diffusion coefficient (D_{lat})

4.3.4.1 Fluorescent lipids

Fluorescent lipids (TRITC-DHPE) carrying a fluorescent probe (TRITC) were diluted in various percentages (0.0012-0.012 %) (w/w) in DPhPC lipids. The fluorescence diffusion in 2-dimensions in lipid bilayers was observed in the DIB system, through TIRF measurements. Droplets (0.5 M KCl, 10 mM HEPES, pH 7.0) were incubated with the fluorescent lipids (TRITC-DHPE/DPhPC). This experiment was conducted in order to provide a fluorescent control at the single molecule level. When labelled ion channels are successfully imaged in a bilayer, their diffusion behaviour and the fluorescent label characteristics (lifetime, intensity, ..) can be compared to fluorescently tagged lipids (Figure 4.10).

4.3.4.2 K_vAP fluorescently tagged with TMR5M

In a similar way, recordings of fluorescently tagged K_vAP-CL embedded in (3:1) POPE:POPG bilayer were used to calculate the lateral coefficient diffusion (Figure 4.11 and Table 4.3). By examining the recordings, it was noticeable that some show a freely diffusing fluorescent spot while in others, the spot was confined to some

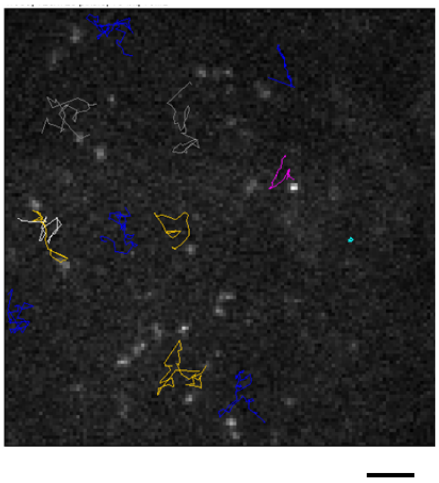


Figure 4.10: Example of the particle tracking results of the Mosaic plugin with ImageJ. 0.00012 % (w/w) of TRITC-DHPE in DPhPC bilayer is visualized in DIB. The coloured lines represent the detected trajectories along the recording. Scale bar: 4 μm.

areas of the bilayer. Therefore, the recordings were divided into two groups, the freely diffusing ion channel and the reduced mobility one, and two lateral diffusion coefficients (D_{lat}) were then calculated. This phenomenon is quite apparent when the fluorescence standard deviation of a whole recording is showed in an image (Figure 4.13). By example in Figure 4.13, the first row presents a much more uniform brightness, through the bilayer with the absence of dark and bright areas. On the other hand, in the second row, structures are apparent, the whiter areas show where fluorescently tagged K_vAP freely diffuse, avoiding the darker areas.

Fluorescently tagged K_vAP-CL demonstrate two distinct diffusion patterns, 6.21 $\pm$ 0.29 μm^2/sec and 6.79 $\pm$ 0.34 μm^2/sec (Figure 4.13), but despite this difference, the lateral diffusion coefficient is not significantly affected by it. The left and center image on the first row on Figure 4.13 show the standard deviation of two recordings of TRITC-DHPE, of 0.0000012 and 0.12 % respectively. No particular diffusion behaviour can be distinguished between these two images, indicating that this diffu-

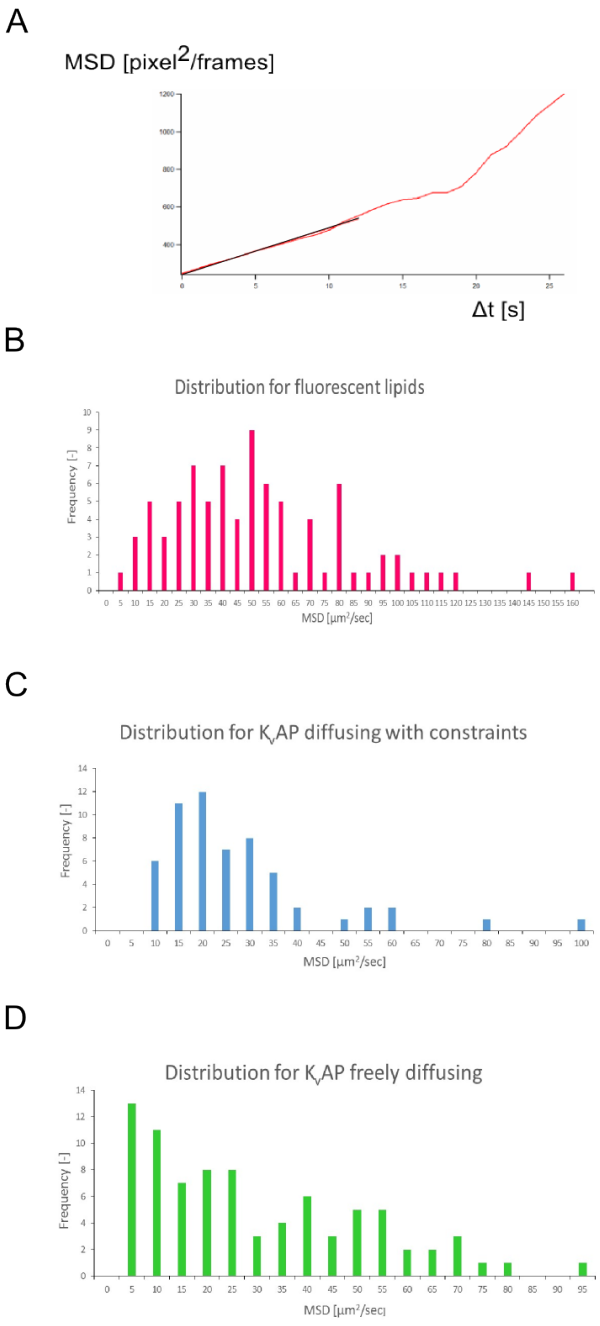


Figure 4.11: Example of the D_{lat} calculation. Panel A: The MSD of each trajectory was plotted and its slope was recorded to calculate the D_{lat}. Panel B: Histogram of the D_{lat} of fluorescent lipids (83 trajectories). Panel C: Histogram of the D_{lat} of K_vAP reduced mobility (57 trajectories). Panel D: Histogram of the D_{lat} of K_vAP freely diffusing (82 trajectories).

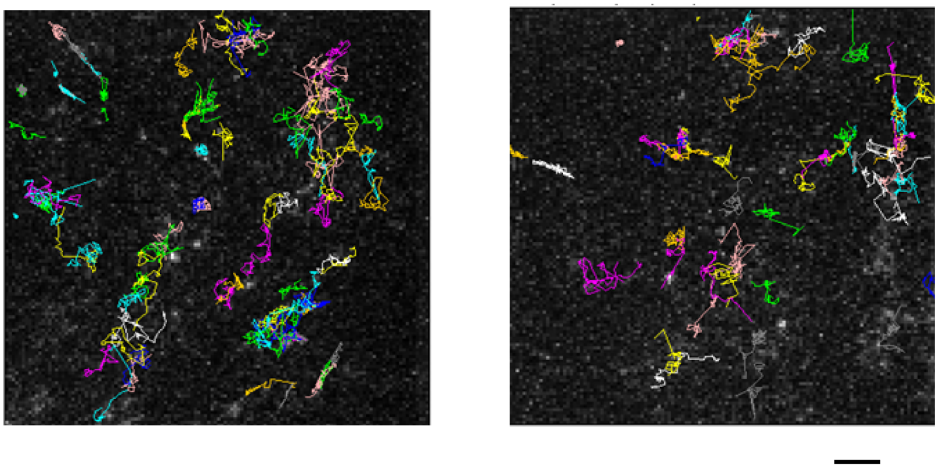


Figure 4.12: Example of the particle tracking results of the Mosaic plugin with ImageJ. Fluorescently tagged K_vAP-CL is visualized in DIB. The coloured lines represent the detected trajectories along the recording. Scale bar: 4 μm.

sion pattern effect is not due to concentration. Either lipid partition has occurred or irregularities of the gel surface affect the mobility of moving species. Pure or mixtures of lipids have been observed to give rise to inhomogenities (phase or domain) on supported bilayers (7, 27). By example, pure POPE and pure POPG show both the presence of dark areas (believed to be the ordered phase) while mixed with the dye NBD-DPPE (1,2-dipalmitoyl-*sn*-glycero-3-phosphoethanolamine-N-[7-nitro-2-1,3-benzoxadiazol-4-yl]) visualised through epifluorescence. The presence of the solid support triggers the formation of dark areas in bilayers made of pure POPG (7). Therefore, the supported gel phase under the bilayer may affect the mobility of moving species through irregularities on the surface (Figure 4.13), and cause a small discrepancy in the diffusion of particles by the presence of higher/lower ordered phase.

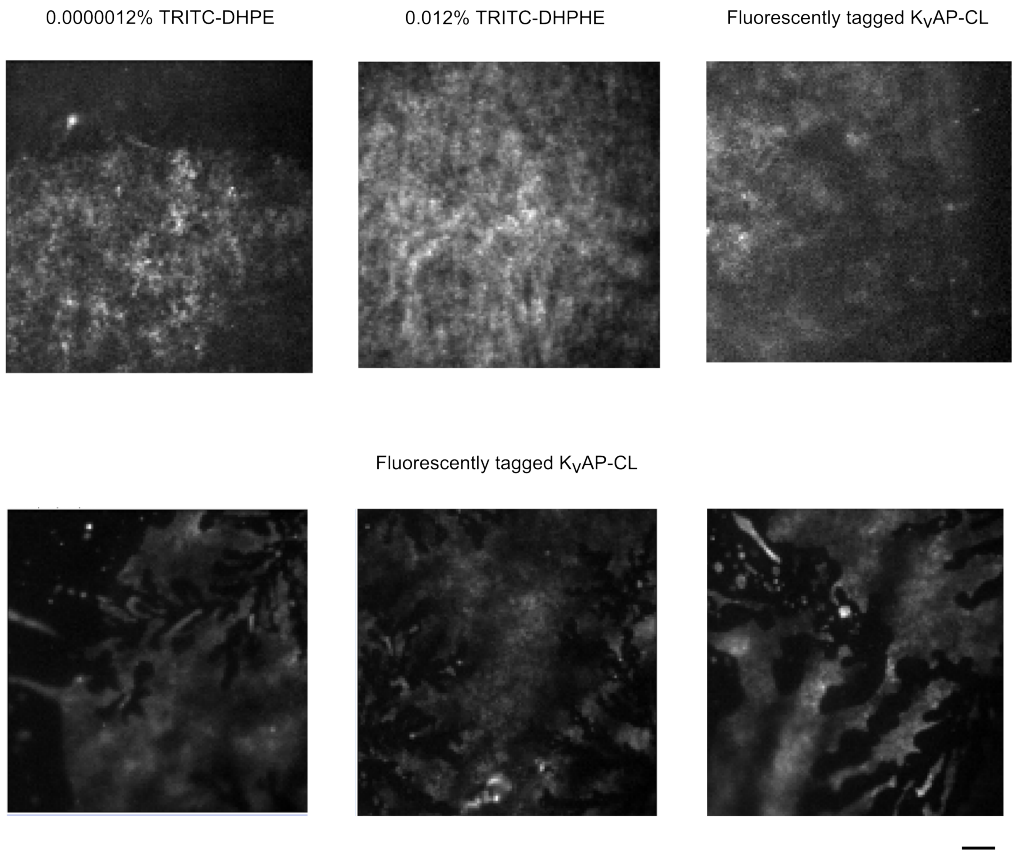


Figure 4.13: Calculated image of the standard deviation of each frame of one recording. A stack-projection of the recording was generated with ImageJ plugin and its standard deviation was calculated. The first row shows the unrestricted diffusion of the ion channel while the second row shows its confined diffusion. Scale bar: 4 μm.

Lipids		K_vAP reduced mobility		K_vAP	
D_{lat} [μm^2/sec]	Standard Deviation [μm^2/sec]	D_{lat} [μm^2/sec]	Standard Deviation [μm^2/sec]	D_{lat} [μm^2/sec]	Standard Deviation [μm^2/sec]
12.59	0.66	6.21	0.29	6.79	0.34

Table 4.3: Coefficient diffusion and standard deviation of K_vAP-L121C-CL and K_vAP-G112C-CL analysed by the software Mosaic. 80, 53 and 79 trajectories were used in the calculation for TRITC-DHPE, K_vAP reduced mobility, and K_vAP freely diffusing.

The lateral coefficient diffusions of fluorescently tagged lipids and K_vAP are within the expected range (order of μm^2/sec) of fluid phase membranes (on supported surfaces) (7). The coefficient diffusion of K_vAP has been previously measured in large GUVs mimicking a planar bilayer (30). The reported measure by a quantum dot attached to the ion channel through a PEG linker is 2.3 μm^2/sec (standard deviation of 0.7 μm^2/sec), in 9:1 EPC (egg phosphatidylcholine) /EPA (egg phosphatidic acid), around half of what has been assessed in DIB in 3:1 POPE:POPG. Both coefficients fall within a similar range and their difference can be accounted to the varied environment in which they have been measured: the lipids, the system and particularly the fluorescent tag.

Other membrane proteins, BKCa and K_v10.1 have shown different diffusion patterns already (102, 103). They have been measured in different cell types and their variations was accounted on the presence of the cytoskeleton and different environment which lead to a more or less restricted diffusion.

This experiment demonstrates the presence of K_vAP-CL in the lipid bilayer along with its expected diffusion.

4.3.5 Correlation of fluorescent, voltage and electrical signals

The fluorescent, electrical and voltage data were recorded as follows. A voltage step protocol was generated by an amplifier to the electrode in the DIB system. In the meantime, the detected responding current was sent to the same apparatus for recording. Both signals are read through the same software (Clampex). The EMCCD camera responsible for fluorescence detection was controlled independently by its own software. Thus, the correlation between the fluorescence and the voltage/electrical signals has to be made through a time delay of approximately 1 second. This param-

eter was included in the analysis of each recording.

4.3.5.1 Single molecule measurements

Analysis of the recordings show in Figure 4.14 shows an incorporation of 2-3 channels in the bilayer. Single channel opening and closing have been identified on the trace, but unfortunately an electrical offset was present. Since a few channels were incorporated into the bilayer, fluorescence arising from TMR5M should come from a few tracks. Due to the dye stability versus contaminations, the longest fluorescent tracks should be the best candidates. Fluorescent tracks longer than 20 frames were thus kept for analysis and were plotted along with the voltage shift (Figure 4.14). We are looking for simultaneous fluorescence and voltage change.

The selected fluorescent tracks (total of 24 and 29 respectively) seem to happen in clusters, some of which begin and end with a voltage shift. Unfortunately, no trends between voltage value and fluorescence behaviour are noticeable, neither can individual fluorescence and electric events be linked to each other with certainity. The number of fluorescent tracks kept for analysis is higher than the number of incorporated ion channels. Fluorescent contaminants are therefore present in the recording, despite all the precautions taken to remove them. If one of tagged ion channels diffuse in the bilayer, it is likely that its signal will be damped in the background noise. In addition, not enough ion channels are incorporated in the bilayer to allow its fluorescent identification among the contaminants.

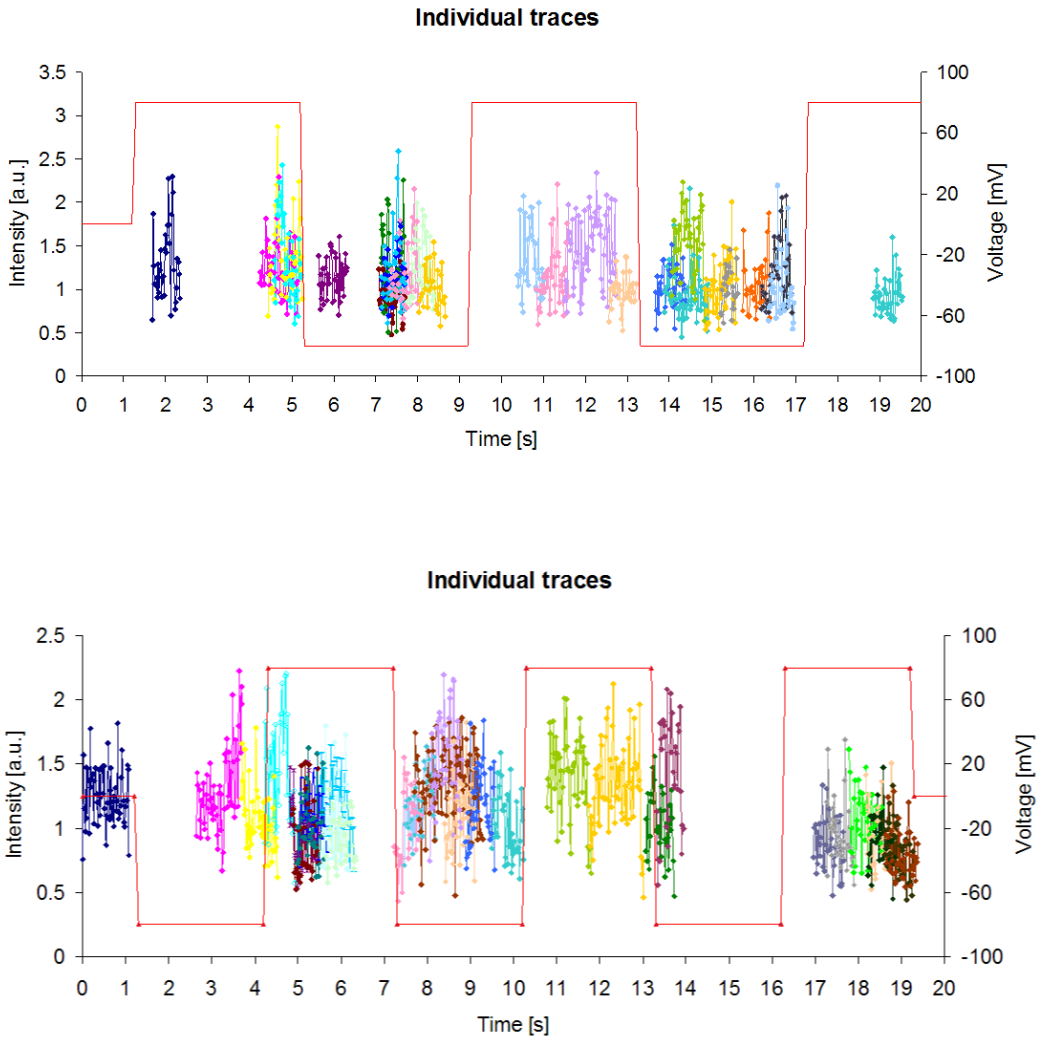


Figure 4.14: Fluorescence recording of K_vAP-L121C-CL fluorescently tagged with TMR5M vs time. Trajectories were analysed with the plugin Mosaic from the software ImageJ and the longest trajectories (longer than 20 frames) were kept. Each individual fluorescent track was plotted along with the voltage (red), automatically applied.

4.3.5.2 Ensemble-averaged measurements

Since no correlation could be found on a single molecule scale between the fluorescence, the voltage and the current, other recordings were analysed similarly as

previously but on a larger scale. In order to see if a correlation exists between fluorescence and current, three recordings where both signals were simultaneously recorded were then analysed. Due to the macroscopic current (corresponding to more than 300 channels in the bilayer), no individual events could be correlated at this scale. Therefore the mean of the overall fluorescence in each recording was plotted along time and compared to the current along with the voltage (Figure 4.15). No particular fluorescence behaviour could be identified with the voltage application, in the three cases. The overall fluorescence constantly decreases over time, without showing any responses to the voltage shifts.

In order to complete the analysis, the fluorescence intensities of the recordings from Figures 4.15 and 4.15 were pooled together. Each datapoint was classed according to its voltage value, V positive (80 mV), V negative (-80 mV), and V null. If the reported fluorescence would change according to the applied voltage, the fluorescent mean value would vary. Therefore the fluorescence recorded at different voltages was plotted as bar-graph and histograms (Figure 4.16).

The three mean, 0.84 ± 0.14, 0.86 ± 0.21, 0.81 ± 0.12 for positive, null and negative voltage respectively confirm the non-correlation. Normalised histograms of the fluorescence at the three voltage values show their value distributions. There is a small shift between each mean, still non-significant. Apart from one, each recording starts by 0 voltage and is followed by a positive voltage shift. Therefore photobleaching is likely to be more prominent at negative voltage than at null or positive voltage, and this might explain the small shift in mean.

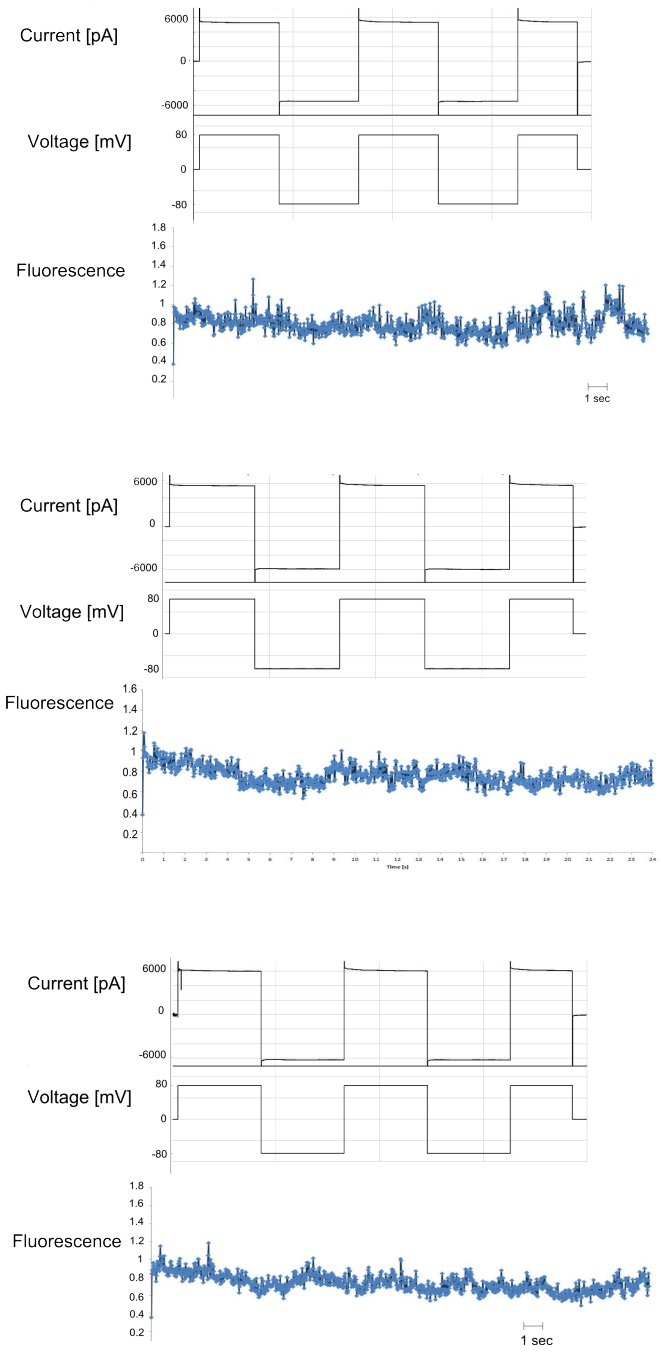


Figure 4.15: Current, Voltage and Fluorescence traces from K_vAP-G112C-CL fluorescently tagged with TMR5M recorded simultaneously. Each graph shows one recording. The fluorescence trace represents the average of every trajectories detected with the plugin Mosaic from the software ImageJ.

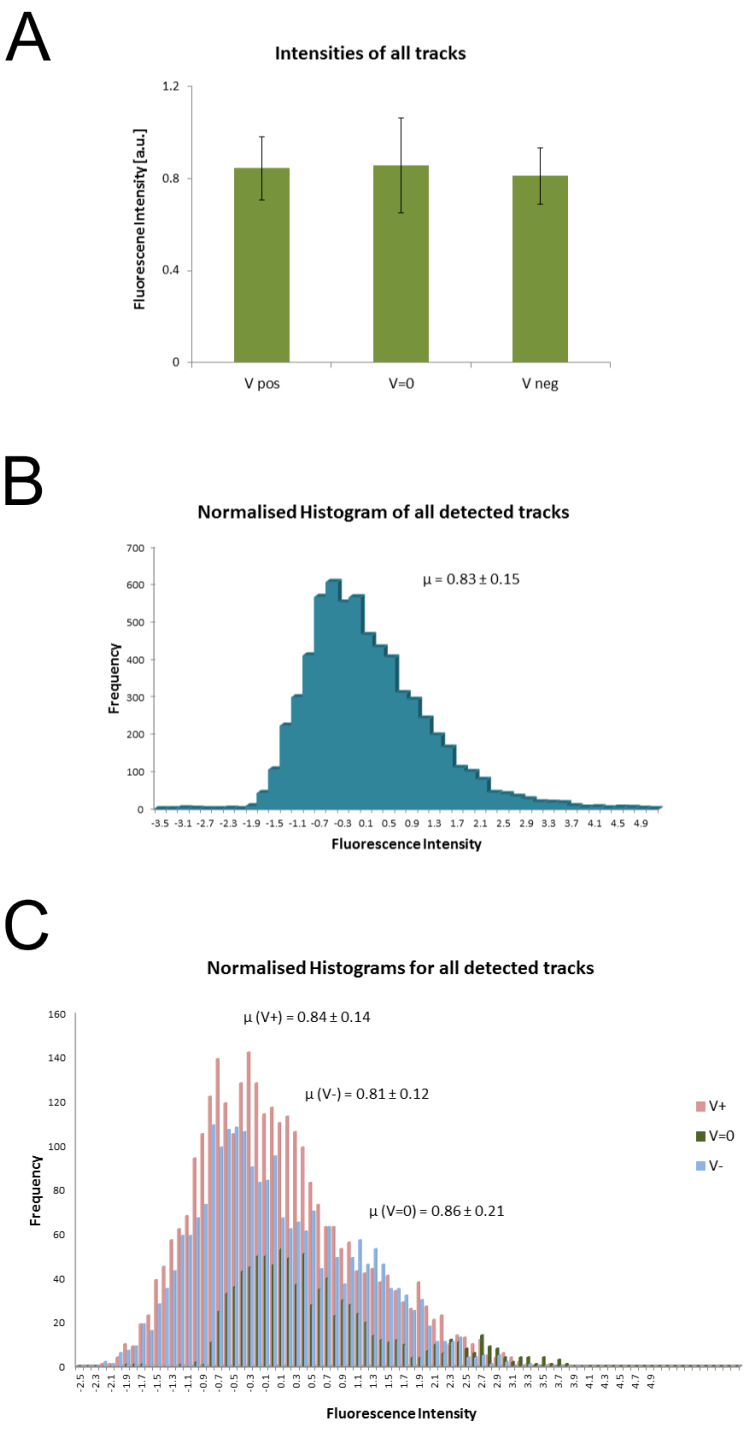


Figure 4.16: Bar-graph (panel A) and normalised histograms (panel B for the overall fluorescence and panel C for the fluorescence classified according to its voltage value) of all fluorescent trajectories detected by the plugin Mosaic of the automated voltage application recordings. Each data point was classified according to its corresponding voltage value (either positive, 0, or negative) and plot separately. The bars represent the standard deviations.

4.4 Discussion

4.4.1 DIB formation

Experiments show that 30 minutes of droplet incubation time in lipid/oil mixture is reliable, whereas less than 20 minutes does not allow the formation of a stable monolayer on the aqueous/oil surface. The lipid in hexadecane concentration is a determining parameter in the bilayer formation and one should ensure that the concentration is optimised for bilayer occurence.

The hygroscopic nature of lipids also makes a precise control of the lipid concentration non trivial. Moreover, the technique requires training, since certain manipulations take time and dexterity to master. However, despite the optimisation process, bilayer formation and especially channel incorporation were not reliable. Some of the reasons are explained below.

4.4.2 Incorporation of vesicles

In the literature (68), vesicle fusion to bilayers is typically made through the use of salt gradients. For example, a 10x KCl gradient is established between the two compartments in planar lipid bilayer to drive the incorporation of K_vAP (83). Once the presence of channel has been established, the KCl concentration is equalised on both sides. Unfortunately this approach is impossible to use for the DIB experiments. The salt concentration in the rehydratation layer or in the droplet cannot be modified once the system has been set-up. The absence of stirring in the DIB also does not drive the vesicle close to the bilayer. Although gravity should help the vesicles settling down in the droplet through time. Positive and negative voltages (up to 50-70 mV)

were applied to help drive the fusion process. Finally, heating the DIB device was also tried, to 30°C. However, no additional incorporation events were observed.

4.4.3 Electrical traces and I/V curve

Many factors influence the quality of the electrical recording. The smaller the bilayer area, the less noisy the electrical recording is going to be. The sample electrode controls the bilayer area, (by moving it up and down); nonetheless any manipulation should be made slowly and carefully since rupture or electrode poping out of the droplet can happen. The electrical and time stability of bilayers vary from droplet to droplet but they are both correlated. Recordings starting with a noisy electrical activity (normally due to electroporation) did not last more than a couple of minutes before droplet rupture. By contrast, some bilayers lasted several hours, sustaining large voltage changes without any electroporation.

A time-dependent current offset (either positive or negative) was observed in all recordings which is certainly caused by the presence of a voltage offset in the system or more channel incorporation. Despite adjustment of the parameters controlling the voltage, it was not possible to start and keep any recordings with a 0 pA baseline. Further in a few recordings, the current baseline was also drifting with time.

Many factors can cause a voltage offset in the electrical system. Firstly, the presence of agarose on one side of the bilayer is having an effect on the osmotic balance. Secondly, the continuous application of voltage is causing salt imbalance, over time, by driving ions on one side of the bilayer. Nonetheless, each positive voltage applied was followed by its negative corresponding voltage step, which should counteract the system. However, electroporation events were observed, causing salt imbalance. Variations in the quality of lipids solutions was observed in the course

of experiments and it is quite likely that some stocks gave rise to better bilayer quality. The presence of a junction potential was also a major potential factor of voltage offset. In the DIB system, both electrodes experience different environment. The sampling electrode despite being agarose-coated is in liquid while the reference electrode is embedded in a gel. Finally, poorly sealed devices and system heat-up cause evaporation, which may also contribute to unequal salt concentration.

4.4.4 Fluorescence experiments

When experiments have to be conducted at the single molecule level, great care needs to be taken at eliminating all potential sources of contaminations. In DIB, fluorescent contamination can come from every component of the system: the lipids, the hexadecane, the chloroform, the plastic tips and the PMMA devices, the equilibration tank. Many controls had to be repetitively performed such as to work in an environment where the fluorescent background is low enough to allow single molecules experiments. It was a constant struggle to eliminate or minimise all of them. Upon my observations, the organic solvent hexadecane was the major source of contamination at the early stage of the experiments. Just a few openings of the stock bottle were enough to dramatically increase the fluorescence background. Therefore, upon opening, the hexadecane was aliquoted and used no more than twice. The same methodology applied with the chloroform (used to dissolve the lipids) and the immersion oil (used on top of the 60x TIRF objective) as well. Both were used as aliquots, in order to minimise the openings of the bottle and the contact with the tips which are all sources of fluorescent contamination. The second major source of contamination are the PMMA devices and equilibration tanks themselves. A cleaning protocol (see Section 4.2.6) was conceived which would be sufficiently stringent

to eliminate the contaminants but not too aggressive to corrode the PMMA material. The PMMA devices are designed with a great accuracy, especially the circular area forming the bottom of the wells needs to be intact for the bilayer to form with an appropriate depth to allow TIRF.

4.4.5 Diffusion coefficient

My studies showed that fluorescently tagged K_vAP-CL could be successfully incorporated into the bilayer and its diffusion tracked (Figure 4.12). Figure 4.13 clearly demonstrates a mobility variation between recordings. K_vAP-CL freely diffuses in some areas but appeared to avoid others. This behaviour was not present with the fluorescently tagged lipids in this document and does not significantly affect the lateral diffusion coefficient (Table 4.3).

4.4.6 Fluorescent, voltage and electrical correlation

4.4.6.1 Technical difficulties

One of the main hurdles to overcome in order to successfully complete fluorescent and electrical recordings with the DIB system is the difficulty to record from both the amplifier and the camera at the same time.

Prior to every experiment, the electrical activity of the bilayer was checked to make sure that K_vAP-CL fluorescently labelled mutants were embedded and functional in the membrane. Once the electrode was successfully placed in the droplet using the 4x magnification, the TIRF 60x oil objective was slowly raised towards the coverslip supporting the hydrogel of the PMMA device. Approaching the 60x objective to the DIB has to be done quite slowly, carefully and smoothly. Time and patience were

needed to make this delicate step work. The difficulty is enhanced by the requirement to find the right focus in the bilayer. Once the objective is in contact with the coverslip through the oil, the right focus has to be found.

The comparison of the fluorescent traces with the electrical ones is a tedious task and does not give any definite answer regarding any correlation between the electrical and fluorescent recordings. Primarily, the difficulty of controlling the number of channels incorporated in the bilayer was one of the main reasons. As discussed previously in this section, the number of ion channels incorporated in vesicles is a parameter which cannot be controlled and will vary from one lipid vesicle to another (68). Therefore the incorporation of K_vAP-CL reconstituted into vesicles will deliver a random number of ion channels into the bilayer. The right conditions for successful incorporation of only a few ion channels into the bilayer could not precisely be pinpointed. Incorporation at the conditions tried, always appear to deliver no K_vAP-CL into the membrane, or tens of channels or so which made the interpretation of the ion channels currents burdensome when one tries to correlate it with single fluorescent traces. This fact is supported by other investigators who have studied incorporation phenomenon of proteo-vesicles into planar lipid membranes (5, 23). All of them show incorporation of ion channels to the planar membrane happening in bursts, dictated by osmosis and Ca^{2+} presence. None of them demonstrates vesicle fusion by sole events.

One straightforward way to resolve this issue would be to decrease the number of proteo-vesicles in the droplet. However, even at the same vesicle concentration giving rise to ten or so ion channel fusion into the bilayer, some experiments show no incorporation at all. Other phenomena contribute to the proteo-vesicle fusion, like vesicle aggregation and stirring of the solution. Thus vesicle fusion is not solely

driven by proteo-vesicle concentration but is a more complex process. Decreasing the proteo-vesicle concentration would not necessarily decrease the number of ion channels incorporated but also its probability of incorporation.

Moreover, the channel can adopt both orientations in the bilayer (it can be orientated both ways in the vesicle) which makes interpretation of the electrical traces even more complicated. K_vAP-CL has also a low single channel conductance (at 50 mV, its ionic current is about 8 pA), which requires a tight voltage control in the system so as to identify the ion channel working in the bilayer. As seen in Section 4.4.3, voltage offset is often present in the system which further complicates the electrical recording readout.

Moreover, the control of the bilayer area plays a huge role both for the fluorescent and electrical recordings. The DHB membrane possesses an intrinsic noise, larger than in the PLB system, which requires the use of digital filtration after digitisation, especially if the current traces are small. The only way to reduce this noise is by decreasing the bilayer area through the sampling electrode control.

Further, correlating fluorescent events with electric ones in these conditions is a difficult task. The first requirement for any potential correlation between fluorescent and electric events is that mutants K_vAP-CL carrying a functional fluorescent tag are captured while they are diffusing in the cameras field of view. The second one is that these channels are producing single channel events while being fluorescently recorded. The first thing to consider is that the bilayer is always going to be larger than the camera field of view. Thus, the electric recording of the bilayer does not match the fluorescent one, since it reads out the entire bilayer area. Ion channels embedded in the bilayer but not imaged by the camera will contribute to the bilayer currents, but no fluorescence-electric correlation can be made. Consequently when there are

tens of embedded mutant K_vAP-CL (Figure 4.14), a significant number needs to be present in the field of view at the instant of a voltage change in order to catch their fluorescent response. Working with such a number does make the correlation of both signals harder due to the unlikelihood of this happening at the same time. Only a few ion channels may diffuse in the field of view during the voltage change, but their electric single events may be damped in the current resulting of the ten or so ion channels in the bilayer. We assume of course that the recorded fluorescence mainly comes from fluorescent dyes attached to the ion channel and that no electroporation is happening.

4.4.6.2 Single molecule behaviour

Figure 4.14 shows the fluorescence of individual tracks plotted along with voltage shifts. Unfortunately, no correlation could be made between the single electrical events and the fluorescence.

Our current knowledge of TMR5M fluorescence moving in a bilayer environment and of fluorescently tagged K_vAP-CL mutant conformation changes do not allow us to predict exactly how the fluorescence may change with voltage shift. Our current knowledge about K_vAP-CL and has been confirmed in these experiments, is that at 0 mV, the channel is closed and at positive or negative voltage, the channel is opened. Upon opening, the S3b-S4 α-helices, which normally lie deeply in the membrane undergo an upward movement (Section 1.8). How the TMR5M tag is going to respond to that cannot be exactly described; its fluorescence should increase in a hydrophobic medium and decrease in a hydrophilic one (18). Nonetheless, we would predict that upon voltage shift, the fluorescence should change in a way or another.

4.4.6.3 Ensemble level

The same type of analysis cannot be undertaken with the result presented in Figure 4.15. The macroscopic current (more than 300 channels) prevents us from correlating any single channel events. Thus, instead of limiting our analysis to the longest trajectories detected by the plugin Mosaic, the mean of fluorescence from every trajectory was plotted through time. No correlation could be made between fluorescence and current signals. The overall fluorescence does not seem to respond to any voltage shift applied through the recording; its slow decay is most probably due to photobleaching.

In the experiment of Figure 4.15, if only 2 channels were present in the bilayer, the probability of capturing one or two in the camera field of view while the voltage is applied would be quite low. However, the number of ion channels in the bilayer makes it quite difficult not to have at least a couple of ion channels diffusing in the field of view at the recording time. These experiments cast doubt on the integrity of the labelled K_vAP-CL. The detected fluorescent could have arisen from either contamination, or from free TMR5M tags embedded in the bilayer. Many efforts made to eliminate/lower contamination sources, but some cannot be avoided. When current flows between the droplet and the hydrogel (K^+ currents or electroporation), there is also the possibility that contaminants present in agarose travel to the bilayer. This contamination can come from the lipids; even very small scale fluorescent contamination will affect the outcome of the experiment, especially at the single molecule level.

In order to confirm the absence of fluorescence–voltage correlation, the fluorescence arising from every detected trajectory of both experiments was pooled together

(Figures 4.14-4.15). Fluorescence happening at positive, negative, or null voltage was grouped together and their average value was compared (Figure 4.16). However, the three calculated mean had very close value and were not significantly different. Figure 4.16 shows the distribution of the fluorescence value at the three voltages. For each one of them, the distribution is skewed toward positive values. In the case of V=0, this fact can be explained by a technical reason, each recording starting with a null voltage. Thus, the overall fluorescence would be less affected by the photo-bleaching effect than for the two other voltage values. In the case of V positive and V negative, the skewed distributions and the slight mean difference between the two may possibly indicate difference of fluorescence at different voltages; an effect which could not be observed at a smaller scale.

4.5 Conclusion

A protocol for a suitable K_vAP-CL incorporation through proteo-vesicle fusion to DIB has been established. An I/V curve was calculated and was in agreement with the published data, which confirms that the channel is present in the bilayer and functional. However, the exact conditions giving rise to reproducible channel incorporation could not be determined, nor could the number of incorporation events be controlled. I believe that the lipids quality and the proteo-vesicle fusion to a bilayer phenomenon itself are responsible for these shortcomings.

The fluorescence experiments on the other hand were not as successful. Lateral coefficients diffusion of fluorescently tagged K_vAP-CL mutants along with fluorescent lipids could be calculated. However, once the fluorescence and the electrical–voltage experiments were performed together, the experiments could not prove any correla-

tion between both signals. Three possibilities can explain this result.

Firstly, the integrity of the fluorescently tagged ion channel has been compromised, maybe through photobleaching, tag loss or degradation.

A second option would be that the fluorescent signal is too modest to be detected, especially if fluorescent contaminants are present. Maybe the fluorescent tag does not experience a significant environmental change (from hydrophobic to hydrophilic), enough to give rise to a detectable fluorescent shift.

At last the third possibility would be that the optimal range of the experiments has not been found yet. The nature itself of the simultaneous fluorescence, electrical and voltage experiment makes it difficult to successfully reproduce. In this specific case, the right number of ion channels, providing that they still carry a functioning fluorescent tag, need to be embedded in the bilayer; not too many to still give rise to single channels events and not too few to have a reasonable probability of their diffusion in the camera field of view during the recording (around 5 active would be perfect). Of course, the electrical system needs to be perfectly balanced, the bilayer quite stable with a minimum of fluorescence contamination. Only correlation of fluorescence to voltage and electrical signals at the single channel events can shed a new light on the dynamic range of the S4 helix motion in the bilayer upon activation/deactivation.

Chapter 5

Conclusions

5.1 Summary

Overall this study aimed to develop an expression, purification and fluorescent labelling strategy for K_vAP so that the resulting channels could be successfully incorporated into lipid bilayers for combined electrical and fluorescent measurements. This would allow a method of probing the mechanism of voltage-sensing in these channels at both the macroscopic and single molecule levels. In particular, successful development of the single molecule approach would enable a level of analysis not previously possible.

Despite the significant technical challenges posed by this study I was able to successfully label K_vAP and incorporate these fluorescently labelled channels into artificial lipid membranes. I was able to record the electrical activity of single channels and also to track their diffusion within the membrane at the single molecule level. However, repeated attempts at correlation of electrical and fluorescent activity were unsuccessful and significant further development of this technique is required before it can be considered as an appropriate approach to study the mechanism of voltage-dependent gating. In the sections below I summarise some of the conclusions that

can be drawn from this study and also highlight steps that might be taken to improve this methodology.

5.2 Expression and purification of K_vAP

Neither the channel production or purification protocols developed in this study gave rise to any concerns. K_vAP could be produced in a satisfactory quantity (especially for an archael channel) within the *E. coli* expression system, and the production and purification conditions could be opimised to give rise to the best yield and purity. No major hurdles were met at this point, and the purification methodology lead to the isolation of functional channels as demonstrated in Chapter 2.

5.3 Labelling of K_vAP

Development of the fluorescent labelling strategy was more troublesome than the previous expression and purification steps. The set-up of a protocol and the quantification of the fluorescent labelling reaction took considerable time and new methodologies had to be determined empirically to answer many questions. In particular, maintaining high purity and consistent concentration appeared to be key factors for a successfull labelling reaction. The purifcation scheme I developed did give rise to high levels of K_vAP protein purity (especially the repetitive IMAC steps) but unfortunately these extra steps resulted in very small quantites of protein being isolated in the final purification step. Previous studies which produced and purified K_vAP did not have to cope with this requirement for high protein purity as they simply measured functional activity within the bilayer and a relative lack of purity was not

a problem. However, purity was a major issue for the fluorescent labelling reaction in all of the mutants tested. In the absence of large fermentation facilities, it would not have been practical to produce and purify more considerable quantities of *E. coli* cells and the large quantities of detergent required for solubilisation would have been prohibitively expensive. Furthermore, the purification scheme required the experiments to be stopped at certain steps and the K_vAP protein did not appear to be stable in the fridge for a long time without proteolysis.

The quantification of the fluorescent labelling also proved troublesome as it gave contradictory results. The successful development of single-molecule fluorescent studies would have required that the number of labels per channel to be correctly determined, especially if there was to be a correlation between movement of individual VSDs (voltage-sensing domain) and channel opening.

Two methods were used for this quantification: an absorbance measurement of protein and dye concentration with the nanodrop (Section 2.4.7) and subunit counting by photobleaching by software analysis (Section 3.3.2).

By simply calculating the dye to protein ratio, all tested mutants had a dye to protein ratio of 1:1 despite the 4 available sites on the tetrameric channel. On the other hand, the detected dye stoichiometry was radically different, ranging from 3 to 6 depending on the mutants, with the SFDA algorithm. The second method was chosen due to the difficulty of reliably measuring the absorbance of the relatively low concentrations of labelled K_vAP.

This second technique was based on counting the number of fluorescent dyes on each protein by photobleaching. It was done at the single-molecule level by examining individual molecules and plotting distribution histograms from the data, rather than measuring an average value from an ensemble. This approach demonstrates the

utility and the precision of single molecule technique. However, using this method the labelling stoichiometry appeared high and in some cases the mutants appeared to have a stiochiometry of >4 which should not be possible due to the presence of only 4 cysteines per channel.

Two explanations might be possible for this result, either the technique overestimates the number of photobleached dyes, or the samples were overlabelled. The controls seemed to indicate that the software does slightly overestimate the number of dyes present, nonetheless the second possibility is also quite possible. The hydrophobicity of the TMR5M dye and its relatively small size may allow the molecule to"stick" to hydrophobic clefts of the ion channel or the detergent. Moreover, many wash steps had to be incoroporated in the protocol to get rid to a maximum of free dye prior to the dialysis in order to minimise contamination. Consequently, reducing the dye concentration (to 5 or 7 times the protein concentration) may seem a sensible approach to remove any uncovalent binding from the fluorescent dye. However, this is very likely to lead to sub-stoichiometric labelling which would introduce its own set of problems.

5.4 Incorporation of K_vAP into DIBs

One major technical difficulty met during this study was finding the conditions which could preserve K_vAP functionality and yet satisfy the technical requirements for incorporation into the DIB. The electrical characterisation of K_vAP needs to be performed in an lipid environment rich in negative charge (88), yet the channel also needs to be delivered to the membrane without any loss of functionality. These two conditions put major restrictions on the choice of lipids that can be used ((3:1)

POPE:POPG) as well as the delivery method. The buffer composition on both side of the bilayer also cannot be modified during the course of the experiments in DIBs and osmotic forces need to be taken into account, as well. Therefore, a balance between the system and the ion channel requirements had to be found. Unfortunately, most combinations tried either did not give rise to constant stable DIBs or ion channel incorporation in the bilayer proved to be inconsistent. More conditions therefore need to be tempted.

5.5 Electrical measurements of K_vAP function

Unfortunately, the planar lipid bilayer methodology produced better and more consistent electrical recordings than the DIBs which I was aiming to use. The planar bilayer method was developped in 1972 (69) and has been standardised for ion channel recordings over many decades. The droplet hydrogel bilayer needs further development and protocols established in order to give rise to the same recording quality and reproducibility. The vesicle fusion method also needs to be adapted to the new conditions of the DIB or another modus operandi for delivering ion channel to the bilayer needs to be found. One future possibility would be the incorporation of purified channels into nanodiscs as this method has been used to successfully deliver KcsA into bilayers and might possibly also be adaptable for use in DIBs (82).

The electrical measurements themselves also proved problematic. In particular, the larger DIB baseline requires extra filtering of the signal after digitisation. This makes channels with small conductance very difficult to identify. Furthermore, voltage-gated potassium channels are very sensitive to their lipid environment. The lipid composition modulates the gating properties and the conductance of the chan-

nel, as shown in (33, 87). In (87), it was demonstrated that the lipid composition and the mechanical force applied to the membrane have a direct influence on the activation and deactivation of K_v channels. Similarly, the effect of different alkane chains, anaesthetics, or cholestrol in the bilayer also has a profound modification on the electrical properties of K_vAP (33). Therefore, the presence of hexadecane used to create these bilayers even at low concentration might cause a shift of the gating behaviour of any voltage-gated potassium channels studied with the DIB or any membrane protein sensitive to its lipid environment (33, 87).

5.6 Measurement of fluorescent signals

Despite these many problems I was eventually able to successfully incorporate labelled K_vAP into the membrane and could visualise single molecules. To confirm that these were labelled K_vAP, and not contaminating labelled lipids I measured the lateral diffusion coefficients. The D_{lat} of K_vAP was found to fall in the expected range for a fluorescently tagged membrane protein diffusing in a bilayer. The discrepancy between the calculated value and the one reported in (30), 6.79 μm^2/sec $\pm$ 0.34 μm^2/sec and 2.3 μm^2/sec $\pm$ 0.7 μm^2/sec respectively, is probably explained by different lipids used(((9:1, mol/mol) EPC/EPA (egg phosphatidylcholine/ egg phosphatidic acid) in (30)) versus (3:1) POPE/POPG). Two modes of diffusion were observed (Section 4.13) by tracking K_vAP diffusion in the PLB (Section 4.3). Their difference was not found to be statistically significant, however it may suggest that confinement of K_vAP to certain regions of the bilayer may happen. This phenomenon can have diverse causes: phase separation in the bilayer or irregularities on the agarose gel surface. It is difficult to determine much the presence of the gel under the bi-

layer affects the bilayer fluidity or diffusion of molecules within the bilayer, but the approach taken by (30) to measure the D_{lat} in vesicles while changing the membrane tube radius may be more representative of the K_vAP diffusion *in vivo*. However, a diffusion rate twice as fast cannot be accounted solely on the two phenomena cited above, since lipid interaction with K_v will still influence its D_{lat}.

5.7 Simultaneous electrical and fluorescent measurements

Incoporation and K_vAP activity was observed before recording any simultaneous electrical and fluorescent traces. No correlation could be observed between the recorded fluorescence, electrical and voltage signals, either at single molecule level, or at the macroscopic level. A few reasons might be able to explain this.

The right number of functional ion channels needs to be present in the bilayer for successful single molecule measurements. If only a couple of channels are incorporated then they are going to be difficult to track in the bilayer, especially if it has a large surface area such as commonly found in the DIBs. The electrical events dictated by the voltage shifts also need to be captured while the channel is passing within the field of view (Section 4.3.5.1). In most of the experiments the field of view is 1024 μm^2 which represents only a small portion of an average bilayer of 100 μm radius (surface: 7850 μm^2). On the other hand, if too many ion channels are present, individually tracking them then becomes unrealistic and the bilayer will cannot physically sustain large currents and repetitive applications of large voltage shifts (Section 4.3.5.2). Therefore, the camera needs to image a significant area of the bilayer with the right

concentration of channels present in order to match the fluorescence with the electrical signal and allow accurate correlation between the two signals.

The inconsistent incorporation rate also put some restrictions on these experiments, and reproducible conditions need to be found before attempting to do any simultaneous recording at single molecule level. In addition, fluorescent contamination can be a major issue (Section 4.3.5.1). No fluorescent identification of incorporated tagged K_vAP can be made if there is significant background signal. A clean bilayer, free from sample was always imaged before any fluorescent experiment, This revealed that the contamination most likely arose from the sample. Despite many dialysis steps to remove free dyes (overall 15 L dialysis) a high background was a continual problem. The free dye may also have arisen from the labelled tetramer itself, either through loss of covalently bound dye or the fact that TMR5M is quite hydrophobic and will likely "stick" with the lipid inner core. However, all components of the system (lipids, chloroform, hexadecane, PMMA devices, buffers) needed to be thoroughly and continuously checked since they get fluorescently contaminated very easily.

In addition, some technical limitations also need to be taken into account during the analysis of any simultaneous electrical and fluorescent data. Firstly, it would be ideal if the camera could image the entire bilayer surface to prevent any events being missed or lost, the electrical and fluorescent recordings would both exactly arise from the same area and every correlated event would be found on both measurements. Anything would not be missed or lost. Secondly, in order to catch single channel events, the frequency of electrical sampling recording has to kept quite high (20-50 kHz). Unfortunately, the camera recording speed cannot match this frequency (recordings were taken at 50 Hz). A discrepancy will therefore persist between both

data sets, and loss of information will automatically occur from electrical to fluorescence traces for any correlated event. Moreover, this limitation makes the analysis of both signals extremely difficult for any manual comparison.

Finally, it is possible that the fluorescence changes from the TMR5M dye may be too modest to be detected. However, this dye has been successfully extensively used in macroscopic voltage-clamp fluorimetry measurements with voltage-gated potassium channels. It reports on a ensemble level a fluorescent change of approximatively 6 % and 10 % for 1 sec at 60 mV for the Shaker K_v and $K_v1.5$ respectively (holding potential: -80 mV) (101). But these magnitude changes depend on the production levels within the cell. We cannot be certain of the extent of the fluorescent change of the dye attached to K_vAP, but its fit is similar to other K_v channels then we can suppose a change of approximately 6 %, at 80 mV. This change would be quite brief and small and would only be detectable in a low fluorescence background. Mostly fluorimetry experiments were performed on eukaryotic K_v; the only prokaryotic channel studied using this technique was NaChBac (13). This channel was produced in *Xenopus* oocytes, and labelled with different dyes. The signals recorded by TIRF were very small (less than 1.5 % normalised fluorescence change) and were dependent on the dye and its position within the voltage sensor. The environment surrounding the attachement site therefore plays a crucial role on the recorded fluorescence and could make the difference between a signal occurence or not. The transfer from hydrophobic to hydrophilic environment and the presence of other residues which may quench the fluorophore are determinant factors, and are also very difficult to predict. Therefore, the mutants tested in this work may have encountered similar problems and other sites within the voltage sensor domain may need to be investigated to obtain a voltage-dependent fluorescent change.

5.8 Future experiments

Significant time still needs to be devoted to optimise the labelling protocol for K_vAP. Since the labelling reaction seems to be complete even at low protein concentration (Section 3.3.2), using a lower dye concentration (by example 5x [protein]) seems a good start to reduce any contaminating free dye. Working with a larger quantity of protein would also allow a better quantification of the labelling reaction and produce a "cleaner" sample. Indeed, the size exclusion purification of the labelled sample partly removes free dye from the sample (Figure 2.28). However, if this step could be repeated without losing the samples then it might significantly reduce dye contamination. Other approaches could also be explored. A different dye could be better, if its fluorescence intensity is dictated by fluorescence changes. The control site (ie the site not predicted to move during voltage-gating) could also be inserted close to the N or C termini, instead of the S2 helix. However, for the reporter sites, more sites on the voltage sensor should be explored.

Regarding the insertion of the protein into the bilayer, the vesicle fusion approach seemed to be the best approach. Indeed, voltage-gated ion channels are fragile proteins and are more likely to conserve their native state surrounded by lipids. A higher [KCl] in vesicle might accentuate the water flux from the trans side (where vesicles have not been added) to their interior (Section 4.1.3). Another possibility would be to incorporate the channels through the hydrogel phase (59), or through the use of nanodiscs. However, care must be taken that fluorescently tagged channels integrity are not compromised using these approaches and that the optical focus on the bilayer is well adjusted. So far ion channels study by TIRF has always been done in cells, not in a reconstituted system. Therefore, protocols needs to be optimised to allow

fluorescent recordings particularly at single molecule level.

Finally, the analysis of fluorescent and electric recordings could also be improved through automation. The manual correlation of events from 3 signals rapidly becomes tedious and troublesome, especially when they are recorded at different sampling rates. If identification and comparison of events on each recording could be automatically implemented in order to find matches in time, then any potential fluorescent response could be throughly examined and the accuracy of analysis would be substantially improved.

5.9 The mechanism of K_vAP voltage-gating and future directions

No experimental evidence has so far brought a definitve answer to the exact physical movements made by the voltage sensor to open the channel, nor has it been determined precisely how many VSDs have to move in order for the channel to open. Bulk fluorescence recordings clearly demonstrate a movement of the S3b-S4 linker upon voltage change, but without allowing any further definitive conclusions at the level of the individual molecule. Consensus seems to agree that movements of the voltage-sensing domains trigger opening or closing of the pore through S4-S5 linkers and that two of the Arg experience a lipid-facing surface while the other two remain buried in the VSD in the open state (62). This seems to indicate that residues on the S3b-S4 helices are in contact with different environments in this conformation.

Furthermore, K_vAP is not the only voltage-gated K^+ channel model available and others might be more suited to resolve those questions. This membrane protein

comes from an extremophile organism living at 95°C, evolutionary distantly related to eukaryotic organsims. Secondly, its crystal structure was resolved due to the addition of a Fab fragment interacting with the voltage-sensor, which may not represent the functional state of the protein. And finally, the poor ion channel electrical activity observed in the DIB may indicate that only a small percentage of the ion channel produced is actually functional, while the rest is in a non-functional state. Therefore the probability to incorporate functional K_vAP to the bilayer is even more limited.

Moreover the recent retraction of a new K_vAP crystal structure (meant to present a new "native" conformation of the protein) highlights the difficulty and the controversy behind those difficult questions and this protein (91). In addition, experiments carried on the selectivity filter of KcsA and K_vAP demonstrate that constricted conformation of the filter does not solely produce C-type inactivation in K^+ channels and this state is more complex than previously inferred (29). Reducing the gap between functional and structural data is a long term process and the intricacy of any functional states should not be underestimated.

Molecular dynamics simulations have been conducted in order to tackle this problem. Recently, one of them focuses on a eukaryotic chimaera, K_v1.2/2.1 and calculate by free energy molecular dynamics the helical motions required to open and close the pore (34). They concluded that the S3b-S4 helices move upward by 8 $\mathring{A}$ in the lipid bilayer upon pore opening, an energetically favourable process since the closed state was less stable. Other computational approaches have shown movements of individual VSDs during extremely long timescale simulations (up to 256 μsec). The same chimaera has been studied by (48) in an all-atomsystem and their result shows a larger translation of the VSD in the bilayer (15 $\mathring{A}$) and closed state more stable than the open state. However, it was not possible to determine if these single VSD move-

ments would actually open the channel. Much more experimental and theoretical work needs to be conducted in order to answer these questions.

In 2011, the first voltage-gated sodium channels (Na_v) was crystallised at high resolution (2.7 $\mathring{A}$) (77). This breakthrough not only has brought a new set of data on the Na_v structure but also on voltage-gated channels in general as the Na_v channels share many common features with the K_v family and may allow many comparisons between presumably conserved mechanisms. Comparison with the mechanism of S4 movement in the related voltage-sensing phophatases will also be important.

Despite all of the work on these channels over the last two decades, many questions still remain about how voltage-gated channels work. The development of these single molecule approaches therefore still remains an attractive method to probe the movement of these dynamic proteins.

Appendix A

A.1 K_vAP(ΔB13)-C247SC

Amino acids sequence of K_vAP(ΔB13)-C247S (K_vAP-CL):

MARFRRGLSDLGGRVRNIGDVMEH
PLVELGVSYAALLSVIVVVVEYTMQLSGEY
LVRLYLVDLILVIILWADYAYRAYKS
GDPAGYVKKTLYEIPALVPAGLLALIEGHLAGL
GLFRLVRLLRFLRILLIISRGSKFLSA
IADAADKIRFYHLFGAVMLTVLYGAFAIYIVE
YPDPNSSIKSVFDALWWAVVTATTVG
YGDVVPATPIGKVIGIAVMLTGISALTLL
IGTVSNMFQKILVGEPEPSSSPAKLAE
MVSSMSEEEFEEFVRTLKNLRRLENSMK

Figure A.1: Amino acids sequence of K_vAP(ΔB13)-C247S. The mutated Serine is marked in pink.

A.2 pQE60-Lac vector

The pQE60-Lac plasmid is a *cis*-repressed plasmid and was constructed by insertion of the β-galactosidase repressor gene into the pQE60 plasmid (Quiagen) (93).

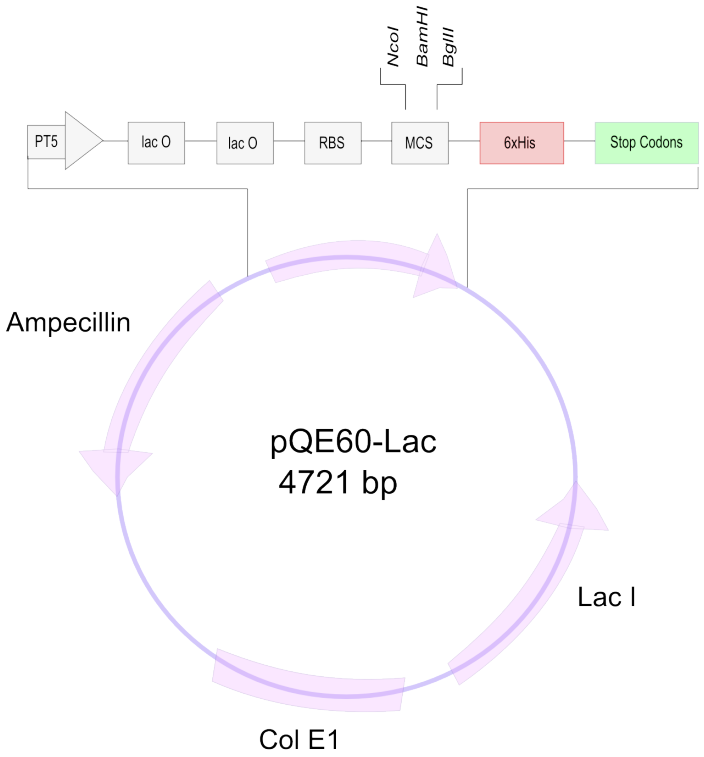


Figure A.2: Map of the pQE60-Lac vector. PT5: T5 promoter. Lac O: lac operator. RBS: Ribosome-binding site. ATG: Start codon. 6xHis: 6xHis tag sequence. MCS: Multiple cloning site. Ampicillin: Ampicillin resistance gene.

A.3 Four Cy3 labelled DNA sample

The control consists of 4 strands carrying the Cy3 dye assembling with a single template.

TAGGCATTAAAGACGGTAGGC

ATTAAAGACGGTAGGCATTAAA

GACGGTAGGCATTAAAGACGG

Figure A.3: Template gene sequence.

Cy3-ATCCGTAATTTCTGCC

Figure A.4: Strand with Cy3 fluorophore gene sequence.

A.4 Microscope calibration

A 1 μm spaced graticule was used for vertical and horizontal calibration of the microscope. The images were taken with a 60x TIRF objective at 1.0x magnification. The average distance between the peaks was calculated by fitting a multi-peak Gaussian to the inverse of the intensity profile of both images.

	Number of pixels	Distance [μm]	Conversion
Vertical resolution	25.25	10	1 pixel = 396 nm
Horizontal resolution	25.5	10	1 pixel = 392 nm

Table A.1: Microscope calibration with a 60x optical magnification.

Bibliography

[1] Langworthy T A. *Membrane Lipids of Prokaryotes Current Topics in Membrane and Transport*, volume 17. Academic Press, 1982.

[2] A Accardi, L Kolmakova-Partensky, C Williams, and C Miller. Ionic currents mediated by a prokaryotic homologue of CLC Cl- channels. *J Gen Physiol*, 123 (2):109–119, 2004.

[3] S K Aggarwal and R MacKinnon. Contribution of the S4 segment to gating charge in the Shaker K+ channel. *Neuron*, 16(6):1169–1177, 1996. URL http://www.ncbi.nlm.nih.gov/pubmed/8663993.

[4] C A Ahern and R Horn. Stirring up controversy with a voltage sensor paddle. *Trends Neurosci*, 27(6):303–307, 2004.

[5] M H Akabas, F S Cohen, and A Finkelstein. Separation of the osmotically driven fusion event from vesicle-planar membrane attachment in a model system for exocytosis. *J Cell Biol*, 98(3):1063–1071, 1984. URL http://www.ncbi.nlm.nih.gov/pubmed/6699082.

[6] W P Ambrose, P M Goodwin, and J P Nolan. Single-molecule detection with total internal reflection excitation: comparing signal-to-background and total

signals in different geometries. *Cytometry*, 36(3):224–231, 1999. URL http://www.ncbi.nlm.nih.gov/pubmed/10404972.

[7] A Arouri, V Kiessling, L Tamm, M Dathe, and A Blume. Morphological changes induced by the action of antimicrobial peptides on supported lipid bilayers. *J Phys Chem B*, 115(1):158–167, 2011. doi: 10.1021/jp107577k. URL http://www.ncbi.nlm.nih.gov/pubmed/21158379.

[8] V J Auld, A L Goldin, D S Krafte, W A Catterall, H A Lester, N Davidson, and R J Dunn. A neutral amino acid change in segment IIS4 dramatically alters the gating properties of the voltage-dependent sodium channel. *Proc Natl Acad Sci U S A*, 87(1):323–327, 1990. URL http://www.ncbi.nlm.nih.gov/pubmed/1688658.

[9] J R Bankston, S S Camp, F DiMaio, A S Lewis, D M Chetkovich, and W N Zagotta. Structure and stoichiometry of an accessory subunit TRIP8b interaction with hyperpolarization-activated cyclic nucleotide-gated channels. *Proc Natl Acad Sci U S A*, 109(20):7899–7904, 2012. doi: 10.1073/pnas.1201997109. URL http://www.ncbi.nlm.nih.gov/pubmed/22550182.

[10] J P Bannister, B Chanda, F Bezanilla, and D M Papazian. Optical detection of rate-determining ion-modulated conformational changes of the ether-a-go-go K+ channel voltage sensor. *Proc Natl Acad Sci U S A*, 102(51):18718–18723, 2005. doi: 10.1073/pnas.0505766102. URL http://www.ncbi.nlm.nih.gov/pubmed/16339906.

[11] F Bezanilla. The voltage sensor in voltage-dependent ion channels. *Phys-*

iol Rev, 80(2):555–592, 2000. URL http://www.ncbi.nlm.nih.gov/pubmed/10747201.

[12] F Bezanilla. How membrane proteins sense voltage. *Nat Rev Mol Cell Biol.*, 9 (4):323–332, April 2008.

[13] R Blunck, D M Starace, A M Correa, and F Bezanilla. Detecting Rearrangements of Shaker and NaChBac in Real-Time with Fluorescene Spectroscopy in Patch-Clamped Mammalian Cells. *Biophysical Journal*, 2004.

[14] R Blunck, H McGuire, H C Hyde, and F Bezanilla. Fluorescence detection of the movement of single KcsA subunits reveals cooperativity. *Proc Natl Acad Sci U S A*, 105(51):20263–20268, 2008. doi: 10.1073/pnas.0807056106. URL http://www.ncbi.nlm.nih.gov/pubmed/19074286.

[15] V Borisenko, T Lougheed, J Hesse, E Füreder-Kitzmüer, N Fertig, J C Behrends, G A Woolley, and G J Schütz. Simultaneous optical and electrical recording of single gramicidin channels. *Biophys J.*, 84(1):612–622, January 2003.

[16] M Carson, D H Johnson, H McDonald, C Brouillette, and L J Delucas. His-tag impact on structure. *Acta Crystallogr D Biol Crystallogr*, 63(Pt 3):295–301, 2007.

[17] O K Castell, J Berridge, and M I Wallace. Quantification of membrane protein inhibition by optical ion flux in a droplet interface bilayer array. *Angew Chem Int Ed Engl*, 51(13):3134–3138, 2012.

[18] A Cha and F Bezanilla. Characterizing voltage-dependent conformational

changes in the Shaker K+ channel with fluorescence. *Neuron*, 19(5):1127–1140, 1997. URL http://www.ncbi.nlm.nih.gov/pubmed/9390525.

[19] A Cha and F Bezanilla. Structural implications of fluorescence quenching in the Shaker K+ channel. *J Gen Physiol*, 112(4):391–408, 1998. URL http://www.ncbi.nlm.nih.gov/pubmed/9758859.

[20] A Cha, G E Snyder, P R Selvin, and F Bezanilla. Atomic scale movement of the voltage-sensing region in a potassium channel measured via spectroscopy. *Nature*, 402(6763):809–813, 1999. doi: 10.1038/45552. URL http://www.ncbi.nlm.nih.gov/pubmed/10617201.

[21] S H Chung and R A Kennedy. Forward-backward non-linear filtering technique for extracting small biological signals from noise. *J Neurosci Methods*, 40(1): 71–86, 1991.

[22] W W Cleland. Dithiothreitol, a New Protective Reagent for Sh Groups. *Biochemistry*, 3:480–482, 1964.

[23] F S Cohen, J Zimmerberg, and A Finkelstein. Fusion of phospholipid vesicles with planar phospholipid bilayer membranes. II. Incorporation of a vesicular membrane marker into the planar membrane. *J Gen Physiol*, 75(3):251–270, 1980.

[24] F S Cohen, M H Akabas, and A Finkelstein. Osmotic swelling of phospholipid vesicles causes them to fuse with a planar phospholipid bilayer membrane. *Science*, 217(4558):458–460, 1982. URL http://www.ncbi.nlm.nih.gov/pubmed/6283637.

[25] F S Cohen, M H Akabas, J Zimmerberg, and A Finkelstein. Parameters affecting the fusion of unilamellar phospholipid vesicles with planar bilayer membranes. *J Cell Biol*, 98(3):1054–1062, 1984. URL http://www.ncbi.nlm.nih.gov/pubmed/6699081.

[26] B Coste, B Xiao, J S Santos, R Syeda, J Grandl, K S Spencer, S E Kim, M Schmidt, J Mathur, A E Dubin, M Montal, and A Patapoutian. Piezo proteins are pore-forming subunits of mechanically activated channels. *Nature*, 483(7388):176–181, 2012. doi: 10.1038/nature10812. URL http://www.ncbi.nlm.nih.gov/pubmed/22343900.

[27] J M Crane and L K Tamm. Role of cholesterol in the formation and nature of lipid rafts in planar and spherical model membranes. *Biophys J*, 86(5):2965–2979, 2004. doi: 10.1016/S0006-3495(04)74347-7. URL http://www.ncbi.nlm.nih.gov/pubmed/15111412.

[28] S K Das, M Darshi, S Cheley, M I Wallace, and H Bayley. Membrane protein stoichiometry determined from the step-wise photobleaching of dye-labelled subunits. *Chembiochem*, 8(9):994–999, June 2007.

[29] P K Devaraneni, A G Komarov, C A Costantino, J J Devereaux, K Matulef, and F I Valiyaveetil. Semisynthetic K+ channels show that the constricted conformation of the selectivity filter is not the C-type inactivated state. *Proc Natl Acad Sci U S A*, 110(39):15698–15703, 2013.

[30] Y A Domanov, S Aimon, G E Toombes, M Renner, F Quemeneur, A Triller, M S Turner, and P Bassereau. Mobility in geometrically confined membranes.

Proc Natl Acad Sci U S A, 108(31):12605–12610, 2011. doi: 10.1073/pnas.1102646108. URL http://www.ncbi.nlm.nih.gov/pubmed/21768336.

[31] D A Doyle, J Morais Cabral, R A Pfuetzner, A Kuo, J M Gulbis, S L Cohen, B T Chait, and R MacKinnon. The structure of the potassium channel: molecular basis of K+ conduction and selectivity. *Science*, 280(5360):69–77, 1998. URL http://www.ncbi.nlm.nih.gov/pubmed/9525859.

[32] G L Ellman. Tissue sulfhydryl groups. *Arch Biochem Biophys*, 82(1):70–77, 1959.

[33] R K Finol-Urdaneta, J R McArthur, P F Juranka, R J French, and C E Morris. Modulation of KvAP unitary conductance and gating by 1-alkanols and other surface active agents. *Biophys J*, 98(5):762–772, 2010. doi: 10.1016/j.bpj.2009.10.053. URL http://www.ncbi.nlm.nih.gov/pubmed/20197029.

[34] P W Fowler and M S Sansom. The pore of voltage-gated potassium ion channels is strained when closed. *Nat Commun*, 4:1872, 2013.

[35] C S Gandhi and E Y Isacoff. Molecular models of voltage sensing. *J Gen Physiol*, 120(4):455–463, 2002. URL http://www.ncbi.nlm.nih.gov/pubmed/12356848.

[36] C S Gandhi, E Loots, and E Y Isacoff. Reconstructing voltage sensor-pore interaction from a fluorescence scan of a voltage-gated K+ channel. *Neuron*, 27(3):585–595, 2000. URL http://www.ncbi.nlm.nih.gov/pubmed/11055440.

[37] C S Gandhi, E Clark, E Loots, A Pralle, and E Y Isacoff. The orientation and

molecular movement of a k(+) channel voltage-sensing domain. *Neuron*, 40(3): 515–525, 2003. URL http://www.ncbi.nlm.nih.gov/pubmed/14642276.

[38] Andrew Garman. *Non-radioactive labeling A practical Introduction*. Elsevier Science Publishing Co, 1997.

[39] C Gell and D A Brockwell D. andSmith. *Handbook of Single Molecule Fluorescence Spectroscopy*, volume 17. Oxford University Press, 2006.

[40] E B Getz, M Xiao, T Chakrabarty, R Cooke, and P R Selvin. A comparison between the sulfhydryl reductants tris(2-carboxyethyl)phosphine and dithiothreitol for use in protein biochemistry. *Anal Biochem*, 273(1):73–80, 1999.

[41] K S Glauner, L M Mannuzzu, C S Gandhi, and E Y Isacoff. Spectroscopic mapping of voltage sensor movement in the Shaker potassium channel. *Nature*, 402(6763):813–817, 1999. doi: 10.1038/45561. URL http://www.ncbi.nlm.nih.gov/pubmed/10617202.

[42] L C Gross, O K Castell, and M I Wallace. Dynamic and reversible control of 2D membrane protein concentration in a droplet interface bilayer. *Nano Lett*, 11(8):3324–3328, 2011.

[43] L C Gross, A J Heron, S C Baca, and M I Wallace. Determining membrane capacitance by dynamic control of droplet interface bilayer area. *Langmuir*, 27(23):14335–14342, 2011. doi: 10.1021/la203081v. URL http://www.ncbi.nlm.nih.gov/pubmed/21978255.

[44] G S Harms, G Orr, B D Montal M. Thrall, S D Colson, and H D Lu. Probing

conformational changes of gramicidin ion channels by single-molecule patch-clamp fluorescence microscopy. *Biophys J.*, 85(3):1826–1836, 2003.

[45] A J Heron, J R Thompson, B Cronin, H Bayley, and M I Wallace. Simultaneous Measurement of Ionic Current and Fluorescence from Single Protein Pores. *JACS*, 131(5):1652–1653, 2009.

[46] R Horn. How S4 segments move charge. Let me count the ways. *J. Gen. Physiol.*, 123(1):1–4, 2004.

[47] S R Jaffrey, H Erdjument-Bromage, C D Ferris, P Tempst, and S H Snyder. Protein S-nitrosylation: a physiological signal for neuronal nitric oxide. *Nat Cell Biol*, 3(2):193–197, 2001.

[48] M O Jensen, V Jogini, D W Borhani, A E Leffler, R O Dror, and D E Shaw. Mechanism of voltage gating in potassium channels. *Science*, 336(6078):229–233, 2012.

[49] Y Jiang, A Lee, J Chen, V Ruta, M Cadene, B T Chait, and R MacKinnon. X-ray structure of a voltage-dependent K+ channel. *Nature*, 423(6935):33–41, 2003. doi: 10.1038/nature01580. URL http://www.ncbi.nlm.nih.gov/pubmed/12721618.

[50] Y Jiang, V Ruta, J Chen, A Lee, and R MacKinnon. The principle of gating charge movement in a voltage-dependent K+ channel. *Nature*, 423(6935):42–48, 2003. doi: 10.1038/nature01581. URL http://www.ncbi.nlm.nih.gov/pubmed/12721619.

[51] A N Kapanidis and T Strick. Biology, one molecule at a time. *Trends Biochem Sci.*, 34(5):234–243, April 2009.

[52] V K Kapoor. Natural toxins and their therapeutic potential. *Indian J Exp Biol*, 48(3):228–237, 2010. URL http://www.ncbi.nlm.nih.gov/pubmed/21046975.

[53] S C Kohout, M H Ulbrich, S C Bell, and E Y Isacoff. Subunit organization and functional transitions in Ci-VSP. *Nat Struct Mol Biol*, 15(1):106–108, 2008. doi: 10.1038/nsmb1320. URL http://www.ncbi.nlm.nih.gov/pubmed/18084307.

[54] M M Kuo, W J Haynes, S H Loukin, C Kung, and Y Saimi. Prokaryotic K(+) channels: from crystal structures to diversity. *FEMS Microbiol Rev*, 29(5):961–985, 2005. doi: 10.1016/j.femsre.2005.03.003. URL http://www.ncbi.nlm.nih.gov/pubmed/16026885.

[55] Leake, Wilson, Gautel, and Simmons. The elasticity of single titin molecules using a two-bead optical tweezers assay. *Biophys. J.*, 87(2):1112–1135, 2004.

[56] J L Ledwell and R W Aldrich. Mutations in the S4 region isolate the final voltage-dependent cooperative step in potassium channel activation. *J Gen Physiol*, 113(3):389–414, 1999. URL http://www.ncbi.nlm.nih.gov/pubmed/10051516.

[57] H C Lee, J M Wang, and K J Swartz. Interaction between extracellular Hanatoxin and the resting conformation of the voltage-sensor paddle in Kv channels. *Neuron*, 40(3):527–536, 2003. URL http://www.ncbi.nlm.nih.gov/pubmed/14642277.

[58] S Y Lee and R Mackinnon. A membrane-access mechanism of ion channel inhibition by voltage sensor toxins from spider venom. *Nature*, 430(6996):232–235, July 2004.

[59] S Leptihn, J R Thompson, J C Ellory, S J Tucker, and M I Wallace. In vitro reconstitution of eukaryotic ion channels using droplet interface bilayers. *J Am Chem Soc*, 133(24):9370–9375, 2011.

[60] S Leptihn, O K Castell, B Cronin, E H Lee, L C Gross, D P Marshall, J R Thompson, M Holden, and M I Wallace. Constructing droplet interface bilayers from the contact of aqueous droplets in oil. *Nat Protoc*, 8(6):1048–1057, 2013.

[61] E R Liman, P Hess, F Weaver, and G Koren. Voltage-sensing residues in the S4 region of a mammalian K+ channel. *Nature*, 353(6346):752–756, 1991. doi: 10.1038/353752a0. URL http://www.ncbi.nlm.nih.gov/pubmed/1944534.

[62] S B Long, E B Campbell, and R Mackinnon. Crystal structure of a mammalian voltage-dependent Shaker family K+ channel. *Science*, 309(5736):897–903, 2005. doi: 10.1126/science.1116269. URL http://www.ncbi.nlm.nih.gov/pubmed/16002581.

[63] S B Long, X Tao, E B Campbell, and R MacKinnon. Atomic structure of a voltage-dependent K+ channel in a lipid membrane-like environment. *Nature*, 450(7168):376–382, 2007. doi: 10.1038/nature06265. URL http://www.ncbi.nlm.nih.gov/pubmed/18004376.

[64] L M Mannuzzu, M M Moronne, and E Y Isacoff. Direct physical measure of conformational rearrangement underlying potassium channel gating.

Science, 271(5246):213–216, 1996. URL http://www.ncbi.nlm.nih.gov/pubmed/8539623.

[65] G I Mashanov and J E Molloy. Automatic detection of single fluorophores in live cells. *Biophys J*, 92(6):2199–2211, 2007.

[66] A R Massensini, J Suckling, M J Brammer, T Moraes-Santos, M V Gomez, and M A Romano-Silva. Tracking sodium channels in live cells: confocal imaging using fluorescently labeled toxins. *J Neurosci Methods*, 116(2):189–196, 2002. URL http://www.ncbi.nlm.nih.gov/pubmed/12044668.

[67] M Milescu, J Vobecky, S H Roh, S H Kim, H J Jung, J I Kim, and K J Swartz. Tarantula toxins interact with voltage sensors within lipid membranes. *J Gen Physiol*, 130(5):497–511, 2007. doi: 10.1085/jgp.200709869. URL http://www.ncbi.nlm.nih.gov/pubmed/17938232.

[68] Christopher Miller. *Ion Channel Reconstitution*. Plenum Press, New York, 1986.

[69] M Montal and P Mueller. Formation of bimolecular membranes from lipid monolayers and a study of their electrical properties. *Proc Natl Acad Sci U S A*, 69(12):3561–3566, 1972. URL http://www.ncbi.nlm.nih.gov/pubmed/4509315.

[70] J H Morais-Cabral, Y Zhou, and R MacKinnon. Energetic optimization of ion conduction rate by the K+ selectivity filter. *Nature*, 414(6859):37–42, 2001.

[71] Y Murata, H Iwasaki, M Sasaki, K Inaba, and Y Okamura. Phosphoinositide phosphatase activity coupled to an intrinsic voltage sensor. *Nature*, 435(7046):

1239–1243, 2005. doi: 10.1038/nature03650. URL http://www.ncbi.nlm.nih.gov/pubmed/15902207.

[72] B P Navas, K Lohner, G Deutsch, E Sevcsik, K A Riske, R Dimova, P Garidel, and G Pabst. Composition dependence of vesicle morphology and mixing properties in a bacterial model membrane system. *Biochimica et Biophysica Acta*, pages 40–48, August 2005.

[73] T P Nguyen and R Horn. Movement and crevices around a sodium channel S3 segment. *J Gen Physiol*, 120(3):419–436, 2002. URL http://www.ncbi.nlm.nih.gov/pubmed/12198095.

[74] C M Nimigean. A radioactive uptake assay to measure ion transport across ion channel-containing liposomes. *Nature Protocols*, 1(3):1207–1212, 2006.

[75] D M Papazian, L C Timpe, Y N Jan, and L Y Jan. Alteration of voltage-dependence of Shaker potassium channel by mutations in the S4 sequence. *Nature*, 349(6307):305–310, 1991. doi: 10.1038/349305a0. URL http://www.ncbi.nlm.nih.gov/pubmed/1846229.

[76] K H Park, C Berrier, B Martinac, and A Ghazi. Purification and functional reconstitution of N- and C-halves of the MscL channel. *Biophys J*, 86(4):2129–2136, 2004.

[77] J Payandeh, T Scheuer, N Zheng, and W Catterall. The crystal structure of a voltage-gated sodium channel. *Nature*, 475:353–358, 2011.

[78] E Perozo, L Santacruz-Toloza, E Stefani, F Bezanilla, and D M Papazian. S4

mutations alter gating currents of Shaker K channels. *Biophys J*, 66(2 Pt 1): 345–354, 1994. URL http://www.ncbi.nlm.nih.gov/pubmed/8161688.

[79] L Picas, M T Montero, A Morros, J L Vazquez-Ibar, and J Hernandez-Borrell. Evidence of phosphatidylethanolamine and phosphatidylglycerol presence at the annular region of lactose permease of Escherichia coli. *Biochim Biophys Acta*, 1798(2):291–296, 2010. doi: 10.1016/j.bbamem.2009.06.024. URL http://www.ncbi.nlm.nih.gov/pubmed/19595667.

[80] A Portis, C Newton, W Pangborn, and D Papahadjopoulos. Studies on the mechanism of membrane fusion: evidence for an intermembrane Ca2+-phospholipid complex, synergism with Mg2+, and inhibition by spectrin. *Biochemistry*, 18(5):780–790, 1979.

[81] W R Redwood, F R Pfeiffer, J A Weisbach, and T E Thompson. Physical properties of bilayer membranes formed from a synthetic saturated phospholipid in n-decane. *Biochim Biophys Acta*, 233(1):1–6, 1971. URL http://www.ncbi.nlm.nih.gov/pubmed/5579131.

[82] T K Ritchie, Y V Grinkova, T H Bayburt, I G Denisov, J K Zolnerciks, W M Atkins, and S G Sligar. Chapter 11 - Reconstitution of membrane proteins in phospholipid bilayer nanodiscs. *Methods Enzymol*, 464:211–231, 2009.

[83] V Ruta, Y Jiang, A Lee, J Chen, and R MacKinnon. Functional analysis of an archaebacterial voltage-dependent K+ channel. *Nature*, 422(6928):180–185, 2003. doi: 10.1038/nature01473. URL http://www.ncbi.nlm.nih.gov/pubmed/12629550.

[84] V Ruta, J Chen, and R MacKinnon. Calibrated measurement of gating-charge arginine displacement in the KvAP voltage-dependent K+ channel. *Cell*, 123 (3):463–475, 2005. doi: 10.1016/j.cell.2005.08.041. URL http://www.ncbi.nlm.nih.gov/pubmed/16269337.

[85] G Sandoz, S C Bell, and E Y Isacoff. Optical probing of a dynamic membrane interaction that regulates the TREK1 channel. *Proc Natl Acad Sci U S A*, 108 (6):2605–2610, 2011. doi: 10.1073/pnas.1015788108. URL http://www.ncbi.nlm.nih.gov/pubmed/21262820.

[86] I F Sbalzarini and P Koumoutsakos. Feature point tracking and trajectory analysis for video imaging in cell biology. *J Struct Biol*, 151(2):182–195, 2005. doi: 10.1016/j.jsb.2005.06.002. URL http://www.ncbi.nlm.nih.gov/pubmed/16043363.

[87] D Schmidt and R MacKinnon. Voltage-dependent K+ channel gating and voltage sensor toxin sensitivity depend on the mechanical state of the lipid membrane. *Proc Natl Acad Sci U S A*, 105(49):19276–19281, 2008. doi: 10.1073/pnas.0810187105. URL http://www.ncbi.nlm.nih.gov/pubmed/19050073.

[88] D Schmidt, Q X Jiang, and R MacKinnon. Phospholipids and the origin of cationic gating charges in voltage sensors. *Nature*, 444(7120):775–779, 2006. doi: 10.1038/nature05416. URL http://www.ncbi.nlm.nih.gov/pubmed/17136096.

[89] D Schmidt, S R Cross, and R MacKinnon. A gating model for the archeal voltage-dependent K(+) channel KvAP in DPhPC and POPE:POPG decane

lipid bilayers. *J Mol Biol*, 390(5):902–912, 2009. doi: 10.1016/j.jmb.2009.05.062. URL http://www.ncbi.nlm.nih.gov/pubmed/19481093.

[90] S A Seoh, D Sigg, D M Papazian, and F Bezanilla. Voltage-sensing residues in the S2 and S4 segments of the Shaker K+ channel. *Neuron*, 16(6):1159–1167, 1996. URL http://www.ncbi.nlm.nih.gov/pubmed/8663992.

[91] L Shi, H Zheng, B A Borkowski, D Shi, T Gonen, and Q X Jiang. Voltage sensor ring in a native structure of a membrane-embedded potassium channel. *Proc Natl Acad Sci U S A*, 110(9):3369–3374, 2013. doi: 10.1073/pnas.1218203110. URL http://www.ncbi.nlm.nih.gov/pubmed/23401554.

[92] F J Sigworth. Voltage gating of ion channels. *Q Rev Biophys*, 27(1):1–40, 1994. URL http://www.ncbi.nlm.nih.gov/pubmed/7520590.

[93] S Sun, J H Gan, J J Paynter, and S J Tucker. {C}loning and functional characterization of a superfamily of microbial inwardly rectifying potassium channels. *Physiol. Genomics*, 26(1):1–7, 2006.

[94] K J Swartz and R MacKinnon. Mapping the receptor site for hanatoxin, a gating modifier of voltage-dependent K+ channels. *Neuron*, 18(4):675–682, 1997. URL http://www.ncbi.nlm.nih.gov/pubmed/9136775.

[95] O Teijido, R Ujwal, C O Hillerdal, L Kullman, T K Rostovtseva, and J Abramson. Affixing N-terminal alpha-helix to the wall of the voltage-dependent anion channel does not prevent its voltage gating. *J Biol Chem*, 287(14):11437–11445, 2012.

[96] J R Thompson, A J Heron, Y Santoso, and M I Wallace. Enhanced stability

and fluidity in droplet on hydrogel bilayers for measuring membrane protein diffusion. *Nano Lett*, 7(12):3875–3878, 2007.

[97] J R Thompson, B Cronin, H Bayley, and M I Wallace. Rapid assembly of a multimeric membrane protein pore. *Biophys J*, 101(11):2679–2683, 2011.

[98] James Thompson. *Imaging the Assembly of the Staphylococcal Pore-Forming Toxin α-Hemolysin*. PhD thesis, University of Oxford.

[99] F Tombola, M H Ulbrich, and E Y Isacoff. The voltage-gated proton channel Hv1 has two pores, each controlled by one voltage sensor. *Neuron*, 58(4):546–556, May 2008.

[100] M H Ulbrich and E Y Isacoff. Subunit counting in membrane-bound proteins. *Nat Methods*, 4(4):319–321, 2007. doi: 10.1038/nmeth1024. URL http://www.ncbi.nlm.nih.gov/pubmed/17369835.

[101] Moninder. Vaid, Thomas. W Claydon, Saman. Rezazadeh, and David. Fedida. Voltage Clamp Fluorimetry Reveals a Novel Outer Pore Instability in a Mammalian Voltage-gated Potassium Channel. *J. Gen. Phys.*, 132(2):209–222, 2008.

[102] L A Veliz, C A Toro, J P Vivar, L A Arias, J Villegas, M A Castro, and S Brauchi. Near-membrane dynamics and capture of TRPM8 channels within transient confinement domains. *PLoS One*, 5(10):e13290, 2010. doi: 10.1371/journal.pone.0013290. URL http://www.ncbi.nlm.nih.gov/pubmed/20948964.

[103] S Won, H D Kim, J Y Kim, B C Lee, S Chang, and C S Park. Movements of individual BKCa channels in live cell membrane monitored by site-specific

labeling using quantum dots. *Biophys J*, 99(9):2853–2862, 2010. doi: 10.1016/j.bpj.2010.08.049. URL http://www.ncbi.nlm.nih.gov/pubmed/21044582.

[104] H Wulff, Castle N.A, and L A Pardo. Voltage-gated potassium channels as therapeutic targets. *Nat Rev Drug Discov.*, 8(12):982–1001, December 2009.

[105] Y Xu, Y Ramu, and Z Lu. A shaker K+ channel with a miniature engineered voltage sensor. *Cell*, 142(4):580–589, 2010. doi: 10.1016/j.cell.2010.07.013. URL http://www.ncbi.nlm.nih.gov/pubmed/20691466.

[106] F H Yu and W A Catterall. The VGL-chanome: a protein superfamily specialized for electrical signaling and ionic homeostasis. *Sci STKE*, 2004(253):re15, 2004.

[107] z. Zhang, P T Rajagopalan, T Selzer, S J Benkovic, and G G Hammes. Single-molecule and transient kinetics investigation of the interaction of dihydrofolate reductase with NADPH and dihydrofolate. *PNAS*, 101(9):2764–2769, March 2004.

[108] Y Zhao, D Terry, L Shi, H Weinstein, S C Blanchard, and J A Javitch. Single-molecule dynamics of gating in a neurotransmitter transporter homologue. *Nature*, 465(7295):188–193, 2010. doi: 10.1038/nature09057. URL http://www.ncbi.nlm.nih.gov/pubmed/20463731.

[109] J L Zimmermann, T Nicolaus, G Neuert, and K Blank. Thiol-based, site-specific and covalent immobilization of biomolecules for single-molecule experiments. *Nat Protoc*, 5(6):975–985, 2010. doi: 10.1038/nprot.2010.49. URL http://www.ncbi.nlm.nih.gov/pubmed/20448543.